Department of Biochemistry of the University of Oxford

St. Anne's College Oxford



Master thesis

in the course Master of Science by Research in Biochemistry

Trinity Term 2021

The linear ubiquitin assembly complex's recruitment to signaling complexes: The role of HOIP's zinc finger domains

Submitted by:

Evangelia Nathanail

Word count: 24,533 words

Acknowledgments

I would like to thank, first and foremost, my supervisors for this thesis, Dr. Paul R. Elliott and Prof. Christina Redfield, for supporting me in my extremely rewarding first endeavor in structural biology. This project would have never taken its true form without Paul's hands-on counseling as well as his insightful feedback and advice on scientific research, for which I am forever grateful. Along with him I would like to whole heartedly thank the Elliott Lab, Cara, Larissa, Maribel and Nunu, for making my year in Oxford an experience I will always remember fondly and for providing me with support, scientific or otherwise, every day along the journey.

I would also like to thank my partner, my friends and my family for their immense help. Even though COVID-19 did not allow us to meet in person as much, or as easily, as we wished, I always know I can rely on you to offer me your love and a little pick-me-up, 24/7. You now all know a bit more about ubiquitin, probably more than you ever thought you would, but that is what you get for supporting my dream of an MRes in Oxford. Thank you, from the bottom of my heart.

Table of Contents

Acknowledgments ii

Abstract v

List of abbreviations vi

List of figures x

List of tables xv

1. Introduction 1

1.1. The ubiquitin code 1

1.2. The writers of the ubiquitin code: the ubiquitin conjugation cascade 2

1.3. Ubiquitin as a target substrate: chain formation and conformation 3

1.4. The readers of the ubiquitin code: ubiquitin-binding domains 6

1.5. The erasers of the code: signal termination 6

1.6. Ubiquitin chains and the M1 code in immunity and inflammation 7

1.7. The assembly and recognition of M1 chains 8

1.8. LUBAC's regulation and its malfunction in disease 10

1.9. LUBAC's role in inflammation and the innate immune response through tumour necrosis factor signaling 11

1.10. NZF domains in inflammatory signaling complexes 13

1.11. LUBAC's recruitment to signaling complexes 16

1.12. HOIP's zinc finger domains as a potential recruitment center for LUBAC 17

1.13. Aims of this thesis 19

2. Materials and Methods 22

2.1. Sequence analysis 22

2.2. Molecular biology 22

2.3. Recombinant protein expression and purification 23

2.4. Nuclear Magnetic Resonance (NMR) spectroscopy and backbone assignment theory 25

2.5. NMR sample preparation and data acquisition 26

2.6. Multi-angle light scattering (MALS) 27

2.7. Isothermal Titration Calorimetry (ITC) 28
2.8. Crystallization 30
3. Results 31
3.1. HOIP's zinc finger domains are highly conserved and fold independently of one another 31
3.2. The Zf domain is a misannotated NZF that does not bind ubiquitin 33
3.3. Backbone assignment of HOIP NZF1-NZF2 (aa 346-451) 34
3.4. NZF1 and NZF2 both bind monoubiquitin via their TF/Φ motif 36
3.5. Binding to monoubiquitin is preserved when both NZF1 and NZF2 are present 41
3.6. NZF1 binds to monoubiquitin stronger than NZF2 47
3.7. NZF2 possesses an extended binding patch for K63-linked chains 50
3.8. NZF1 binds ubiquitin chains tighter than NZF2 and the HOIP N-terminus shows specificity for K63 chains 62
3.9. Construct crystallization aimed to elucidate HOIP's specificity for K63-linked ubiquitin chains 66
3.10. Phosphorylation in S383 does not significantly affect polyubiquitin binding 70
3.11. HOIP's oligomerization is controlled by the B-box domain and does not influence ubiquitin chain affinity 72
3.12. The ubiquitin-binding patch of NZF1 overlaps partially with its NEMO binding interface, hindering binding to monoubiquitin 76
3.13. Other signaling partners do not bind directly to the HOIP N-terminus 83
4. Discussion 88
5. Limitations of the study 92
6. Concluding remarks 93
Appendix 95
References 109

Abstract

The linear ubiquitin chain assembly complex (LUBAC) regulates NF-κB activation and prevents cell death by conjugating M1 polyubiquitin on inflammatory complexes through its catalytic subunit HOIP. Although the conjugation of M1 chains is well described, less is known about the mechanism of LUBAC's recruitment to inflammatory signaling complexes. This thesis elucidates the role of HOIP's zinc finger region, which encompasses its B-box, Zf and NZF domains, in the binding and recruitment to ubiquitin chains, by employing biophysical techniques such as NMR and ITC to characterize the mechanism. The HOIP NZF1 domain is the driving force behind ubiquitin-binding and interacts with monoubiquitin with a higher affinity than previously studied NZF domains, while HOIP NZF2 employs a similar interface as NZF1 to bind to monoubiquitin weakly. HOIP's specificity for K63-linked chains is determined by the tandem NZF domains, which cooperatively decrease the protein's affinity to monoubiquitin and increase its affinity to polyubiquitin, as shown by ITC binding experiments. The interaction of HOIP NZF1 with the downstream signaling effector NEMO hinders, but does not abolish, ubiquitin binding due to an overlap in the binding interfaces for ubiquitin and NEMO. To widen the scope of the regulation of LUBAC's recruitment, phosphorylation of S383 of the NZF1-NZF2 linker region and HOIP oligomerization via the B-box domain are studied as regulatory mechanisms for the affinity to K63-linked polyubiquitin and found to not affect it. It is therefore proposed that HOIP NZF1 and NZF2 jointly drive LUBAC's recruitment to preformed K63-linked polyubiquitin in inflammatory signaling complexes. A novel binding mechanism for linkage-specific NZF domains is described, in which binding is driven by NZF1 while K63 diubiquitin specificity is established independently by each NZF domain.

List of abbreviations

ΔG	Gibb's free energy change
ΔH	reaction enthalpy change
ΔS	entropy change
2xYT	Yeast Tryptone Broth
Å	Ångström
ABIN	A20-Binding Inhibitors of NF-κB
aa	amino acids
ATP	Adenosine Triphosphate
B-box	B-box-type zinc finger
BEST-TROSY	Band-Selective Excitation Short-Transient Transverse relaxation optimised spectroscopy
CARMA1	CARD-containing MAGUK protein 1
cIAP1/2	cellular Inhibitor of Apoptosis Proteins ½
CoZi	coil-zipper
cpdm	Sharpin-chronic proliferative dermatitis
CSP	Chemical Shift Perturbation
CYLD	Cylindromatosis
DAMP	Damage-associated Molecular Pattern
DD	intracellular Death-Domain
DTT	Dithiothreitol
DUB	Deubiquitinating enzyme
FID	Free Induction Decay
HECT	Homologous to the E6-associated protein (E6AP) C-terminus
HEPES	4-(2-hydroxyethyl)-1-piperazineethanesulfonic acid
HOIL-1L	Heme-oxidized IRP2 ubiquitin Ligase 1
HOIP	HOIL-1-Interacting Protein

HSQC	Heteronuclear Single Quantum Coherence
IκB	Inhibitor of κB
IKK	IκB Kinase
IPTG	Isopropyl β-D-1-thiogalactopyranoside
K_d	Dissociation constant
ITC	Isothermal Titration Calorimetry
LDD	Linear ubiquitin chain Determining Domain
LTD	LUBAC-Tethering motif Domains
LUBAC	Linear Ubiquitin chain Assembly Complex
NDP52	nuclear dot protein 52 kDa
NEMO	NF-κB Essential Modulator
NF-κB	nuclear factor κ-light-chain-enhancer of activated B cells
NMR	Nuclear Magnetic Resonance
NOD	Nucleotide-binding Oligomerization Domain-containing protein
NOE	Nuclear Overhauser Effect
Npl4	Nuclear protein localization 4
NUS	non-uniform sampling
NZF	Npl4 Zinc Finger
OD600	optical density at 600 nm
OPTN	Optineurin
ORAS	OTULIN-related Autoinflammatory Syndrome
OTULIN	OTU domain-containing deubiquitinase with Linear linkage specificity
PAMP	Pathogen-associated Molecular Pattern
PEG	polyethylene glycol
PIM	PUB-interacting Motif
ppm	parts per million
PRR	Pattern Recognition Receptor
PTM	Post-translational Modification

PUB	Peptide:N-glycanase/UBA- or UBX containing proteins
RanBP2	RAN Binding Protein 2
RBR	RING-Between-RING
RING	Really Interesting New Gene
RIP	Receptor-interacting Protein 1
RIPK1	RIP Kinase 1
RNF213	Ring Finger protein 213
SDS-PAGE	Sodium Dodecyl Sulphate - Polyacrylamide Gel Electophoresis
SEC	Size-exclusion Chromatography
SEC-MALS	SEC coupled with Multi-angle Light Scattering
SHARPIN	Shank-associated RH domain-interacting protein
SKICH	SKIP carboxyl homology
SPATA2	Spermatogenesis-associated protein 2
SUMO	Small Ubiquitin-like Modifier
TAB2/3	Mitogen-activated protein kinase kinase kinase 7-interacting protein 2/3
TAK	Mitogen-activated protein kinase kinase kinase 7
TCEP	tris(2-carboxyethyl)phosphine
TNF	Tumour Necrosis Factor
TNFR	TNF Receptor
TRABID	TRAF-binding domain-containing protein
TRAF2/6	TNFR-associated Factor 2/6
TNF-RSC	TNFR Signaling Complex
TRADD	TNFR1-associated via DD
TRIM	Tripartite protein
Ub_2	Diubiquitin
UBA	Ubiquitin-associated
UBAN	Ubiquitin Binding in ABIN and NEMO
UBD	Ubiquitin-Binding Domain

UBL	Ubiquitin-like
UBZ	Ubiquitin-binding zinc finger
USP	Ubiquitin Specific Protease
Zf	Zinc finger

List of figures

Figure 1: The ubiquitin code. 2

Figure 2: The structure of ubiquitin 5

Figure 3: An overview of canonical TNF signaling with an emphasis on linear ubiquitination. 12

Figure 4: Comparison of NZF structures bound to ubiquitin. 14

Figure 5: Graphic illustration of HOIP, HOIL-1L and SHARPIN and their domains. 17

Figure 6: Graphic illustration of HOIP's domains and the constructs used in this thesis..... 23

Figure 7: Sequence alignment for the extended zinc finger domains of HOIP (aa 200-468) across orthologues. 31

Figure 8: BEST-TROSY spectra of ^{15}N-labelled HOIP constructs B-box-Zf-NZF1-NZF2 (aa 215-451, orange), Zf-NZF1-NZF2 (aa 280-451, pink), Zf (aa 280-340, green), NZF1-NZF2 (aa 346-451, purple) and NZF2 (aa 380-451, red). 33

Figure 9: Sequence comparison of HOIP's Zf with other zinc finger domains. 33

Figure 10: BEST-TROSY spectra of ^{15}N-labelled HOIP NZF0 (aa 280-340, green) and HOIP NZF0 mixed with 1:6 molar excess monoubiquitin. 34

Figure 11: Snapshot of the NMR assignment of ^{13}C-^{15}N-labelled HOIP NZF1-NZF2 (aa 346-451)..... 35

Figure 12: BEST-TROSY spectra of ^{13}C-^{15}N-labelled HOIP NZF1-NZF2 (aa 346-451). 36

Figure 13: BEST-TROSY spectra of ^{15}N-labelled HOIP NZF1 (aa 346-400) and HOIP NZF1 mixed with monoubiquitin. 37

Figure 14: BEST-TROSY spectra of ^{15}N-labelled HOIP NZF2 (aa 380-451) and HOIP NZF2 mixed with monoubiquitin. 38

Figure 15: Chemical shift perturbation maps of HOIP NZF1 (aa 346-400) and HOIP NZF2 (aa 380-451), derived from their titrations with monoubiquitin. 39

Figure 16: Comparison of the NZF1 of HOIP and the NZF of TAB2 and superposition on the NZF1 of HOIP and K63-linked diubiquitin. 41
Figure 17: BEST-TROSY spectra of ^{15}N-labelled HOIP NZF1-NZF2 (aa 346-451) and HOIP NZF1-NZF2 mixed with monoubiquitin. 42
Figure 18: Chemical shift perturbation map of HOIP NZF1-NZF2 (aa 346-451), derived from its titration with monoubiquitin. 43
Figure 19: BEST-TROSY spectra of ^{15}N-labelled HOIP NZF1-NZF2 T360A (aa 346-451) and HOIP NZF1-NZF2 T360A mixed with monoubiquitin. 44
Figure 20: BEST-TROSY spectra of ^{15}N-labelled HOIP NZF1-NZF2 T419A (aa 346-451) and HOIP NZF1-NZF2 T419A mixed with monoubiquitin. 45
Figure 21: Chemical shift perturbation maps of HOIP NZF1-NZF2 wild-type (aa 346-451), HOIP NZF1-NZF2 T360A (aa 346-451) and HOIP NZF1-NZF2 T419A (aa 346-451), derived from their titrations with monoubiquitin. 46
Figure 22: ITC titration curves and graphic illustration of the interaction of monoubiquitin with HOIP NZF1 (aa 346-400), NZF2 (aa 380-451), NZF1-NZF2 wild-type (aa 346-451), NZF1-NZF2 T419A (aa 346-451) and NZF1-NZF2 T360A (aa 346-451). 48
Figure 23: BEST-TROSY spectra of ^{15}N-labelled HOIP NZF1-NZF2 (aa 350-438) and HOIP NZF1-NZF2 mixed with K48-linked diubiquitin in (A) and K63-linked diubiquitin in (B). 52
Figure 24: Chemical shift perturbation maps of HOIP NZF1-NZF2 (aa 350-438), derived from its titrations with K48-linked (A) and K63-linked diubiquitin (B). 53
Figure 25: Comparison of the NZF2 of HOIP with the NZF1 of HOIP and the NZF of TAB2 and superposition on the NZF2 of HOIP and K63-linked diubiquitin 55
Figure 26: BEST-TROSY spectra of ^{15}N-labelled HOIP NZF1 (aa 346-400) and HOIP NZF1 mixed with K48-linked diubiquitin in (A) and K63-linked diubiquitin in (B) 56
Figure 27: Chemical shift perturbation maps of HOIP NZF1 (aa 346-400), derived from its titrations with K48-linked (A) and K63-linked diubiquitin (B). 57

Figure 28: BEST-TROSY spectra of ^{15}N-labelled HOIP NZF2 (aa 380-451) and HOIP NZF2 mixed with K48-linked diubiquitin in (A) and K63-linked diubiquitin in (B)..... 58
Figure 29: Chemical shift perturbation maps of HOIP NZF2 (aa 380-451), derived from its titrations with K48-linked (A) and K63-linked diubiquitin (B). 59
Figure 30: BEST-TROSY spectra of ^{15}N-labelled HOIP NZF1-NZF2 T360A (aa 346-451) and HOIP NZF1-NZF2 mixed with K48-linked diubiquitin in (A) and K63-linked diubiquitin in (B). 61
Figure 31: Chemical shift perturbation maps of HOIP NZF1-NZF2 T360A (aa 346-451), derived from its titrations with K48-linked (A) and K63-linked diubiquitin (B). 62
Figure 32: ITC titration curves and graphic illustration of the interaction of HOIP NZF1 (aa 346-400), NZF2 (aa 380-451), NZF1-NZF2 wild-type (aa 346-451), NZF1-NZF2 T419A (aa 346-451) and NZF1-NZF2 T360A (aa 346-451) with K63 diubiquitin or K48 diubiquitin. 65
Figure 33: ^{1}H-^{15}N HetNOE values for HOIP NZF1-NZF2 (aa 346-451). 67
Figure 34: BEST-TROSY spectra of ^{15}N-labelled HOIP NZF1-NZF2 (aa 346-451) and the truncated construct HOIP NZF1-NZF2* (aa 350-438). 68
Figure 35: Coomassie-stained SDS-PAGE analysis of the proteins used for crystallization. From left to right: HOIP NZF1-NZF2 (aa 350-438), K63-linked diubiquitin, K63-linked triubiquitin. 69
Figure 36: (A) Exemplary image of ubiquitin crystals, typically adopting cubic forms in zinc-containing conditions. (B, C) Uniform crystals appearing in conditions using microseeding. 70
Figure 37: ITC titration curves and graphic illustration of the interaction between HOIP NZF1-NZF2 wild-type or HOIP NZF1-NZF2 S383E with K63-linked diubiquitin (A) and K48-linked diubiquitin (B). 71
Figure 38: SEC-MALS analysis of HOIP's zinc finger domains and their mutants L219D, L219I, L219R, L219Y on a Superdex 75 column. 73

Figure 39: ITC titration curves and graphic illustration of the interaction between HOIP NZF1-NZF2 wild-type (aa 346-451), HOIP B-box-NZF0-NZF1-NZF2 wild-type (aa 215-451) and HOIP B-box-NZF0-NZF1-NZF2 L219R (aa 215-451) with long K63-linked polyubiquitin chains. 75
Figure 40: (A) BEST-TROSY spectra of ^{15}N-labelled HOIP NZF1 and HOIP NZF1 mixed with NEMO CoZi domain. (B) BEST-TROSY spectra of ^{15}N-labelled HOIP NZF1-NZF2 R375A alone and mixed with 1:4 molar excess NEMO CoZi domain. 77
Figure 41: BEST-TROSY spectra of ^{15}N-labelled HOIP NZF1-NZF2 wild-type (aa 346-451) and HOIP NZF1-NZF2 R375A. 78
Figure 42: BEST-TROSY spectra of ^{15}N-labelled HOIP NZF1 (aa 346-400) mixed with 1:6 excess NEMO CoZi domain and subsequently mixed with monoubiquitin. 79
Figure 43: Chemical shift perturbation maps of HOIP NZF1 (aa 346-400), derived from its titration with NEMO CoZi domain and subsequently with monoubiquitin. 79
Figure 44: Crystal structure of HOIP NZF1 with NEMO CoZi domain, with the ubiquitin-binding patch in blue, the NEMO binding patch in orange and their overlap in green, and with the surface coloured according to its sequence conservation using ClustalW in (B). 81
Figure 45: Thermodynamic parameters for the ITC titration curves of HOIP NZF1-NZF2 wild-type, and HOIP NZF1-NZF2 R375A binding to monoubiquitin. 81
Figure 46: BEST-TROSY spectra of ^{15}N-labelled HOIP NZF0 (aa 280-340, orange) or ^{15}N-labelled HOIP NZF2 (aa 380-451, red) mixed with 1:4 molar excess NEMO CoZi domain. 82
Figure 47: BEST-TROSY spectra of ^{15}N-labelled HOIP B-box-NZF0-NZF1-NZF2 construct (aa 215-451), mixed with CARMA1. 83
Figure 48: BEST-TROSY spectra of ^{15}N-labelled HOIP PUB domain (aa 1-184), B-box (aa 195-291), NF0 (aa 280-340), NZF1 (aa 346-451) and NZF2 (aa 380-451) mixed with TRAF6 RING and Zf domains. 84

Figure 49: BEST-TROSY spectra of ^{15}N-labelled HOIP PUB domain (aa 1-184), B-box (aa 195-291), NF0 (aa 280-340), NZF1 (aa 346-451) and NZF2 (aa 380-451) mixed with NDP52 SKICH domain. 85
Figure 50: BEST-TROSY spectra of ^{15}N-labelled HOIP PUB domain (aa 1-184), B-box (aa 195-291), NF0 (aa 280-340), NZF1 (aa 346-451) and NZF2 (aa 380-451) mixed with NDP52 UBZ domain. 85
Figure 51: BEST-TROSY spectra of ^{15}N-labelled HOIP NZF0 (aa 280-340) or ^{15}N-labelled HOIP NZF1 (aa 346-400) mixed with ABIN2 UBAN domain. 86
Figure 52: BEST-TROSY spectra of ^{15}N-labelled HOIP NZF0 (aa 280-340) or NZF1-NZF2 (aa 346-451) mixed with SHARPIN UBL domain. 87

List of tables

Table 1: Concentrations and repeats of all ITC experiments studied in this thesis. 29

Table 2: Thermodynamic parameters for the ITC titration curves of HOIP NZF1-NZF2 wild-type, HOIP NZF1, HOIP NZF1-NZF2 T419A, NZF2 and HOIP NZF1-NZF2 T360A binding to monoubiquitin..... 49

Table 3: Thermodynamic parameters for the ITC titration curves of HOIP NZF1, HOIP NZF1-NZF2 T419A, NZF2, HOIP NZF1-NZF2 T360A and HOIP NZF1-NZF2 wild-type, binding to K48- and K63-linked diubiquitin..... 65

Table 4: Thermodynamic parameters for the ITC titration curves of HOIP NZF1-NZF2 wild-type and S383E (aa 346-451) binding to K63- and K48-linked diubiquitin. 71

Table 5: Calculated molar masses of the HOIP B-box-NZF0-NZF1-NZF2 wild-type and mutant constructs..... 74

Table 6: Thermodynamic parameters for the ITC titration curves of HOIP NZF1-NZF2 wild-type, HOIP B-box-NZF0-NZF1-NZF2 wild-type and HOIP B-box-NZF0-NZF1-NZF2 L219R binding to long K63-linked ubiquitin chains. 75

Table 7: Thermodynamic parameters for the ITC titration curves of HOIP NZF1-NZF2 wild-type and HOIP NZF1-NZF2 R375A binding to monoubiquitin..... 82

1. Introduction

1.1. The ubiquitin code

Proteins are the driving engines of life, determining and executing nearly all vital processes in organisms. The fine control and regulation of these processes is therefore necessary and is often realized through post-translational modifications (PTMs). Alongside phosphorylation and acetylation, one of the most common ways to modify expressed proteins is through ubiquitination. Ubiquitin is a small protein of 8.6 kDa with a β-grasp fold and a flexible C-terminus [1]. It is highly conserved in all eukaryotes and was initially thought to only regulate protein degradation by marking proteins to be destroyed by the 26S proteasome. In the past 40 years the study of ubiquitination has broadened its role to include a multitude of signaling processes, from cell cycle regulation to innate immunity [2, 3].

Without enzymatic activity of its own, ubiquitin plays its vital role as a modifier through its attachment to target substrates via the formation of a bond between the C-terminus of the ubiquitin and a lysine residue in the target protein [4, 5]. One ubiquitin molecule may be attached onto a substrate (monoubiquitination), or multiple residues of the target protein may be ubiquitinated (multi-monoubiquitination). In addition, as ubiquitin has several lysine residues polyubiquitin chains may be formed [6]. This conjugation serves as a signal to determine the processes mentioned above, and therefore the ubiquitin system involves writers, readers and erasers: writers to conjugate ubiquitin onto substrates and create the code, readers to correctly decipher the code and erasers to remove previously attached ubiquitin and terminate the signal (**Figure 1**).

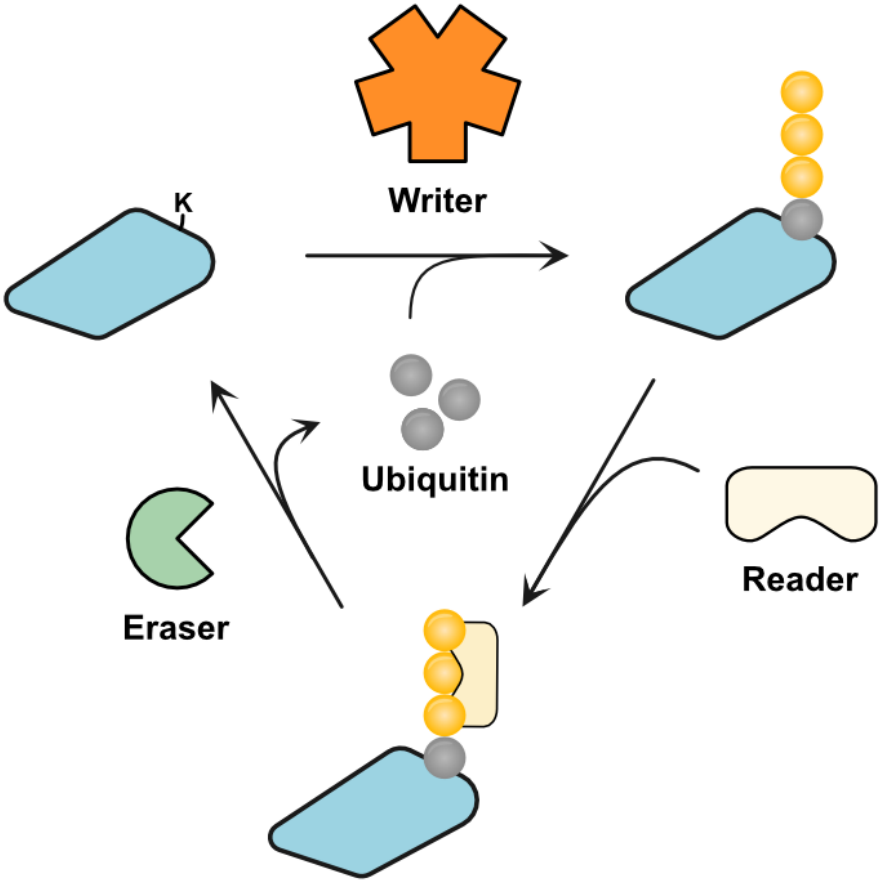


Figure 1: The ubiquitin code. A writer (orange) attaches ubiquitin to a lysine on the substrate (blue) and subsequently extends it to form a ubiquitin chain. A reader (yellow) binds to the chain. The eraser (green) cleaves the chain, terminating the signal and returning the ubiquitin to the cell's ubiquitin pool.

1.2. The writers of the ubiquitin code: the ubiquitin conjugation cascade

The ubiquitin conjugation system attaches ubiquitin moieties to target substrates, making its enzymes the writers of the ubiquitin code. The system is ATP-dependent and requires three categories of enzymes: an E1 (ubiquitin-activating enzyme), an E2 (ubiquitin-conjugating enzyme) and an E3 (ubiquitin-ligating enzyme) [7]. The cascade is initiated by the E1, which activates the ubiquitin by acyl-adenylating its terminal glycine Gly76 with the use of ATP and subsequently binds it to an active site cysteine on the E1. The activated ubiquitin is then transferred onto the active site cysteine of the E2.

In the final step the ubiquitin-loaded E2 is recruited to the E3, which is responsible for transferring the ubiquitin to the target substrate, usually a lysine but serines, threonines or lipids have also been described [4, 5, 8]. The mechanism of the transfer varies across the four families of E3s: Really Interesting New Gene (RING), U-box, Homologous to the E6-associated protein (E6AP) C-terminus (HECT) and RING-Between-RING (RBR) E3s. RING and U-box E3s facilitate the transfer of ubiquitin directly from the activated E2 cysteine to the target residue in the substrate, meaning that the E2 defines the specificity of the ligation in terms of ubiquitin linkage specificity. HECT E3s, on the other hand, possess a catalytic cysteine in their HECT domain which allows them to be loaded with the ubiquitin, forming an E3~Ub conjugate and afterwards selectively labelling the target, where ~ symbolizes a thioester bond [9]. RBR E3s use a HECT/RING hybrid mechanism to conjugate ubiquitin onto proteins. While they possess a RING domain, it is followed by an In-Between-RING and a RING-like domain. The E2-Ubiquitin is recruited to the RING domain, much like RING E3s, however RBRs then load the ubiquitin onto the RING-like domain and build an E3~Ub complex before transferring it to the substrate, making them similar to HECT E3s. RBRs therefore also determine the specificity of the ligation, much like their HECT counterparts [10, 11]. The ligase studied in this thesis, HOIL-1-Interacting Protein (HOIP, also named RNF31, ZIBRA or PAUL), is a RBR E3 ligase. To ensure the tight regulation of ubiquitin signaling, the system becomes more specific as the cascades progresses. There are therefore 4 genes that encode ubiquitin, 2 E1s, 35 E2s and more than 500 E3s in humans, enabling a multitude of highly specific ubiquitin conjugating cascades to take place [12].

1.3. Ubiquitin as a target substrate: chain formation and conformation

Canonical ubiquitination requires the C-terminus of ubiquitin to be attached to a free amino-group of the substrate, creating an (iso)peptide bond between the two proteins. Ubiquitin consists of 76 amino acids and itself contains eight residues with a free amino-

group: its N-terminal methionine (M1) and seven lysines (K6, K11, K27, K29, K33, K48, K63). It is therefore possible for ubiquitin to serve as a target for ubiquitination, having further ubiquitin molecules attached to it to create polyubiquitin, also called a ubiquitin chain. In such a cascade the substrate is initially monoubiquitinated by an E3 on the substrate's target lysine. This ubiquitin moiety is called the proximal ubiquitin. A second ubiquitin, named the distal ubiquitin, is attached onto the proximal ubiquitin via an (iso)peptide bond. The process is repeated to create chains of variable lengths [4]. E2s and E3s can achieve specificity in ubiquitin chain assembly, in which the target residue of the proximal and the C-terminus of the distal ubiquitins are sterically coordinated in proximity that allows covalent bond formation. This is often complemented by positioning the ubiquitin so that other acceptor residues (e.g. other lysines or M1) are shielded and unavailable to the active site [13].

Since the attachment sites (lysines and N-terminus) are dispersed across the surface of ubiquitin polyubiquitin chains adopt different conformations [9]. For example, K48 chains adopt a closed conformation as shown by structural and solution studies, while K63 chains can adopt both open and compact conformations in solution [14].

In addition, different hydrophobic patches are found across the surface of ubiquitin which mediate non-covalent interactions between other proteins. The main ubiquitin patches are the Ile44, Phe4 and Ile36 patches, encompassing three to five residues per patch (**Figure 2**). These patches facilitate the recognition of ubiquitin by the enzymes of the ubiquitin code. Ile44 is the canonical binding patch for the readers of the code, but by forming additional hydrophobic interactions with other patches proteins can selectively position ubiquitin for enzymatic activity (e.g. chain formation by an E3) or bind polyubiquitin of a specific linkage type (see *The readers of the ubiquitin code: ubiquitin-binding domains* and **Figure 4**) [15].

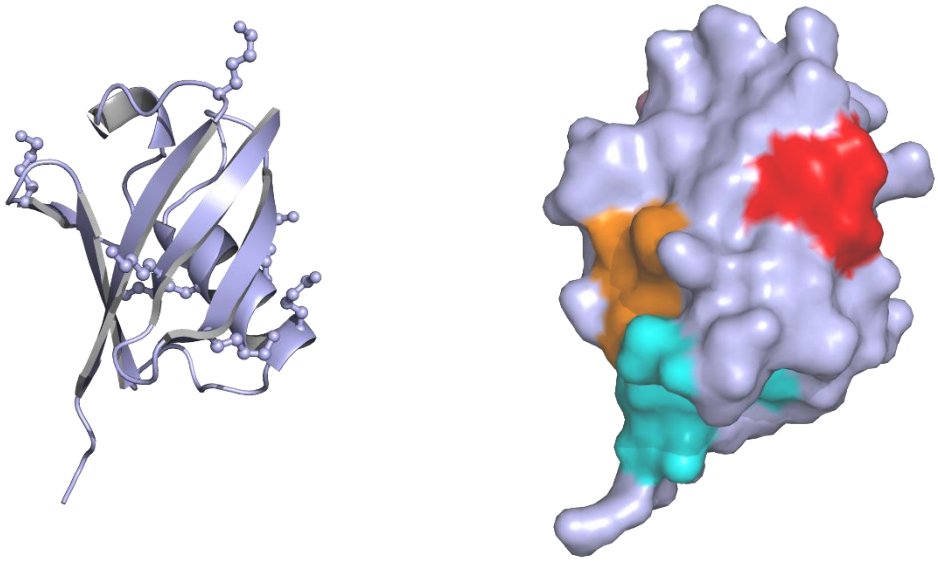


Figure 2: The structure of ubiquitin is displayed on the left as a cartoon (pale blue). The residues used for canonical chain formation (lysines and N-terminus) are shown in ball-and-stick format. The surface of ubiquitin is displayed on the right, with the hydrophobic ubiquitin patches illustrated with different colours: Ile44, orange; Ile36, cyan; Phe4, red.

With dozens of lysines in target proteins and eight acceptor residues per ubiquitin, there is potential for the ubiquitin code to become highly complex. Monoubiquitination and polyubiquitination with homologous chains are often referred to as canonical ubiquitination, however atypical polyubiquitination with a variety of forms has also been described. Firstly, heterotypic ubiquitin chains whereby an existing linkage contains another ubiquitin linkage either through a branch or, as in the case of K63-M1, the addition of a different linkage. Heterotypic K11-K48 and K63-M1 chains have been identified and in the case of K63-M1 chains are important in innate immune signaling [16]. Secondly, there is non-canonical ubiquitin conjugation: E3 ligases have been described that attach the C-terminal glycine to serines or threonines through an oxyester rather than an (iso)peptide bond, and the resulting monoubiquitin is then extended with a canonical chain [8]. Lastly, apart from proteins lipids have been described to become ubiquitinated, also through an oxyester bond [5]. This illustrates that the ubiquitin code creates highly complicated signaling and therefore requires a plethora of proteins capable of recognizing these signals and differentiating them from one another.

1.4. The readers of the ubiquitin code: ubiquitin-binding domains

This complicated ubiquitin code requires proteins which can identify ubiquitin chains and translate them into signaling effectors. The architecture of these readers includes ubiquitin-binding domains (UBDs): domains capable of binding ubiquitin via transient, non-covalent interactions through one or more of the aforementioned hydrophobic patches [17, 18]. Highly conserved UBD families point at the significance of the ubiquitin code.

UBDs vary greatly in regard to their structure and the mechanisms they employ to bind different mono- or polyubiquitin conjugates. Proteins may possess one or multiple UBDs in tandem to facilitate binding. One such example are the Ubiquitin-Interacting Motifs of Arsenite Inducible RNA-Associated Protein-Like proteins that bind K48 chains [19]. UBDs can bind one or more ubiquitin moieties simultaneously through hydrophobic-interactions with the Ile44 patch of ubiquitin. Some UBDs bind polyubiquitin in a linkage-specific manner. Additional contacts with the Phe4 and Ile36 patches allow UBDs to recognize the orientation of the distal and proximal ubiquitin to one another, thereby restricting binding to specific linkage types [19, 20].

1.5. The erasers of the code: signal termination

The key in fine-tuned signaling events is regulating not only when the signal is initiated and amplified, but also when it is terminated. Deubiquitinating enzymes (DUBs) are the erasers of the ubiquitin code. With over 100 DUBs in humans, these proteases counteract the ligase activity of the conjugation cascade by cleaving ubiquitin from proteins, whether that is trimming a ubiquitin chain with or without chain specificity or removing mono- or polyubiquitin from target proteins [21]. Their action regulates ubiquitination two-fold; firstly, they counteract E3s and ensure that ubiquitin is not attached or extended indefinitely and secondly, DUBs remove autoubiquitination from

E3s, allowing them to ubiquitinate the desired signaling partners instead of extending autoubiquitinating chains on themselves [22].

1.6. Ubiquitin chains and the M1 code in immunity and inflammation

The complexity, diversity and fine regulation of the ubiquitin chain system allows ubiquitination to act as a signaling effector for a variety of distinct signaling events. Such signaling would be initiated by activation of the E1-E2-E3 cascade, followed by the addition of mono- or polyubiquitin to the target protein. The PTM would subsequently be recognized, leading to the recruitment of downstream signaling factors to the complex and, lastly, the termination of the signal by DUBs and/or the deactivation of the E3 to reduce ubiquitination [23].

A multitude of signaling pathways use different ubiquitin chains at different stages of their cascade to control and coordinate signaling outcomes. By establishing patterns in these cascades the general role of some ubiquitin chain types has been established. For example, K48 chains are the most abundant in cells and serve as a signal for degradation by the 26S proteasome, while K11 chains regulate the cell cycle [24]. K6, K27, K29 and K33 chains remain more elusive, although K6 has been involved in mitophagy and K27, K29 and K33 influence protein aggregation, secretion and trafficking [25-29]. Lastly, K63 and M1 are involved as codes in inflammation and autophagy.

Also known as linear chains, M1 chains are distinct since the C-terminus of the distal ubiquitin is bound not to a lysine, but to residue methionine 1, the N-terminus, of the proximal ubiquitin. The bond between the two ubiquitin moieties is therefore formed with an α- and not an ε-amino-group, making it a peptide bond, naturally restrained in flexibility due to the delocalized nature of its electron pairs. Its flexibility is further diminished compared to the isopeptide bonds of other chain types because, for the latter, the chemical structure of the lysine side chain allows for more movement in relation to the amide backbone. The chemical environment of the peptide bond of M1 chains is also

affected by its proximity to the side chain of M1, ultimately making it unique to this chain type [23, 30].

M1-linked polyubiquitin can adopt an open, linear conformation, with no contact between the hydrophobic patches of moieties, although closed conformations have been reported in solution [14, 31]. On the surface of ubiquitin residue M1 is situated close to K63, only 7Å apart, leading M1 and K63 chains to adopt similar folds. UBDs that recognize one of the two types specifically must therefore take advantage of the aforementioned differences between peptide and isopeptide bonds or ensure a sterical clash with the non-target acceptor residue [20, 32]. Specific mechanisms are discussed later in the thesis (see *The assembly and recognition of M1 chains*). Polyubiquitin binding by M1-specific UBDs is necessary for inflammatory signaling. Inhibiting M1 chain conjugation or abrogating this binding leads to decreased levels of nuclear factor κ-light-chain-enhancer of activated B cells (NF-κB) activation upon immune receptor stimulation, meaning a weakened immune response, and increased levels of induced cell death [33-37]. M1 chains are vital for maintaining the balance between inflammation and apoptosis and details on the enzymes of the M1 code shed light on the molecular details of this balance.

1.7. The assembly and recognition of M1 chains

M1 chains are assembled by the multisubunit E3 ligase linear ubiquitin chain assembly complex (LUBAC), the only ligase known to conjugate M1 chains [38]. LUBAC consists of three subunits: HOIP; heme-oxidized IRP2 ubiquitin ligase 1 (HOIL-1L, also named RBCK1) and Shank-associated RH domain-interacting protein (SHARPIN) in a ratio of 1:1:1, forming monomers of 222 kDa or dimers of 444 kDa, although the apparent weight of the complex is 600 kDa [38-40]. HOIP is the main catalytic component of LUBAC and builds linear ubiquitin chains through its RBR E3 ligase activity. Specificity for M1 linkage is achieved through an extension of the RBR called the Linear ubiquitin chain

Determining Domain (LDD), which binds and orients the proximal ubiquitin so that only the N-terminus is close enough to the catalytic C885 to allow for conjugation to the distal ubiquitin [41]. HOIL-1L is also an E3 RBR ligase, however more recently HOIL-1L has been shown to catalyse atypical oxyester bonds rather than (iso)peptide bonds between ubiquitin moieties [42]. SHARPIN was only later identified as a component of LUBAC and ongoing studies have shown it is necessary for LUBAC's stability and for its recruitment to signal complexes through its NZF domain [39, 43, 44].

The stable assembly of the complex is necessary for the efficient generation of linear ubiquitin as well as inflammatory responses, as shown in deficient or mutated models (see *LUBAC's regulation and its malfunction in disease*). Although HOIP is the E3 that generates linear polyubiquitin, all subunits are necessary to achieve LUBAC's full activity. When isolated from other LUBAC components, HOIP's ubiquitin-associated domains (UBAs) are bound to its RBR region, trapping it in an autoinhibited state [45]. HOIL-1L and SHARPIN bind to HOIP UBA through their UBLs and release HOIP from its inhibitory state, forming the active LUBAC complex [39, 46]. SHARPIN and HOIL-1L further stabilize the complex by associating to one another through their LUBAC-tethering motif domains (LTD) [47].

In addition to LUBAC efficiently conjugating M1 chains, the readers of inflammatory pathways must bind to and specifically recognize them. Two examples of UBD families capable of M1-linkage specificity are Ubiquitin binding in ABIN and NEMO (UBAN) domains and Npl4 (nuclear protein localization 4) zinc fingers (NZF). UBAN domains are coiled-coil homodimers that bind polyubiquitin with a concentration-dependent polyubiquitin:UBD stoichiometry. The UBAN domains of proteins such as Optineurin (OPTN), NF-κB essential modulator (NEMO) or A20-binding inhibitors of NF-κB (ABIN) preferentially bind M1 diubiquitin, with phosphorylation altering the binding affinity to regulate the interaction [48]. Specificity is achieved as the UBAN domain engages the distal and proximal ubiquitin via different patches, namely Ile44 for the former and Phe4

for the later, requiring a polyubiquitin chain with an open conformation for binding [33]. This can correspond to M1 or K63 chains. UBAN domains bind to M1 chains selectively, although they also bind K63 chains with an approximately 100-fold lower affinity [32].

The second UBD family are NZF domains. NZF domains are zinc finger domains capable of binding to mono- or polyubiquitin when they possess a TF/Φ ubiquitin binding motif [49]. Not all NZF domains possess this motif, meaning that not all NZF zinc fingers can bind to ubiquitin. By employing a variety of mechanisms, which are elaborated on in chapter *NZF domains in inflammatory signaling complexes*, some NZF domains can show linkage-specificity in polyubiquitin binding. HOIL-1L binds to M1 chains via its elongated NZF domain. Its NZF core adopts the canonical fold and shows little specificity alone, but possesses an α-helical tail region that increases binding to the proximal ubiquitin of M1 ubiquitin and ultimately leads the NZF to be M1 specific (**Figure 4F**) [50].

1.8. LUBAC's regulation and its malfunction in disease

M1 chains are a vital component of inflammatory signaling and their conjugation by LUBAC must be regulated closely to fulfill their pathophysiological functions. The enzymes OTU domain-containing deubiquitinase with linear linkage specificity (OTULIN) and cylindromatosis (CYLD) are the only DUBs known to cleave linear ubiquitin chains and thereby counteract HOIP's E3 activity, making them the main regulators of M1 chains [51, 52]. OTULIN and CYLD are recruited to and interact with LUBAC through HOIP's peptide:N-glycanase/UBA- or UBX containing proteins (PUB) domain, directly in the case of OTULIN and indirectly through Spermatogenesis-associated protein 2 (SPATA2) for CYLD [53, 54]. Phosphorylation of OTULIN's PUB-interacting motif (PIM) domain disables it from binding HOIP, leading to increased M1 chain conjugation and adding further regulatory steps to this interaction [55]. Disrupting OTULIN's activity or its interaction with HOIP distorts the balance of inflammatory signaling and cell death in the TNF-RSC. A knock-down of OTULIN leads LUBAC to autoubiquitinate and inactivate

itself, while OTULIN knock-out mouse models show diminished expression of HOIP and SHARPIN [22, 56]. Knock-in mice with catalytically inactive OTULIN were also destabilized in assembling LUBAC, indicating that OTULIN is an essential regulator of the M1 code [22].

The vital role of LUBAC and its regulators becomes clear in animal models of LUBAC knock-outs or mutations and clinical cases of LUBAC-related autoimmune diseases. In all instances immune responses are significantly dysregulated, while knocking out one subunit leads to a diminished protein expression for all of LUBAC, possibly due to the destabilization of the complex [57]. Deficiency in HOIP or HOIL-1L leads to embryonic lethality and SHARPIN deficiency causes acute inflammation as found in mouse models [58, 59]. Two clinical cases of HOIP deficiency have been described, one based on an L72P mutation in HOIP's PUB domain and the other on the partial deletion of HOIP's UBA-1 domain through which it binds to SHARPIN [60, 61]. Deletion alleles of *HOIL1* have also been found, along with numerous point mutants, all resulting in different defective immunophenotypes [62-64]. Sharpin-chronic proliferative dermatitis (cpdm) mice are SHARPIN deficient and develop severe inflammation on their skin as well as in internal organs [65]. Due to the destabilization of LUBAC in these mice they are often used as an approximation to a LUBAC knock-out model [44]. The insufficient regulation of LUBAC due to mutations in OTULIN also leads to disease models, labeled OTULIN-related Autoinflammatory Syndrome (ORAS), generally leading to hyperinflammation [66].

1.9. LUBAC's role in inflammation and the innate immune response through tumour necrosis factor signaling

The destructive impact of LUBAC mutants to NF-κB signaling stem from its crucial role in its regulation. NF-κB is a family of transcription factors responsible for regulating inflammation and immunological responses [67]. It is initially induced when harmful

pathogen- or damage-caused factors named PAMPs and DAMPs are recognized by cells of the innate immune system via pattern recognition receptors (PRRs) [68]. This leads to an overall increase of pro-inflammatory signaling, including the secretion of cytokines, chemokines and anti-apoptotic factors as well as the activation of T cells, all aiming to protect the organism from the cause of the inflammation [69]. The recognition of cytokines and chemokines by somatic cells propagates the immune signal. Due to the variety of cells involved with immunity there is a variety of NF-κB-inducing receptor signaling pathways (e.g. Toll-Like Receptor, inflammasome signaling, Interleukin-1, nucleotide-binding oligomerization domain-containing protein (NOD)), but they all hold a similar signaling scaffold [70].

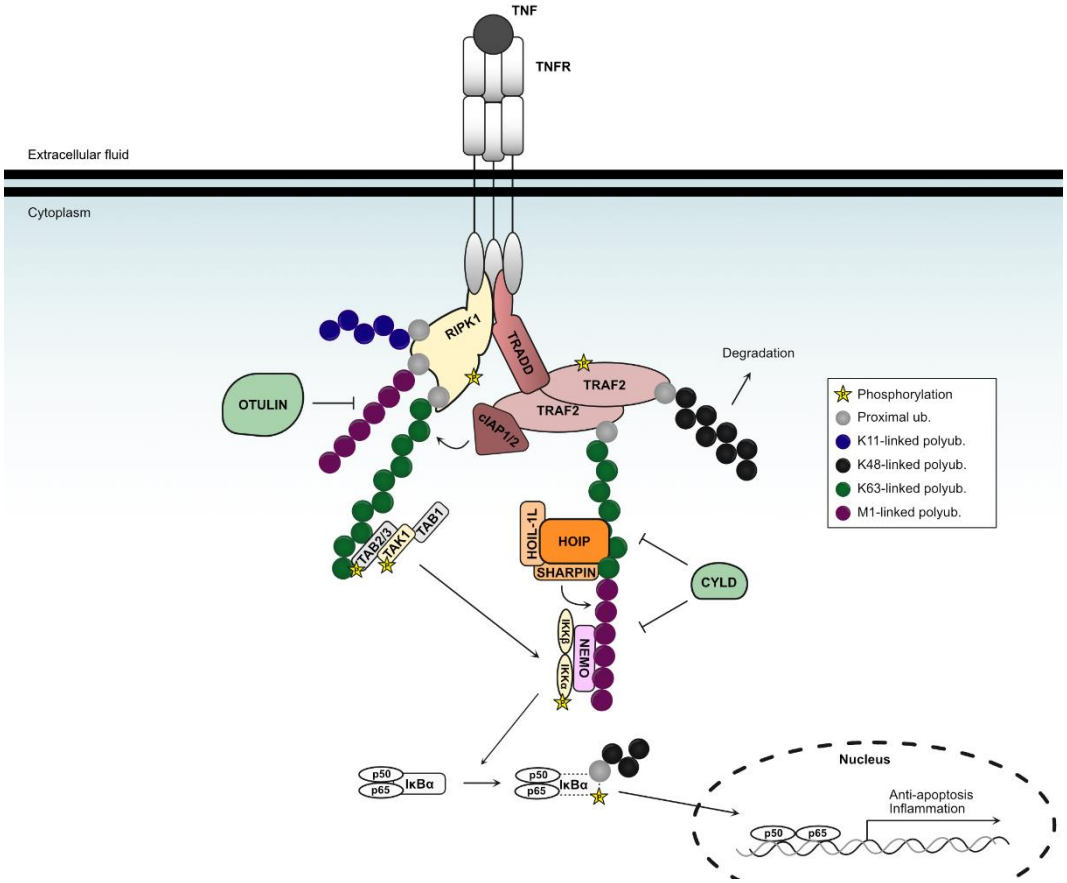


Figure 3: An overview of canonical TNF signaling with an emphasis on linear ubiquitination. Following receptor activation effectors and adaptors (TRADD, RIPK1) are recruited and E3 ligases (cIAP1/2, TRAF2) decorate the complex with ubiquitin chains, leading to the recruitment of further effectors and LUBAC. LUBAC assembles linear ubiquitin chains on the receptor complex, leading to the recruitment of the IKK complex, the liberation of NF-κB and the upregulation of inflammatory and anti-apoptotic genes.

The signaling pathway of Tumour Necrosis Factor (TNF) is a canonical model for inflammatory signaling (**Figure 3**). Upon TNF binding to the TNF receptor (TNFR), the receptor trimerizes and its intracellular death-domain (DD) changes its conformation. This allows for the recruitment of adaptor proteins with similar DDs, such as TNFR1-associated via DD (TRADD). TRADD recruits RIP kinase 1 (RIPK1), as well as TNFR-associated factor 2 (TRAF2), bound by the E3 ligases cellular inhibitor of apoptosis proteins 1 and 2 (cIAP1/2). cIAPs ubiquitinate RIPK1, recruiting the TAK1-TAB complex to the conjugated K63 chains. LUBAC is also recruited to ubiquitin chains, possibly K63. LUBAC then adds linear ubiquitin chains to the TNFR signaling complex (TNF-RSC), using RIPK1 and K63 chains as substrates [35]. NEMO-driven recruitment of the IKK complex to M1 chains places the NEMO-IKK complex in proximity to the TAK1-TAB complex, with TAK1-TAB phosphorylating IKKα, allowing NF-κB to translocate to the nucleus to increase NF-κB transcription and inflammation [70, 71]. M1 chains are therefore necessary signaling platforms for the TNF-RSC to be assembled appropriately and induce pro-inflammatory signals [48].

1.10. NZF domains in inflammatory signaling complexes

NZF, also known as RAN Binding Protein 2 (RanBP2) zinc finger, is a sub-category of zinc finger with the consensus sequence x(4)-W-x-C-x(2)-C-x(3)-N-x(6)-C-x(2)-C-x(5) and a length of approximately 30 amino acids [72]. NZF domains can bind a variety of interaction partners, from single stranded RNA to ubiquitin, depending on whether they possess further consensus sequences withing their NZF fold [49, 72, 73]. For ubiquitin binding this pattern is TF/Φ, where Φ is a hydrophobic residue positioned 10 amino acids C-terminally of the phenylalanine. The affinity to monoubiquitin is usually moderate, with

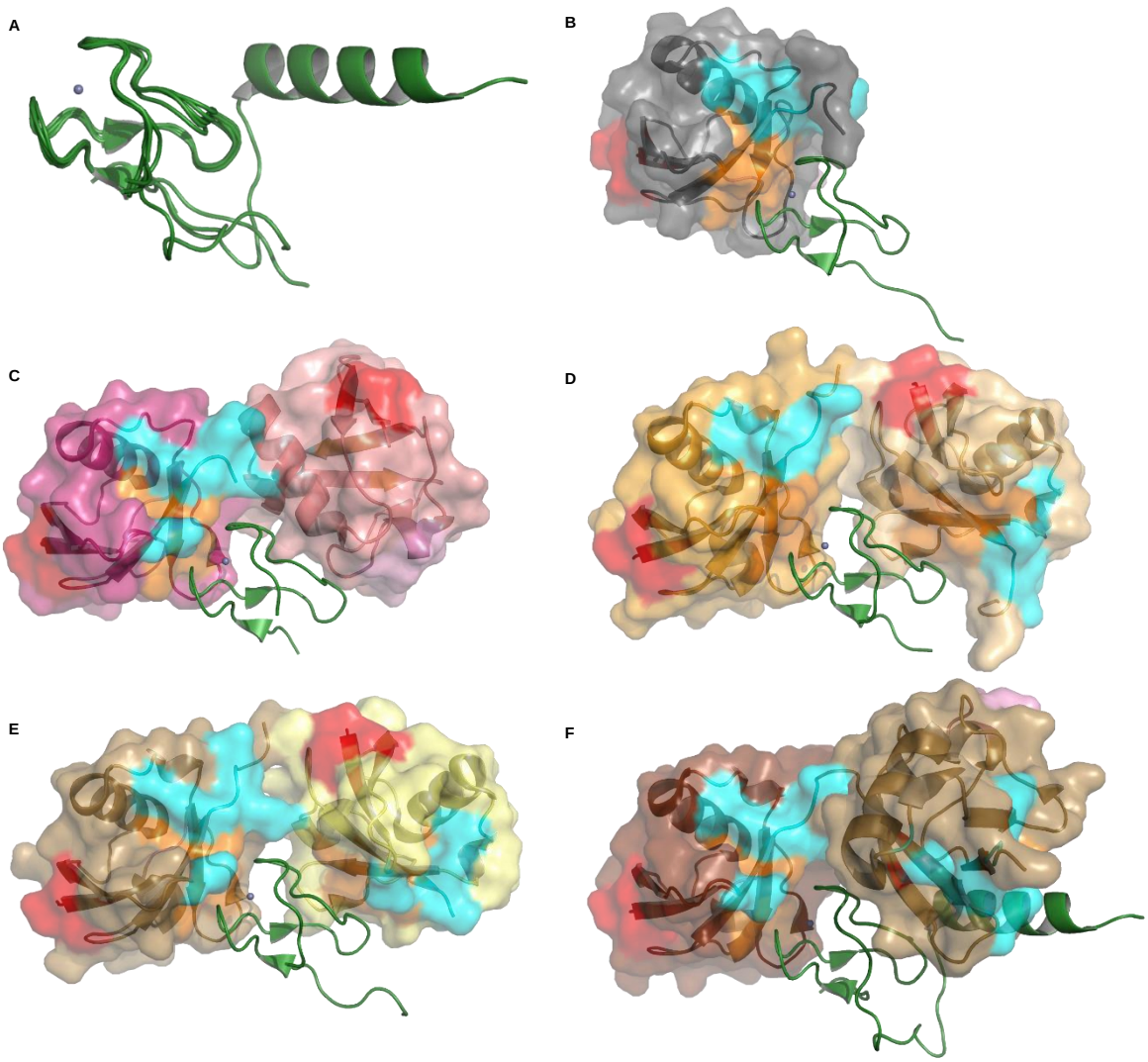


Figure 4: Comparison of NZF structures bound to ubiquitin. (A) Overlay of the structures of Npl4 NZF (PDB: 1Q5W), TRABID NZF1 (PDB: 4S1Z), TAB2 NZF (PDB: 2WWZ), TAB3 NZF (PDB: 3A9K) and HOIL-1L NZF (PDB: 3B08). (B) Structure of monoubiquitin (black surface, hydrophobic patches coloured as in Figure 2) bound to Npl4 NZF (green cartoon) (PDB: 1Q5W) (C) Structure of K29 diubiquitin (distal ubiquitin surface in raspberry, proximal ubiquitin surface in salmon, hydrophobic patches coloured as in Figure 2) bound to TRABID NZF1 (green cartoon) (PDB: 4S1Z) (D) Structure of K63 diubiquitin (distal ubiquitin surface in orange, proximal ubiquitin surface in wheat, hydrophobic patches coloured as in Figure 2) bound to TAB2 NZF (green cartoon) (PDB: 2WWZ) (E) Structure of K63 diubiquitin (distal ubiquitin surface in sand, proximal ubiquitin surface in yellow, hydrophobic patches coloured as in Figure 2) bound to TAB3 NZF (green cartoon) (PDB: 3A9K) (F) Structure of M1 diubiquitin (distal ubiquitin surface in dark brown, proximal ubiquitin surface in olive, hydrophobic patches coloured as in Figure 2) bound to HOIL-1L NZF (green cartoon) (PDB: 3B08).

a K_d of more than 100μM, and mutations to this ubiquitin-binding fold abrogate binding [72]. The canonical NZF of Npl4 binds to monoubiquitin as well as polyubiquitin and interacts with nearly all chain types, except for K6 and K29 [74, 75]. Structural studies reveal that this interaction centers around the domain's TF/Φ binding patch with which it

binds one ubiquitin moiety via its I44 patch (**Figure 4B**). Since it does not bind a second ubiquitin moiety the NZF of Nlp4 cannot differentiate between chain types and therefore does not show specificity [72].

While several NZF domains have not been reported to show specificity, those that do achieve this through different mechanisms. They do so while preserving a similar overall fold for the NZF domain, as shown by the little variation between known ubiquitin-binding NZF structures in **Figure 4A**. All NZF domains with linkage specificity bind the distal ubiquitin moiety via its I44 patch, with an interface similar to the one employed by the NZF of Npl4 to bind monoubiquitin. Specificity arises from the binding of the NZF to the proximal ubiquitin moiety of the chain. In the case of the NZF of TAK1-binding protein 2/3 (TAB2 and TAB3), they interact with K63 diubiquitin, binding both ubiquitin moieties via their Ile44 patch and measuring the spacing between them to recognize the linkage type (**Figure 4D-E**) [20]. The NZF domain of HOIL-1L, in contrast, requires the additional structural element of the NZF α-helical tail region to establish M1 chain preference by binding the Phe4 patch of the proximal ubiquitin (**Figure 4F**). Another interesting model for NZF-based chain specificity is TRAF-binding domain-containing protein (TRABID) binding to K29/K33 chains. TRABID contains three NZF domains in tandem, all of which can bind monoubiquitin [75]. Overall, NZF1 drives polyubiquitin binding and establishes TRABID's K29 and K33 specificity by contacting the proximal ubiquitin via an atypical binding pocket that includes Ub. E24 (**Figure 4C**). NZF2 and NZF3 have been postulated to contribute to TRABID's interaction with polyubiquitin filaments, binding different ubiquitin moieties of the chain, possibly with the same mechanism as NZF1 [74]. The NZF fold is therefore highly versatile in its specificity and crystal structures of NZF·Ub_2 complexes have been crucial in understanding the molecular basis by which this specificity is achieved.

1.11. LUBAC's recruitment to signaling complexes

LUBAC plays a vital role in a large number of inflammatory cascades, but the question remains: ***What is the mechanism underlying LUBAC's recruitment to signaling complexes?***

Initially only HOIP and HOIL-1L were considered necessary for recruitment. Through immunoprecipitation assays using truncated constructs it was shown that the N-termini of both proteins, including their zinc finger and ubiquitin-like (UBL) and/or UBA domains (**Figure 5**), are necessary for recruitment to TNF-RSC [35]. In the case of HOIP this was later narrowed down to NZF1 and NZF2, which bind to ubiquitin chains, preferring long K63 chains over shorter M1 or K48 chains. It should be noted that the affinity of NZF1 and NZF2 to K48, K63 and M1 chains was determined using polyubiquitin of varying lengths as binding substrates, namely M1 tetraubiquitin and the pooled products of K48 and K63 assembly reactions, thereby disregarding the importance of avidity effects in binding to longer chains for K48 and K63 linkages [35]. The T360A mutation to the NZF ubiquitin-binding motif of NZF1 abolished the interaction with these chains and, importantly, recruitment to the TNF-RSC, meaning that it is directly binding to ubiquitin and not to another signaling effector that dictates LUBAC's involvement with this cascade [76]. HOIP T360A also abrogated the recruitment of LUBAC to cytosol-invading bacteria, confirming the vital role of HOIP NZF1 in LUBAC recruitment [77]. HOIL-1L's NZF is the component responsible for ubiquitin chain binding in HOIL-1L, as dictated by its preference for M1 chains [43]. The model of recruitment to K63 chains was supported upon studying the NZF module of SHARPIN. It binds K63 and M1 chains with similar affinities and its removal or replacement with the M1-specific HOIL-1L NZF led to TNF-α induced cell death. It was therefore determined that ability of the NZF of SHARPIN to bind K63 chains, rather than M1, allowed for LUBAC recruitment to and stabilization of TNF-RSC [43, 44].

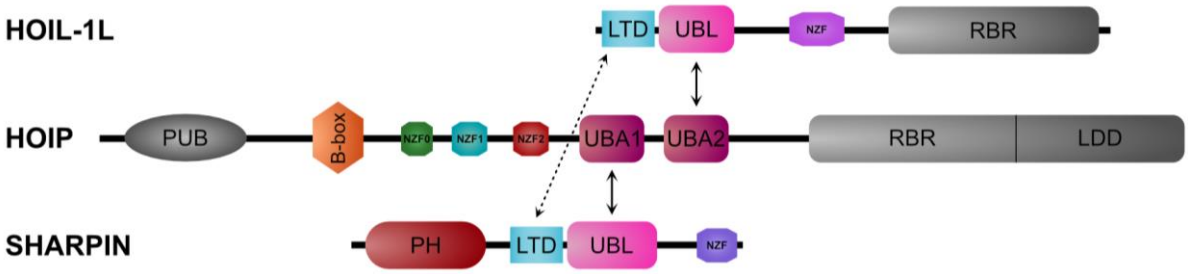


Figure 5: Graphic illustration of HOIP, HOIL-1L and SHARPIN and their domains. Arrows indicate that these domains interact. Abbreviations: LTD Lubac Tethering Domain, UBL Ubiquitin-like domain, NZF nuclear protein localisation 4 (Npl4) zinc finger, RBR RING-Between-RING, RING Really Interesting New Gene, PUB peptide:N-glycanase/UBA- or UBX containing proteins, B-box B-box-type zinc finger, UBA ubiquitin associated domain, LDD linear ubiquitin chains determining domain, PH pleckstrin homology.

Interestingly, Noad et al. established that the removal of HOIP's linear ubiquitin conjugating domain also negatively affected recruitment. They interpreted this, together with the NZF domains' ability to bind M1 chains, as a feed-forward mechanism; upon LUBAC recruitment to K63 chains on signaling complexes, LUBAC creates M1 chains to which it is then itself recruited to increase signal intensity [77]. While this is an interesting model for LUBAC recruitment, further studies on LUBAC's ubiquitin binding abilities are necessary to provide quantitative rather than qualitative insight on these interactions, allowing us to answer the question of LUBAC recruitment.

1.12. HOIP's zinc finger domains as a potential recruitment center for LUBAC

Among LUBAC's components and their domains, HOIP's N-terminal domains and particularly NZF1 are indispensable for the recruitment to signaling complexes. The study of these domains could therefore be the key in determining the answer of HOIP and LUBAC recruitment.

HOIP consists of the N-terminal PUB domain, which is vital for interaction with and regulation by DUBs, followed by a B-box-type zinc finger, three RanBP2 type zinc fingers, two of which are annotated as NZF domains, and two UBA domains for the

recruitment of HOIL-1L and SHARPIN and subsequent LUBAC assembly. The catalytic E3 RBR domain is found C-terminally and is responsible for the generation of linear ubiquitin chains with the help of its LDD extension (**Figure 5**) [23].

The C-terminus, including the UBA domains and catalytic center, only dictates LUBAC's recruitment indirectly in the context of the incomplete assembly of the complex or the feed-forward mechanism described above. Mutational studies on these domains have not shown an effect in LUBAC's binding to K63 chains to initiate the recruitment. Our attention is therefore turned to the N-terminus for answers to the question of recruitment. Even though the PUB domain has been carefully studied in its interaction with DUBs, no direct binding has been reported between HOIP PUB and ubiquitin chains [53, 78]. The remaining candidate is therefore the poorly studied region of HOIP that is comprised of its zinc fingers.

B-box domains are cysteine-rich zinc fingers that coordinate two zinc atoms per fold [79]. The B-box module in HOIP was described in the first paper published on the protein and has since been largely misannotated and partially postulated to be involved in HOIP's dimerization [53]. An unpublished structure of HOIP's B-box domain from the Elliott Lab displays its ability to dimerize, and highlights a key residue, L219, in the dimer interface. The functional effect of the dimerization and generally of the B-box remains unknown, although recently an interaction between HOIP B-box and CARD-containing MAGUK protein 1 (CARMA1) was reported [78].

The RanBP2 type zinc fingers of HOIP were first identified in 2004 [80]. They were later separated into RanBP2-zf (here Zf, aa 299-329) and two NZF domains (aa 350-379 and 409-438). It should be noted that RanBP2-zf and NZF are alternate names for zinc fingers with the NZF fold and consensus sequence [38, 72]. Nevertheless, nothing is known about the physiological role of Zf and studies have focused on NZF1 and NZF2.

NZF1, as mentioned in previous chapters, presents the NZF ubiquitin-binding fold through residues T360, F361 and I372. It binds to K63 and M1 chains with comparable affinity, followed by K48 linkages [35, 44]. NZF1 T360A is unable to bind ubiquitin and

abolishes LUBAC's recruitment to TNF receptor complexes [77]. NZF1 is further able to bind to NEMO CoZi (coil-zipper) domain in a low affinity interaction via a highly conserved patch in NZF1 [76]. The crystal structure of the NZF1·NEMO complex points at conserved residue R375 of the interface, the R375A mutation of which hinders NEMO binding but does not fully abolish ubiquitin binding, placing NEMO recruitment downstream of LUBAC recruitment to TNF-RSC. Reciprocally, the T360A mutant does not abolish NEMO binding, thereby uncoupling the two binding events and illustrating that NZF1 is capable of binding NEMO and ubiquitin simultaneously [76]. It is unknown whether the interaction with NEMO is specific only for this UBAN domain. Other downstream effectors of inflammatory signaling, such as OPTN and ABINs, are known to interact with linear ubiquitin, much like NEMO, and also possess UBAN domains.

NZF1 is followed by NZF2, with a linked region of approximately 30 amino acids between them. This linker region contains an uncharacterized phosphorylation site S383 [81]. NZF2 also presents a ubiquitin-binding motif through residues T419, F420 and M431. Though it was initially thought to not bind to ubiquitin, in affinity experiments using an NZF1-NZF2 T360A construct, where NZF2 is the only domain theoretically able to bind ubiquitin, weak binding to diubiquitin was measured, with binding to K63 and M1 being slightly stronger [44, 77]. This showed that NZF2 could possibly bind to ubiquitin after all, but no signaling effects of such binding have been investigated.

1.13. Aims of this thesis

LUBAC is an essential effector of inflammatory signaling and its activity determines the balance between inflammation and cell death in innate immunity. Even though LUBAC's catalytic activity through its subunit HOIP is well described and as the regulation of this activity through DUBs and PTMs gains more detail, little information is known about how LUBAC is recruited to signaling complexes in order to decorate them with M1 chains. Answering this question is imperative in understanding how the TNF-RSC and other

inflammatory signaling complexes are assembled, how LUBAC's recruitment stabilizes them and prevents cell death and how this interaction fails in autoimmune disease models. Previous studies on LUBAC's recruitment to the TNF-RSC illustrate the vital role of HOIP and more specifically the domain NZF1 in the recruitment to complexes. However, various questions remain open in order to establish a detailed mechanism of this recruitment. Towards this end and specifically regarding LUBAC recruitment, the poorly studied zinc finger domains of HOIP display numerous interesting features that can be studied.

Firstly, biophysical studies need to establish the binding of ubiquitin chains to the NZF domains unequivocally and provide a detailed mechanism of how the NZF domains achieve linkage specificity. Such studies must be completed not only for individual units, as performed previously for NZF1, but using a combination of all ubiquitin-binding domains in order to determine each domain's contribution to the recruitment. The binding mechanism, coupled with affinity measurements, would aid in locating HOIP and LUBAC's designated recruitment partner.

Secondly, further insight are needed into how interaction with signaling partners such as NEMO or novel interactions for the zinc finger domains interfere with this affinity for ubiquitin chains to promote or deter recruitment and whether upstream and downstream signaling are fully uncoupled for HOIP. This question has not been approached previously using biophysical studies. Therefore, the interplay between ubiquitin and signaling partner binding needs to be examined for us to understand this double function of HOIP's zinc finger domains.

Furthermore, to characterize the recruitment model in more detail, possible regulatory mechanisms, for example phosphorylation in the uncharacterized site S383, need to be studied further and assessed regarding their effect on HOIP's affinity and specificity for ubiquitin chains. By determining these finer details of LUBAC's recruitment our understanding of this complex mechanism can be solidified. Lastly, it is vital to examine

the until now hypothesized oligomeric state of HOIP and determine how dimerization affects complex recruitment and, possibly, activity.

This thesis will attempt to answer these questions using a unified structural, biophysical and biochemical approach to determine a holistic model of the role of HOIP's zinc finger domains in LUBAC recruitment. It will first investigate the interaction of HOIP zinc fingers with monoubiquitin, to determine the domains responsible for ubiquitin chain binding and establish a molecular model for their interaction with ubiquitin moieties. This model will then be expanded with information on linkage-specific polyubiquitin and how its binding differs among domains and among chain types to monoubiquitin binding, resulting in HOIP's overall chain specificity. Lastly, the effect of dimerization, of post-translational modifications and of the interaction with signaling partners will be established in order to discover possible regulatory mechanisms and form a more global picture of the recruitment of HOIP to signaling complexes.

2. Materials and Methods

2.1. Sequence analysis

Multiple sequence alignment of HOIP orthologues from the Ensemble database (**Figure 7**) was performed using Clustal Omega and processed with Jalview [82]. The Ensemble accession numbers and species abbreviations are as follows: human (*homo sapiens*, ENSP00000315112), cow (*Bos taurus*, ENSBTAP00000053642), gorilla (*Gorilla gorilla gorilla*, ENSGGOP00000015643), gibbon (*Nomascus leucogenys*, ENSNLEP00000018559), rat (*Rattus norvegicus*, ENSRNOP00000026333), mouse (*Mus musculus*, ENSMUSP00000019443), zebrafish (*Danio rerio*, ENSDARP00000109107), coelacanth (*Latimeria chalumnae*, ENSLACP00000001666), tropical clawed frog (*Xenopus tropicalis*, ENSXETP00000031992). The Consurf server (https://consurf.tau.ac.il/) was used in calculating the conservation and mapping the values on the existing structure of the HOIP NZF1·NEMO CoZi peptide complex (PDB: 4OWF).

2.2. Molecular biology

The majority of plasmids encoding the constructs of interest were prepared by Dr. Paul Elliott using a pOPINS backbone, which provides kanamycin resistance and further includes an inducible T7 promoter and an N-terminal His_6-SUMO tag, with two plasmids generated by myself (HOIP aa 215-451 wild-type and L219R). The constructs were generated as described previously (see HOIP PUB domain construct, [23]) using Q5 High-Fidelity Polymerase and the following primers:

HOIP-215-Fwd GCGAACAGATCGGTGGTGGTCCTTGCTTCCTGTGCGGT for the wild-type, HOIP-215-L219R

GCGAACAGATCGGTGGTGGTCCTTGCTTCAGATGCGGTTCCGCTCCTG for L219R and HOIP-451-Rev ATGGTCTAGAAAGCTTTATTAGGAGCTAGCGTAAGGACGGGG. The PCR products were cloned into a pOPINS vector. An overview of the constructs used in this thesis can be found in **Figure 6**.

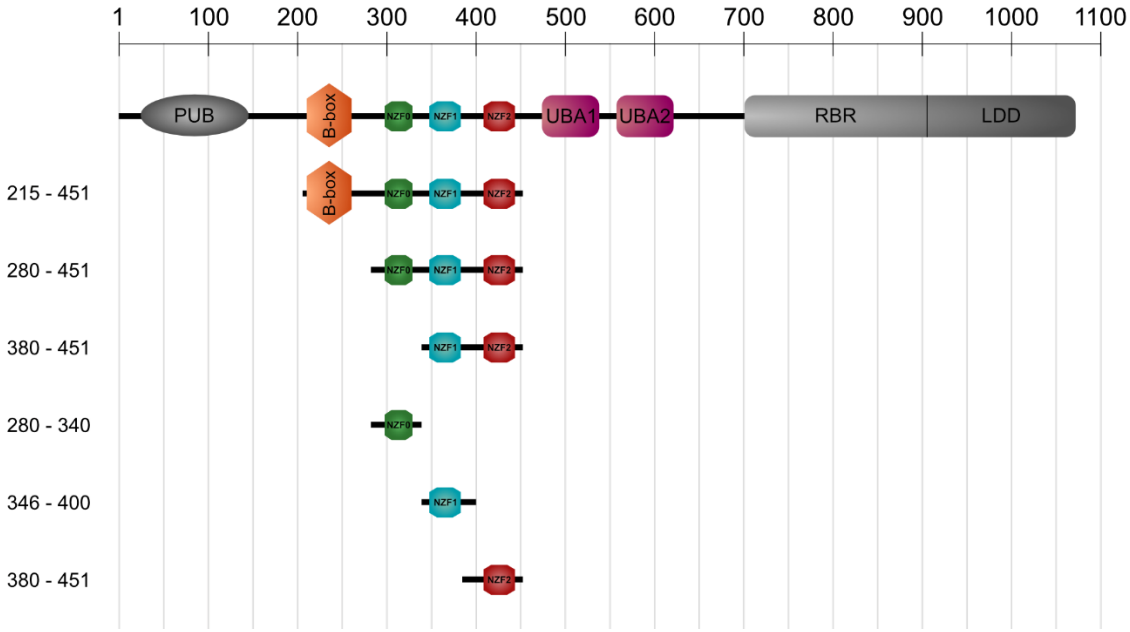


Figure 6: Graphic illustration of HOIP's domains and the constructs used in this thesis. Abbreviations: PUB peptide:N-glycanase/UBA- or UBX containing proteins, B-box B-box-type zinc finger, NZF nuclear protein localisation 4 (Npl4) zinc finger, UBA ubiquitin associated domain, RBR RING-Between-RING, RING Really Interesting New Gene, LDD linear ubiquitin chains determining domain.

2.3. Recombinant protein expression and purification

In order to conduct experiments using a protein of interest, it is vital to determine how to obtain large and pure amounts of the protein by using cell systems, usually mammalian, insect or bacterial, to express the protein. We proceeded with a bacterial expression system, known for its simple culture conditions, potential for high yields and suitability for isotopic labelling for NMR. Monoubiquitin was expressed in Rosetta2 (DE3) cells and purified as described previously [83]. Ubiquitin chains were assembled from purified monoubiquitin as described previously [83]. In summary, purified monoubiquitin was incubated with mouse E1 and a linkage-specific E2 enzyme in the presence of ATP. The

reaction was stopped after 3 hours and the products were separated using cation exchange chromatography (Resource S cation exchange chromatography column, cytiva, cation exchange buffer 50 mM sodium acetate pH 4.5), with polyubiquitin of increasing length being eluted at higher salt concentrations (**Supplementary Figure 22**). The fractions of distinct polyubiquitin species were pooled, concentrated and further separated using size-exclusion chromatography (Superdex 75 10/300, GE Life Sciences, buffer consisted of 20 mM Tris pH 7.5, 150 mM NaCl). They were finally concentrated and flash-frozen.

All constructs mentioned in this thesis were expressed and purified by myself, with the exception of constructs derived from TRAF6 and nuclear dot protein 52 kDa (NDP52), which were prepared by Dr. Paul Elliott, and ABIN2 UBAN domain, which was purified by Maribel Schönewolff. Protein constructs were expressed in Rosetta2 (DE3) cells and grown at 30 °C in medium supplemented with 34 µg/mL chloramphenicol and 30 µg/mL kanamycin. 2xYT medium was used for biophysical assays and crystallization constructs, while 2M9 medium supplemented with 1 g $^{15}NH_4Cl$ or 1 g $^{15}NH_4Cl$ and 2.5 g ^{13}C glucose was used for NMR studies. Upon reaching an OD600 of 0.8 the cells were cooled to 18 °C and induced overnight with 400 µM IPTG and 100 µM $ZnSO_4$. They were harvested by centrifugation, resuspended and lysed by sonication in lysis buffer. All constructs were purified by gravity flow metal affinity chromatography using Ni-NTA Agarose (QIAGEN) and a previously described protocol. The eluate was subsequently dialysed overnight into anion exchange chromatography buffer (20 mM Tris pH 8.0, 4 mM DTT). The constructs were purified using anion exchange chromatography (Resource Q anion exchange chromatography column, cytiva) and the His_6-SUMO-tag of the pooled fractions was cleaved with SUMO protease overnight. Further purification of the target protein was achieved through another use of anion exchange chromatography, followed by size-exclusion chromatography (Superdex 75 10/300, GE Life Sciences, buffer consisted of 20 mM Tris pH 7.5, 150 mM NaCl, 4 mM DTT). The purity of the fractions was assessed by SDS-PAGE analysis and found to be higher than

95%. Exemplary SDS-PAGE gels of each purified construct can be found in the Appendix (**Supplementary Figure 22**). The proteins were concentrated and flash-frozen.

2.4. Nuclear Magnetic Resonance (NMR) spectroscopy and backbone assignment theory

Atoms with an odd number of neutrons and/or protons have a nuclear spin, which describes their ability to interact with magnetic fields and occupy different energy states. By exposing such atoms to a constant, high strength magnetic field of a spectrometer their spins orient themselves to this field (e.g. along spatial axis z). Introducing a second, oscillating field, (e.g. along spatial axis y) will change their orientation towards the magnetic field, and the removal of the second field will force them to relax back to their initial orientation to the spectrometer's field in axis z. This relaxation is detected as a signal called the Free Induction Decay (FID). The FID of an atom is dependent on its chemical environment, leading different atoms to have different FID signals. By Fourier transforming FIDs the frequencies can be measured and registered as a unique signal for the atom studied [84]. By introducing different atom types more FIDs can be measured, adding further dimensions to the measurements. Some atoms commonly used in protein NMR are ^{1}H, ^{15}N and ^{13}C, offering at least three dimensions to conduct experiments in by ensuring these heavier atom isotopes for N and C are incorporated into the protein of interest. Considering the amide group of an amino acid contains both ^{1}H and ^{15}N and that each amino acid has its own chemical environment, 2D ^{1}H-^{15}N spectra provide the "protein fingerprint" where each residue can be seen as an individual peak. The interaction with a ligand can further affect the chemical surroundings, leading the signals and therefore the position of the peaks of the interacting amino acids to shift, making NMR a powerful tool to study protein interactions [85].

To identify which specific amino acid corresponds to every peak 3D experiments are necessary, requiring the incorporation of a further isotope, namely ^{13}C. The carbon atoms relevant to 3D NMR are CO, meaning the carbonyl, the C_α of the amino acid backbone and the C_β of the side chain. More and less sensitive experiments are used in combination to detect the CO, C_α and C_β signal of the preceding (i-1) and the observed (i) amino acid, allowing for pairs of sequential amino acids to be identified until the entire sequence is mapped. This is named a “sequential walk” or “backbone assignment”. Although HNCO/HNCACO backbone assignment, meaning an assignment that correlates only the carbonyl signal between two sequentially adjacent amino acids, is a good start for a sequential walk, the chemical environment of CO atoms does not vary enough for there to only be one certain match for an amino acid pairing. HN(CO)CACB/HNCACB experiments detect the C_α and C_β atoms of the previous residue (i-1) and of both the current and previous residue (i, i-1) respectively and can be used along with HNCO/HNCACO experiments to provide solid matches between amino acid pairs. Together with the characteristic C_α and C_β pattern of certain amino acids (for example glycine, serine, threonine, alanine), amino acids can be ordered sequentially and then backbone assigned by recognizing these key amino acids and the spacing between them in the protein sequence. Therefore, interesting interactions with signaling partners and shifts observed in a 2D spectrum can be traced to specific, backbone-assigned residues, a characteristic unique to NMR.

2.5. NMR sample preparation and data acquisition

Purification was carried out as stated above and all samples were exchanged to NMR buffer (20 mM Tris pH 7.5, 150 mM NaCl, 4 mM DTT) and supplemented with 5% D_2O (v/v) prior to measurement. Data acquisition was performed at 25 ˚C on a Bruker BioSpin 600MHz Avance III HD spectrometer with a 5 mM TCl cryoprobe. Samples were typically measured at a concentration of 100 µM and a volume of 600 µL, while the 3D sample of

NZF1-NZF2 (^{13}C, ^{15}N HOIP aa 346-451) was measured at 350 µL of 270 µM. In titration experiments the titrant was mixed with the labelled protein, originally at 100 µM, to achieve the desired molar ratio between the labelled protein and titrant. In titration series increasing amounts of titrant were added to the mixture at each titration point. Heteronuclear Nuclear Overhauser Effect (NOE) experiments to determine construct flexibility were carried out as described previously using a ^{1}H saturation time of 3 s [86]. Titration experiments were completed using the BEST-TROSY method, while the assignment of backbone resonances of HOIP was completed using BEST-TROSY triple resonance experiments (HNCA, HN(CO)CA, HNCO, CBCA(CO)NH, HNCACB) [87]. The spectra were collected using 25% non-uniform sampling (NUS) to minimize sample collection time while ensuring good spectral resolution [93]. In NUS not all points of the FID are collected, but rather enough to enable in silico reconstitution of the full FID. Data processing and analysis were carried out using Topspin 3.2 (Bruker), NMRPipe (https://www.ibbr.umd.edu/nmrpipe/install.html) and CCPN Analysis V2.4 and V3 software to visualize the processed spectra. NMRPipe is a multidimensional NMR data processing software, which allows for phase adjustment, NUS reconstruction and for the conversion of the measured spectrometer data to FIDs and their Fourier transform, resulting in 2D projections of the 3D spectra, displayable in CCPN Analysis.

2.6. Multi-angle light scattering (MALS)

SEC-MALS (size-exclusion chromatography combined with MALS) is a technique to determine the absolute molar mass of a protein in solution. After being separated in a SEC column, the different species are run through a light scattering detector, which determines the molecular weight of the individual SEC peaks by measuring the intensity of the scattered light. When comparing the absolute molar mass to the molecular weight of a construct, its oligomeric state can be determined [88, 89].

The molar mass of HOIP B-box-NZF0-NZF1-NZF2 (aa 215-451) and its mutant constructs (L219D, L219I, L219R, L219Y) were determined by SEC-MALS using a Superdex 75 10/300 column (GE Life Sciences) in combination with a Wyatt Heleos 8+ angle light scattering instrument and a T-rEX refractive index detector. Protein samples (110 µL of 1 mg/mL and 3 mg/mL) were loaded at 500 µL/min in SEC-MALS buffer (20 mM Tris pH 8.5, 150 mM NaCl, 2 mM TCEP). The differential refractive index applied for all calculations was 0.186 RI per 1 g/mL. The observed molecular weight is lower than that of a pure dimer due to the partial dissociation of the dimer. For SEC-MALS measurements an error of 10% is assumed.

2.7. Isothermal Titration Calorimetry (ITC)

ITC is a biophysical method to determine the thermodynamic parameters of the interaction of two molecules. At a constant temperature one partner remains in the same concentration while its interaction partner is titrated in small, finite increments of time and concentration. The production or loss of heat upon addition of the second molecule is measured and fitted to establish parameters such as the enthalpy, entropy and K_d of the reaction [90, 91].

A Malvern PEAQ-ITC microcalorimeter was used to perform the experiments. All constructs were exchanged to ITC buffer (20 mM HEPES pH 7.5, 100 mM NaCl, 2 mM TCEP) prior to measurement to minimize heat changes due to buffer inconsistencies. 300 µL of HOIP constructs in concentrations between 40 µM and 300 µM (see **Table 1**) were placed in the sample cell while interaction partners such as ubiquitin, ubiquitin chains and other protein constructs were titrated in with injection volumes of 3 µL and equilibration pauses of 120s, again in varying concentrations. The monoubiquitin and ubiquitin chains were purified as described in chapter 2.3. and their purity was assessed by SDS-PAGE analysis.

Table 1: Concentrations and repeats of all ITC experiments studied in this thesis. Constructs and their mutants correspond to those illustrated in Figure 6. The total repetitions for each experiment are mentioned only if they are greater than one.

Cell construct	Cell concentration (μM) (repeats)	Syringe protein	Syringe concentration (mM) (total repeats)
NZF1	80 (3)	Monoub.	2 (3)
	40, 80	K48 diub.	1 (2)
	40, 80	K63 diub.	1 (2)
NZF2	150 (2), 300 (1)	Monoub.	3 (1), 4 (2)
	300	K48 diub.	1.8
	300	K63 diub.	1.83
NZF1-NZF2	80 (2)	Monoub.	2 (2)
	70, 80	K48 diub.	1 (2)
	40, 80	K63 diub.	1 (2)
	40	K63 long chains	0.8
NZF1-NZF2 T360A	150	Monoub.	4
	150	K48 diub.	1.8
	150	K63 diub.	1.83
NZF1-NZF2 T419A	150	Monoub.	4
	80	K48 diub.	1
	80	K63 diub.	1
NZF1-NZF2 S383E	70	K48 diub.	1
	40	K63 diub.	1
NZF1-NZF2 R375A	80	Monoub.	2
B-box-NZF0-NZF1-NZF2	40	K63 long chains	0.8
B-box-NZF0-NZF1-NZF2 L219R	40	K63 long chains	0.8

2.8. Crystallization

In supersaturated solutions and under distinct conditions such as temperature, salt concentration and pH, proteins have the ability to form ordered crystals. Upon illumination with X-ray beams, the crystal's atoms scatter the X-rays and, due to their ordered nature, produce unique diffraction patterns. Because these patterns stem from the positioning of the atoms in the crystal, it is possible to use mathematical operations to reconstruct the electron density of the protein from which the diffraction pattern was collected. The 3D modelling of this electron density can be evaluated and possibly provide a structure model for the crystallized protein.

The construct selected for crystallization was the HOIP NZF1-NZF2 domains (aa 350-438) mixed with a 1.2 molar excess of K63 diubiquitin and, in separate experiments, K63 triubiquitin. The method used was sitting drop diffusion, in which the peptide complex was mixed with the equivalent volume of reservoir.

3. Results

3.1. HOIP's zinc finger domains are highly conserved and fold independently of one another

Initially the zinc finger domains were studied regarding their conservation across ubiquitinating organisms with the exception of yeast, which does not possess an orthologue of HOIP. HOIP is present as far back as Drosophila, under the name LUBEL, although LUBEL shows significant differences to HOIP in its domain architecture.

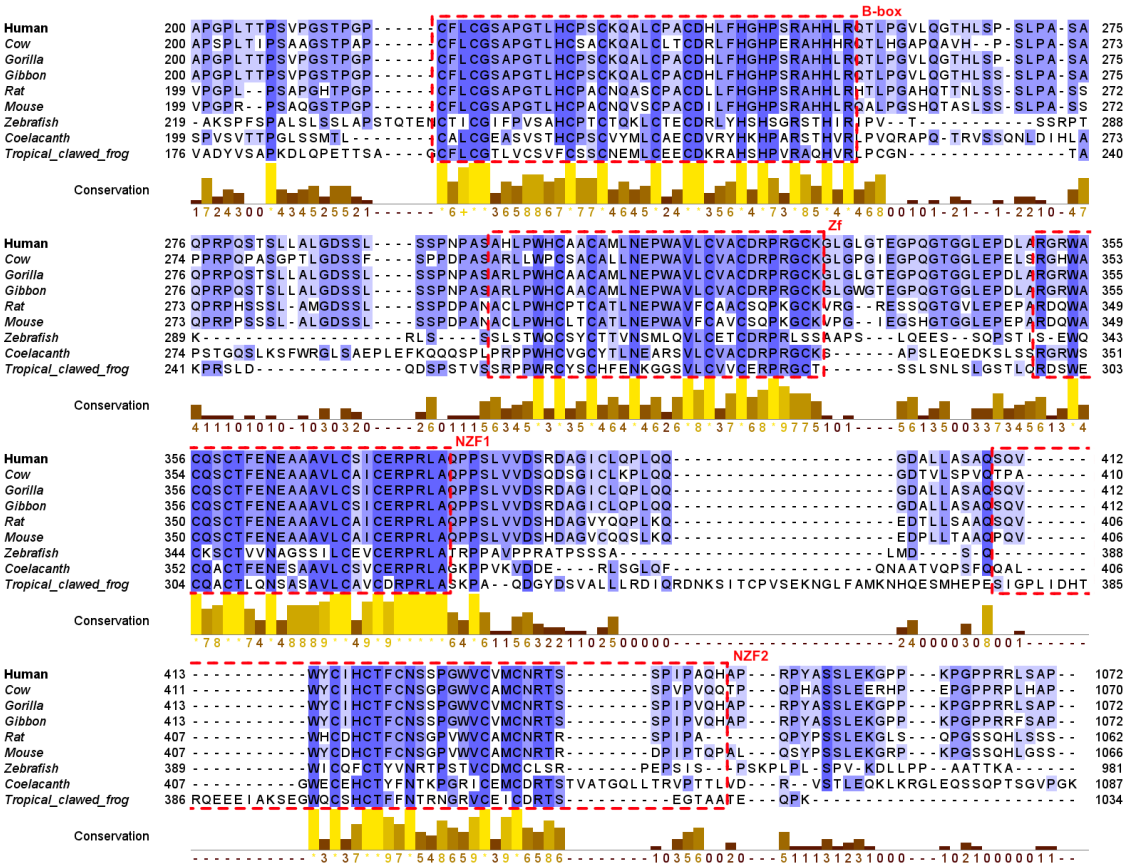


Figure 7: Sequence alignment for the extended zinc finger domains of HOIP (aa 200-468) across the orthologues human *(homo sapiens)*, cow *(Bos taurus)*, gorilla *(Gorilla gorilla gorilla)*, gibbon *(Nomascus leucogenys)*, rat *(Rattus norvegicus)*, mouse *(Mus musculus)*, zebrafish *(Danio rerio)*, coelacanth *(Latimeria chalumnae)* and tropical clawed frog *(Xenopus tropicalis)*. Conservation is mapped below each sequence and more highly conserved residues are coloured in deep blue. The domains B-box, Zf, NZF1 and NZF2 are framed in a red box.

The curated sequences of the zinc finger domains of prototypical organisms can be seen

in **Figure 7**, with highly conserved residues coloured according to identity percentage. The domains, as annotated by previous publications or identified by homology in Uniprot, are highly conserved, especially the domain consensus sequences (e.g. NZF, B-box type I etc.) and particularly NZF1 [38, 92]. They are separated by less conserved linker regions of varying length.

These domains are therefore highly conserved across organisms except for yeast. As a foundation for the subsequent structural and biophysical studies, it was vital to investigate the fold of these domains in relation to one another, namely whether they show cooperativity in folding or whether they can be studied independently of one another. 2D NMR is the most effective way to study such an effect in folding since it provides information on the chemical environment of each amino acid and therefore how this environment may change if the domain fold is altered, for example through cooperative folding. ^{1}H-^{15}N spectra were collected for each protein fragment, so that each amino acid is present as a definite point or “peak” on the spectrum. This can also be called the “protein fingerprint” of the construct. Such spectra were collected for individual domains and then for constructs that include more than one domains, until the entire studied region was included in the final construct. All constructs provided well-defined 2D spectra with little to no overlap within a construct’s peaks. Overlaying these spectra as in **Figure 8** (**Supplementary Figure 1**) shows a clear overlap of the peaks in the protein fingerprint of individual domains and of longer constructs. This indicates that the amino acids have a highly similar chemical environment regardless of whether other domains are present, meaning they fold independently of one another, much like beads on a string, and therefore likely function as independent domains.

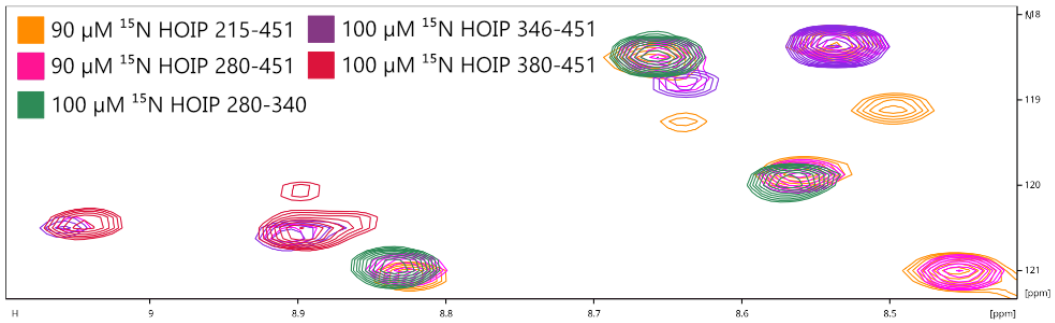


Figure 8: BEST-TROSY spectra of ^{15}N-labelled HOIP constructs B-box-Zf-NZF1-NZF2 (aa 215-451, orange), Zf-NZF1-NZF2 (aa 280-451, pink), Zf (aa 280-340, green), NZF1-NZF2 (aa 346-451, purple) and NZF2 (aa 380-451, red), showing overlapping peaks for spectra with overlapping regions. Full spectra can be found in Supplementary Figure 1.

3.2. The Zf domain is a misannotated NZF that does not bind ubiquitin

As stated previously, NZF domains are equivalent to RanBP2 type zinc fingers and both possess the consensus sequence x(4)-W-x-C-x(2)-C-x(3)-N-x(6)-C-x(2)-C-x(5) [72]. When they possess the additional motif TF/Φ they are able to bind ubiquitin through its Ile44 patch [49]. HOIP's Zf was first identified together with NZF1 and NZF2 as a RanBP2 type zinc finger and was then isolated as a non-NZF RanBP2 type Zf some years later [38, 92].

The amino acid sequences of these three zinc fingers was aligned with the prototypical

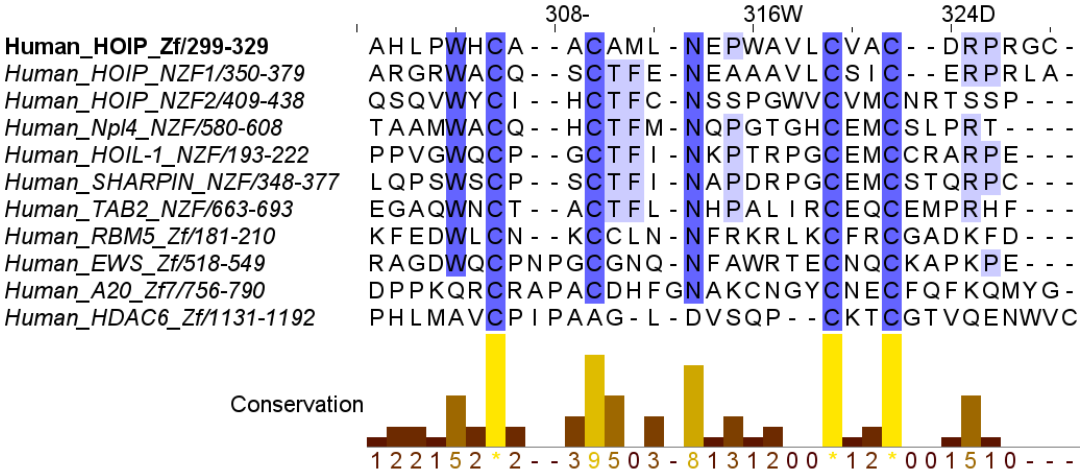


Figure 9: Sequence comparison of HOIP's Zf with ubiquitin binding NZF domains (prototypical Npl4, inflammatory proteins HOIP, HOIL-1L, SHARPIN, TAB2), non-ubiquitin-binding NZF domains (RBM5, EWS), A20's Zf and the HDAC6 Zf. Conservation is mapped below each sequence and more highly conserved residues are coloured in deep blue.

NZF of Npl4 as well as other NZF domains of inflammatory complexes and NZF domains that do not bind ubiquitin. **Figure 9** shows that HOIP Zf possesses the canonical NZF sequence, but not the NZF ubiquitin-binding motif. Zf is therefore a misannotated NZF0 and will be referred to as NZF0 for the purposes of this thesis.

To determine the role of NZF0 in HOIP's binding to polyubiquitin chains its binding to monoubiquitin was studied by NMR, which can detect very low affinity interactions. The 2D NMR spectrum of NZF0 was collected, the protein was mixed with monoubiquitin in a 1:6 molar excess and the spectrum was collected anew. The position of the amide peaks remains the same between the two spectra (**Figure 10**, **Supplementary Figure 2**). Their chemical environment is therefore not altered upon ubiquitin addition, meaning that NZF0 does not bind to monoubiquitin, even in a very low affinity interaction, or only binds extremely weakly.

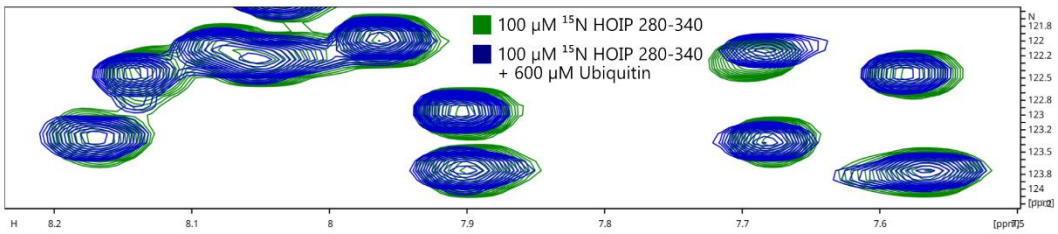


Figure 10: BEST-TROSY spectra of ^{15}N-labelled HOIP NZF0 (aa 280-340, green) and HOIP NZF0 mixed with 1:6 molar excess monoubiquitin (blue), showing an overlap of the two spectra. Full spectra can be found in Supplementary Figure 2.

3.3. Backbone assignment of HOIP NZF1-NZF2 (aa 346-451)

NMR is a powerful tool to study protein interactions, with the unique potential to deliver amino acid specific information of even weak interactions. Determining which peak represents which amino acid in the sequence, also called a backbone assignment, is vital in mapping interaction surfaces on the protein sequence. Since in this thesis emphasis is laid on the ubiquitin-binding abilities of NZF1 and NZF2, mapping their binding to ubiquitin with amino acid specificity is necessary to elucidate finer details of

this binding event which cannot be determined by affinity or other biophysical studies. Backbone assigning NZF1-NZF2 is therefore necessary in order for us to create detailed models of the interaction of these tandem NZF domains with ubiquitin chains.

Through a combination of more and less sensitive experiments the carbon signal of the preceding (i-1) and the observed (i) amino acid is collected, allowing one to trace the protein backbone backwards and to assign residues according to their chemical structure and known shifts. This is known as a “sequential walk” and utilizes experiments involving both the carbonyl and the C_α and C_β atoms of an amino acid. For the backbone assignment of HOIP NZF1-NZF2 (aa 346-451) an HNCO/HNCACO approach, coupled with HN(CO)CACB/HNCACB measurements, was applied. An example of this can be seen in **Figure 11** for residues C429 and V430 (here C84 and V85). The HNCO and HN(CO)CACB spectra of V430 display the CO, C_α and C_β resonances of the residue

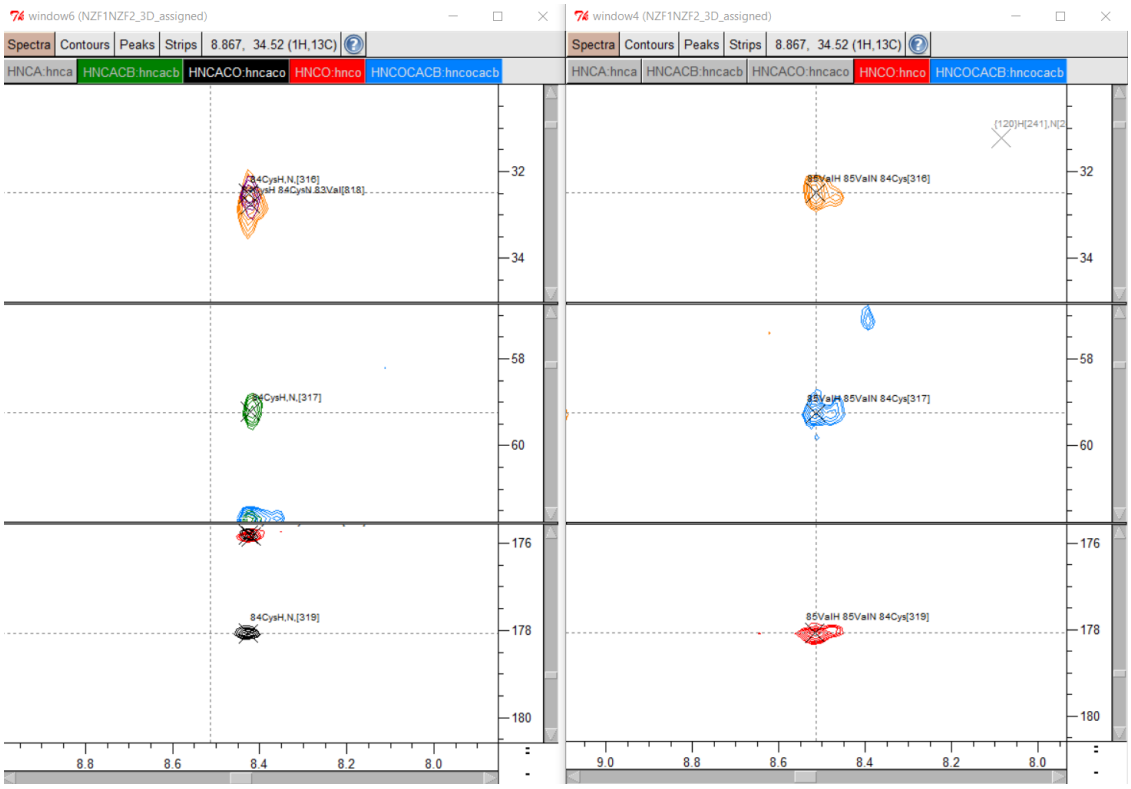


Figure 11: Snapshot of the NMR assignment of ^{13}C-^{15}N-labelled HOIP NZF1-NZF2 (aa 346-451). (Left) HNCO (red), HNCACO (black), HN(CO)CACB (blue, orange) and HNCACB (green, purple) spectra for C429 (here C84). (Right) HNCO (red) and HN(CO)CACB (blue, orange) spectra for V430 (here V85). The horizontal markers indicate that the HNCO and HN(CO)CACB spectra of V430 overlap with the HNCACO and HNCACB spectra of C429, suggesting that C429 is the residue before V430 and assigning them sequentially to one another.

before it. The HNCACO and HNCACB spectra of C429 have resonances in exactly these positions. Moreover, these resonances do not overlap with the HNCO and HN(CO)CACB spectra of C429, meaning that they belong to C429 itself and not to its previous amino acid V428.

The 3D experimental data needed to be processed with NMRPipe, to correct phasing and reconstitute NUS, before being imaged and evaluated on CCPN Analysis. NZF1-NZF2 was backbone assigned by manually picking the peaks and by using the semi-automated sequential backbone assignment function, as illustrated in **Figure 11**. The N-terminus cannot be detected due to the rapid hydrogen exchange with the solvent and was therefore not assigned, along with the residues Q411, W427, A444 and S450 and all prolines. In total 96% of the expected residues were successfully assigned and can be identified on the BEST-TROSY spectrum of HOIP NZF1-NZF2 (**Figure 12**, **Supplementary Figure 3**).

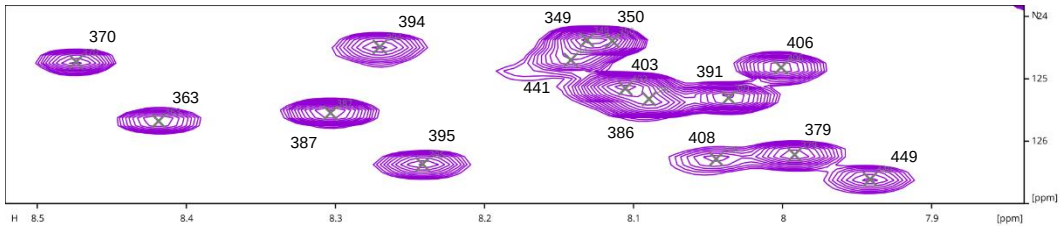


Figure 12: BEST-TROSY spectra of ^{13}C-^{15}N-labelled HOIP NZF1-NZF2 (aa 346-451, purple), showing nearly all resonances backbone assigned to the corresponding amino acid of the sequence. Full spectra can be found in Supplementary Figure 3.

3.4. NZF1 and NZF2 both bind monoubiquitin via their TF/Φ motif

HOIP's NZF domains have been the focal point of HOIP recruitment studies since 2006. NZF1 was reported to bind ubiquitin chains, while NZF2 did not coimmunoprecipitate with linear ubiquitin and was therefore considered incapable of binding ubiquitin [44]. **Figure 9** illustrates that NZF1 but also NZF2 possess the TF/Φ ubiquitin-binding motif of NZF domains, making them both candidates for ubiquitin binding and justifying further biophysical studies into their binding abilities.

To study this interaction NMR titrations of ^{15}N-labelled constructs of NZF1 and NZF2 with monoubiquitin were completed (**Figures 13 and 14, Supplementary Figures 4 and 5**). The constructs partially overlap in the linker region between the two domains,

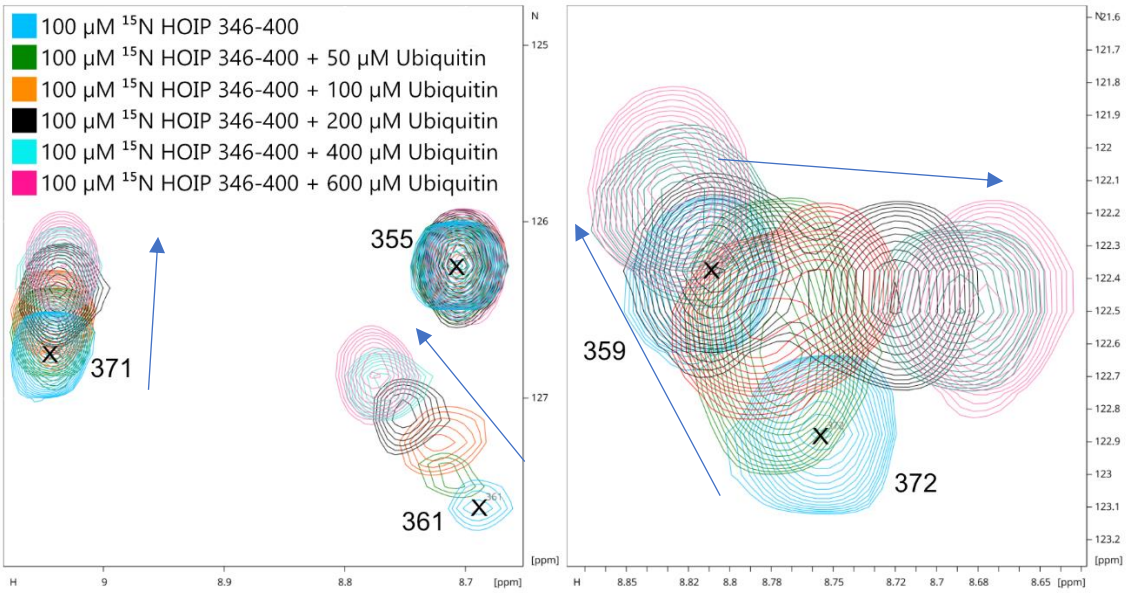


Figure 13: BEST-TROSY spectra of ^{15}N-labelled HOIP NZF1 (aa 346-400, skyblue) and HOIP NZF1 mixed with 1:0.5 molar excess (green), 1:1 molar excess (orange), 1:2 molar excess (black), 1:4 molar excess (turquoise), 1:6 molar excess monoubiquitin (pink), showing several peaks shifting upon ubiquitin addition. Close-up of spectral regions of interest, displaying the shifts of residues A355, F361 and S371 (Left) and C359 and I372 (Right). Full spectra can be found in Supplementary Figure 4.

particularly for the NZF2 construct. Chemical shift perturbations are already observed in a molar ratio of 1:0.5 NZF:Ub for both constructs. The amide shifts show that both NZF domains bind to monoubiquitin. The existence of peaks with different spectral positions for each individual titration point indicates a fast exchange in binding and therefore an interaction with weak affinity. In contrast, high affinity interactions present two peak positions, one for the bound and one for the unbound state, with the proportion between the two populations migrating from unbound to bound throughout the titration [94].

The chemical shifts reach saturation by the end of the titration series for NZF1, as shown by the overlap of the peaks for the ratios 1:4 and 1:6 NZF1:Ub (turquoise and pink spectra), while for NZF2 the overlap between these two titration points is smaller, meaning it does not reach saturation at a 1:4 molar ratio. This hints towards the two NZF

domains having different affinities to monoubiquitin. NZF1 could have a higher affinity, thereby being in a mostly bound state when mixed with 400 µM or 600 µM monoubiquitin (1:4, 1:6 molar ratios), while the affinity of NZF2 is expected to be lower.

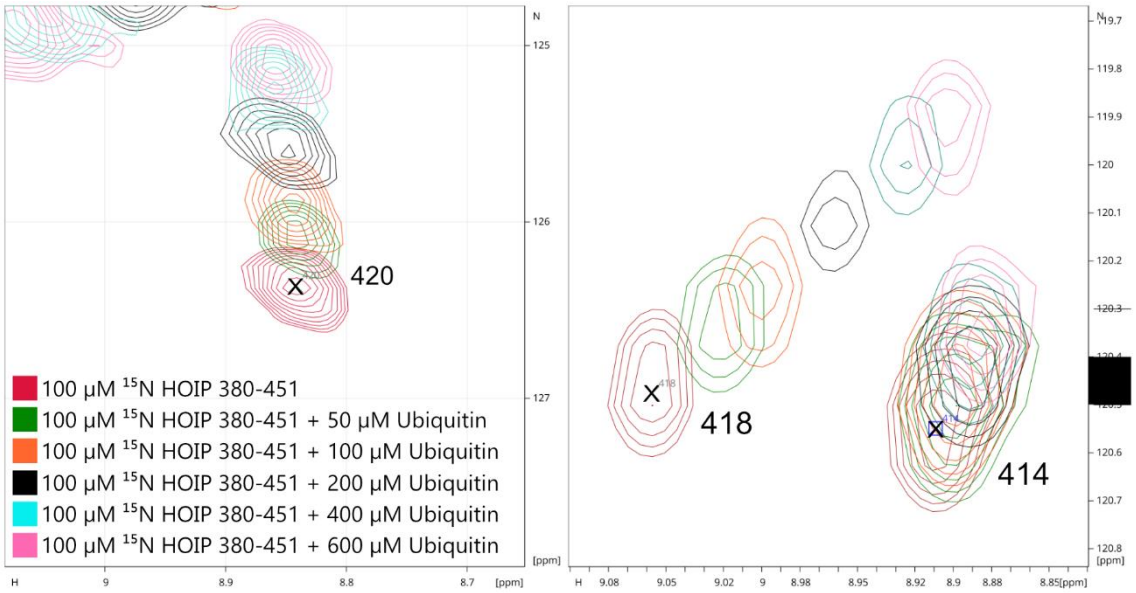


Figure 14: BEST-TROSY spectra of ^{15}N-labelled HOIP NZF2 (aa 380-451, crimson) and HOIP NZF2 mixed with 1:0.5 molar excess (green), 1:1 molar excess (orange), 1:2 molar excess (black), 1:4 molar excess (turquoise), 1:6 molar excess monoubiquitin (pink), showing several peaks shifting upon ubiquitin addition. Close-up of spectral regions of interest, displaying the shifts of residue F420 (Left) and Y414 and C418 (Right). Full spectra can be found in Supplementary Figure 5.

Owing to the assignment of the NZF1-NZF2 backbone resonances, chemical shift perturbation (CSP) maps can be derived. The CSP maps display how far each residue has shifted by tracking the spectral length covered throughout the titration. By statistically analyzing these shifts the standard deviation and therefore a cut-off value is established in order to determine what constitutes a significant shift, meaning an interaction, and what does not (**Figure 15**). Peaks and chemical shifts are dependent on the chemical environment of the amino acid, meaning that the CSP values are specific to each amino acid and each interaction. They provide qualitative insight in order to compare the shift strength between equivalent titrations, e.g. monoubiquitin binding to NZF1 and NZF2, and most importantly to observe trends or binding patches for the interaction between two proteins.

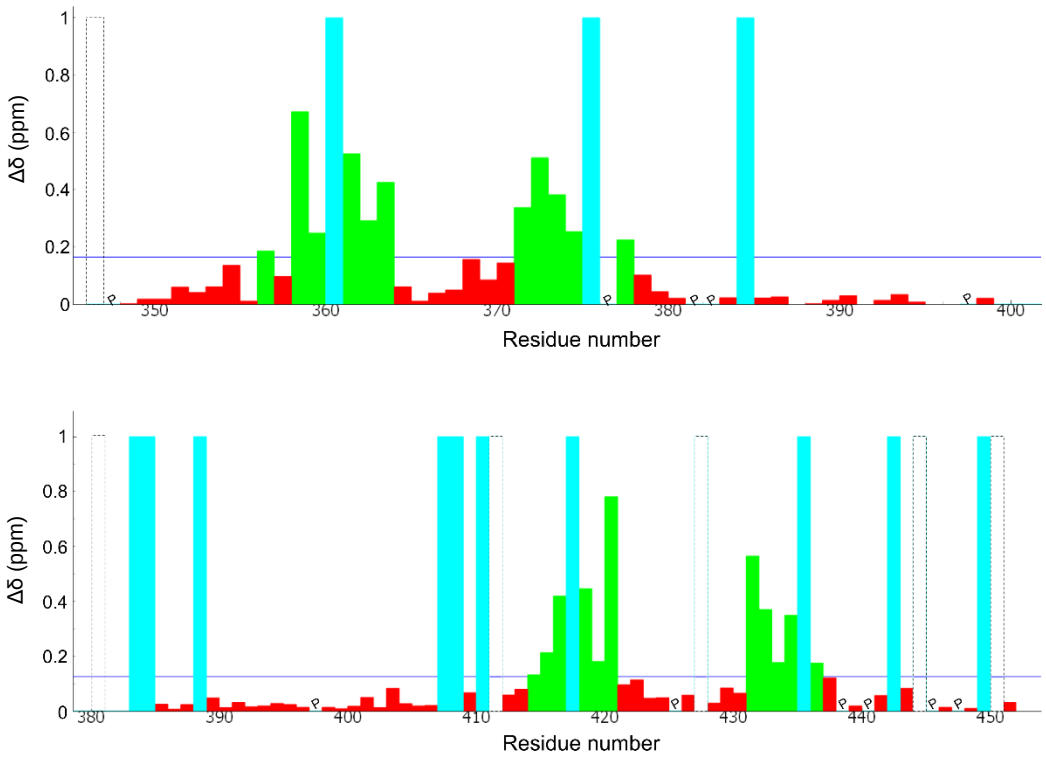
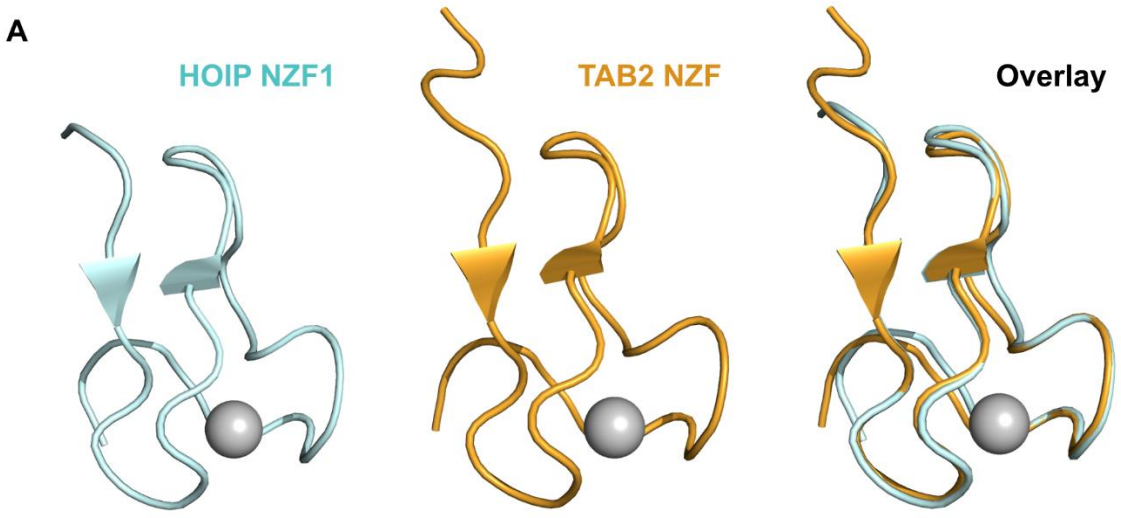


Figure 15: Chemical shift perturbation maps of HOIP NZF1 (aa 346-400, top) and HOIP NZF2 (aa 380-451, bottom), derived from their titrations with monoubiquitin as seen in Figures 13 and 14, respectively. The cut-off for significant shifts was set as the standard deviation and illustrated as a blue horizontal line. Peaks shifting significantly as defined by the cut-off are coloured in green, peaks not shifting coloured in red, peaks disappearing during the titration coloured in blue with shift value set at 1, not assigned peaks presented as transparent boxes and prolines indicated with a P.

The CSP maps of ubiquitin binding to the two NZF domains illustrate that shifts are stronger along the TF/Φ NZF ubiquitin-binding motif, namely T360F361/I372 for NZF1 and T419F420/M431 for NZF2. This demonstrates that monoubiquitin binds not only to NZF1 but also to NZF2, using a similar binding interface as seen in other NZF domains. NZF1 and NZF2 residues have similar CSP values, with a maximum of approximately 0.7 ppm for NZF1 and 0.8 ppm for NZF2, but as stated previously no absolute conclusion about binding characteristics can be drawn from quantitative comparisons of independent CSP maps.

A structure of NZF1 bound to NEMO CoZi domain has been published (PDB: 4OWF), allowing for the ubiquitin-binding patch to be mapped onto the structure (**Figure 16**). Numerous structures of NZF domains bound to mono- or polyubiquitin are available,

including the crystal structure of TAB2 NZF bound to K63 diubiquitin (PDB: 2WWZ), which is the ubiquitin chain postulated to be the preferred binding substrate of NZF1. Overlaying the structure of the two NZF domains highlights the similarity between the two folds (**Figure 16A**), while aligning the K63 diubiquitin bound to the TAB2 NZF with the NZF1 provides insight on the monoubiquitin-binding patch of NZF1 (**Figure 16B**). The patch covers the interface between NZF1 and the distal ubiquitin moiety of the diubiquitin. This is in agreement with NZF literature, in which binding to monoubiquitin represents the same site as a distal ubiquitin in a diubiquitin. Importantly, each chain-specific NZF then employs a different mechanism to orient the proximal ubiquitin and achieve linkage specificity, often present as an extended ubiquitin-binding interface, capable of facilitating not only the distal but also the proximal ubiquitin of the chain. Such an extension cannot be observed in NZF1 through its monoubiquitin-binding patch, illustrated by the lack of shifting residues in the surface of NZF1 which contacts the proximal ubiquitin moiety of the K63 diubiquitin. However, monoubiquitin binding to the proximal site is much weaker than to the distal site, disallowing its observation in the titration with monoubiquitin. Chemical shifts corresponding to this additional interaction site may only be observable in a titration with ubiquitin chains, rather than monoubiquitin.



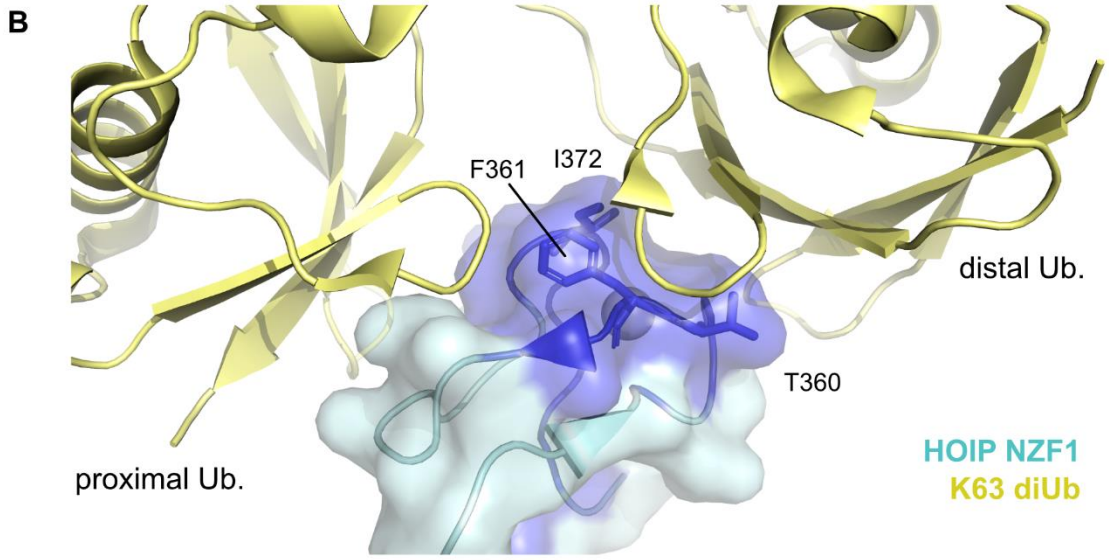


Figure 16: (A) Superposition on the NZF1 of HOIP (PDB: 4OWF, cyan, left) and the NZF of TAB2 (PDB: 2WWZ, orange, center) shows alignment of the NZF fold. (B) Superposition on the NZF1 of HOIP (PDB: 4OWF, cyan, ubiquitin-binding patch established by NMR in blue) and K63-linked diubiquitin (PDB: 2WWZ, gold) showing alignment of the ubiquitin-binding patch with the distal ubiquitin moiety of the diubiquitin. The NZF ubiquitin-binding pattern T360F361/I372 is shown as sticks.

3.5. Binding to monoubiquitin is preserved when both NZF1 and NZF2 are present

To confirm whether NZF1 and NZF2 bind monoubiquitin independently of one another, the titration with monoubiquitin was repeated with a construct containing both NZF1 and NZF2 (HOIP NZF1-NZF2, aa 346-451). In this case twice the concentration of ubiquitin was used to ensure a final 1:6 molar excess monoubiquitin per binding site, unlike the NZF1 and NZF2 titrations. As shown in **Figure 17** (**Supplementary Figure 6**), NZF1 residues reach saturation at an earlier titration point (see F361, **Figure 18** left and right) in proportion to the total concentration of ubiquitin in the sample. For example the spectrum of NZF1 bound to 1:1 molar excess monoubiquitin (100 µM monoubiquitin) is equivalent to the spectrum of NZF1-NZF2 bound to 1:0.5 molar excess monoubiquitin (also 100 µM monoubiquitin) etc.

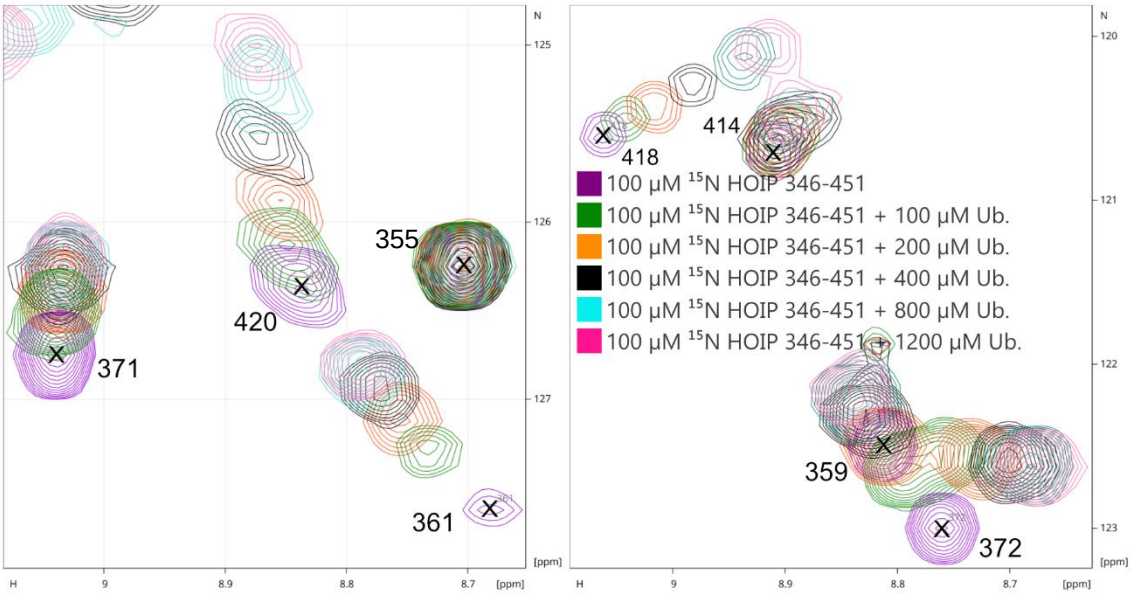


Figure 17: BEST-TROSY spectra of ^{15}N-labelled HOIP NZF1-NZF2 (aa 346-451, purple) and HOIP NZF1-NZF2 mixed with 1:0.5 molar excess (green), 1:1 molar excess (orange), 1:2 molar excess (black), 1:4 molar excess (turquoise), 1:6 molar excess monoubiquitin per binding site (pink), showing several peaks shifting upon ubiquitin addition. Close-up of spectral regions of interest, displaying the shifts of residues A355, F361, S371 and F420 (Left) and C359, I372, Y414 and C418 (Right). Full spectra can be found in Supplementary Figure 6.

In order to compare these shifts qualitatively and gain a better overview of NZF1 versus NZF2 shifts in the NZF1-NZF2 construct a CSP map was finalized (**Figure 18B**). In the NZF1-NZF2 construct both NZF1 and NZF2 residues shift slightly stronger than they do when the domains are present alone, again due to the higher final concentration of ubiquitin. The shifts of the individual titration points for NZF1 in the NZF1 and the NZF1-NZF2 constructs overlap, with NZF1 binding largely unaffected by the presence of NZF2 as a second binding site. This is not the case for NZF2, where the titration points of the NZF2 and the NZF1-NZF2 constructs overlap based on the molar ratio of binding site to monoubiquitin rather than the final ubiquitin concentration. NZF2 is therefore affected by the presence of NZF1 as a binding site for monoubiquitin, possibly because NZF1 binds the available ubiquitin, removing it from the substrate pool of NZF2 and ultimately reducing the concentration of free ubiquitin that determines the shifts of NZF2 residues. It should furthermore be noted that even with 1200 µM ubiquitin present in the sample, NZF2 shifts have not reached saturation while NZF1 shifts have, hinting that the

two domains preserve their lower and higher affinities to monoubiquitin respectively in the NZF1-NZF2 construct.

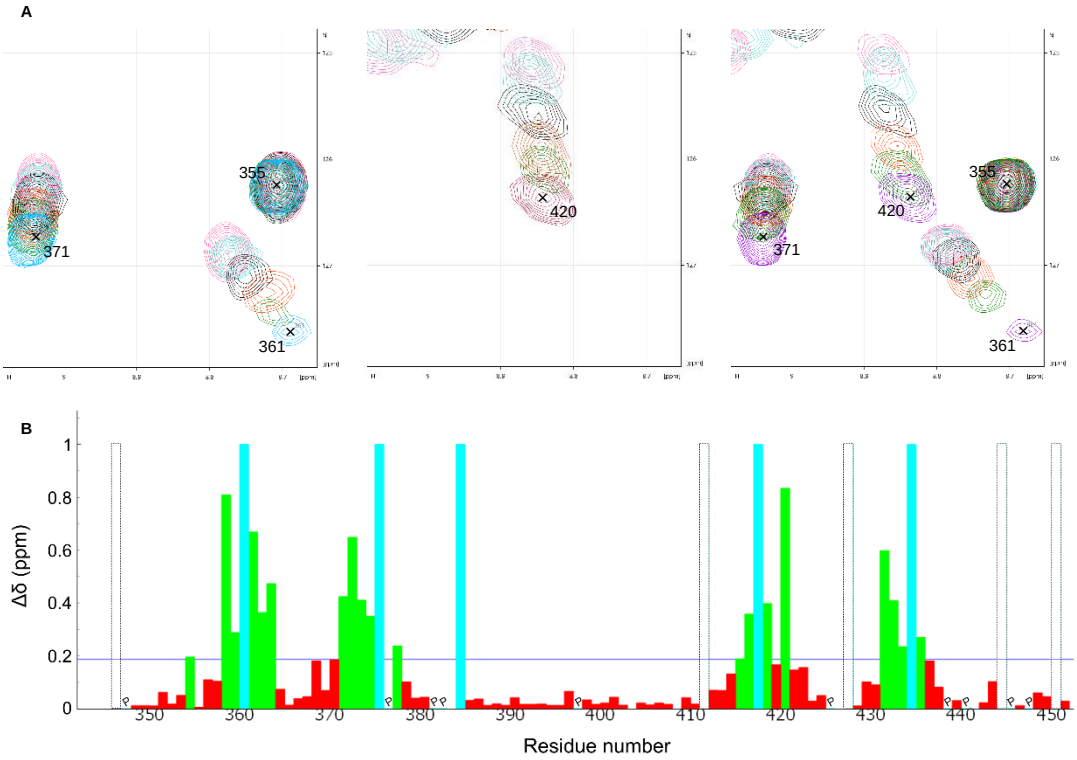


Figure 18: (A) Close-up of a spectral region of interest, displaying the shifts of residues A355, F361, S371 and F420 for the constructs HOIP NZF1 (aa 346-400, left), HOIP NZF2 (aa 380-451, center) and HOIP NZF1-NZF2 (aa 346-451, right) as seen in Figures 13, 14 and 17, respectively. Note the difference in shifts for F361 and the similarity for F420. (B) Chemical shift perturbation map of HOIP NZF1-NZF2 (aa 346-451), derived from its titration with monoubiquitin as seen in Figure 17. The cut-off for significant shifts was set as the standard deviation and illustrated as a blue horizontal line. Peaks shifting significantly as defined by the cut-off are coloured in green, peaks not shifting coloured in red, peaks disappearing during the titration coloured in blue with shift value set at 1, not assigned peaks presented as transparent boxes and prolines indicated with a P.

In order to delve further into the how each NZF binds to ubiquitin, ubiquitin-binding mutants were developed for NZF1-NZF2. These mutants would help elucidate the binding of the individual domains while the second domain is present while ensuring substrate availability is not influenced due to the observed difference in the binding affinities of NZF1 and NZF2. Based on previous experiments with the prototypical Npl4 NZF, mutating the threonine of the NZF ubiquitin-binding patch greatly reduces ubiquitin binding [49]. Such a mutant has been described for NZF1 before (T360A) and was shown to reduce overall diubiquitin binding in NZF1-NZF2 and recruitment to the TNF

receptor signaling complex [76, 77]. An equivalent mutant for NZF2 has not yet been described.

The constructs NZF1-NZF2 T360A and T419A were designed, in which T360A is only able to bind ubiquitin via NZF2 and T419A which can bind only through NZF1. The same titration with the same amount of ubiquitin as for NZF1-NZF2 was completed for the mutant constructs (**Figures 19 and 20, Supplementary Figures 7 and 8**). All assigned peaks retained their positions, except for the mutated site and surrounding residues, illustrating that the constructs' fold is not affected by the mutation. For NZF1-NZF2 T360A only NZF2 residues shift significantly, except for one NZF1 residue, meaning that ubiquitin binding takes place only with NZF2. For NZF1-NZF2 T419A only NZF1 binds to monoubiquitin, except for one NZF2 residue.

The analysis of the spectral shifts on CSP maps confirms that the mutated domains did not bind to ubiquitin (**Figure 21** center and bottom). In the T360A mutant NZF2 was able to bind to ubiquitin in a manner similar to that of the NZF2 construct. NZF2 residues shifted stronger in the T360A mutant than in the NZF2 construct (**Figure 21** center). The

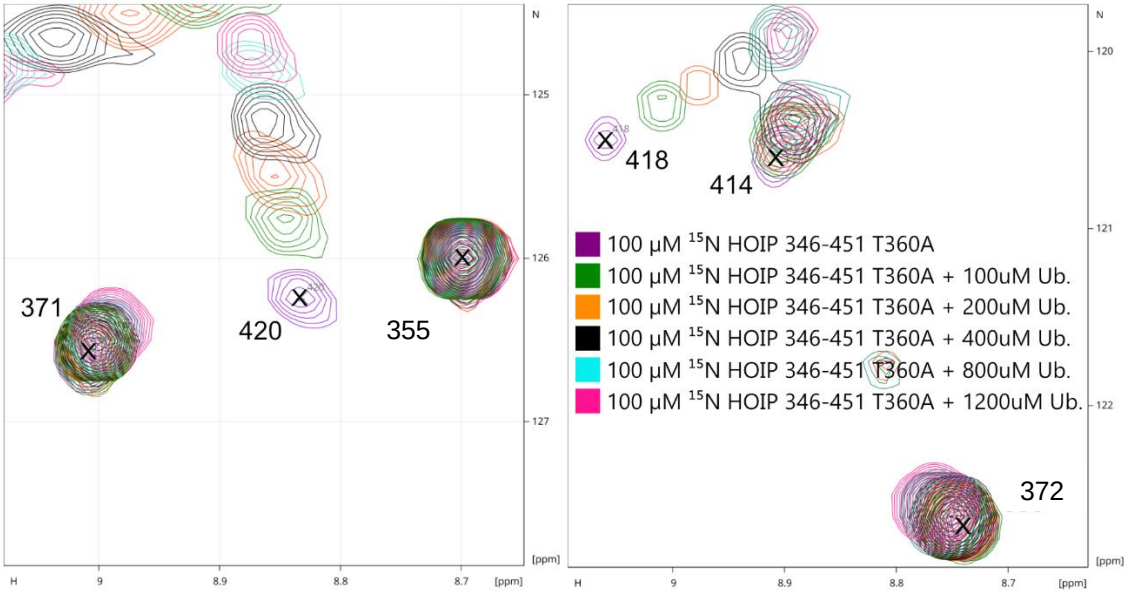


Figure 19: BEST-TROSY spectra of ^{15}N-labelled HOIP NZF1-NZF2 T360A (aa 346-451, purple) and HOIP NZF1-NZF2 T360A mixed with 1:0.5 molar excess (green), 1:1 molar excess (orange), 1:2 molar excess (black), 1:4 molar excess (turquoise), 1:6 molar excess monoubiquitin (pink), showing several peaks shifting upon ubiquitin addition. Close-up of spectral regions of interest, displaying the shifts of residues A355, S371 and F420 (Left) and I372, Y414 and C418 (Right). The peaks of residues C359 and F361 have changed their spectral position due to their proximity to the mutated residue T360A. Full spectra can be found in Supplementary Figure 7.

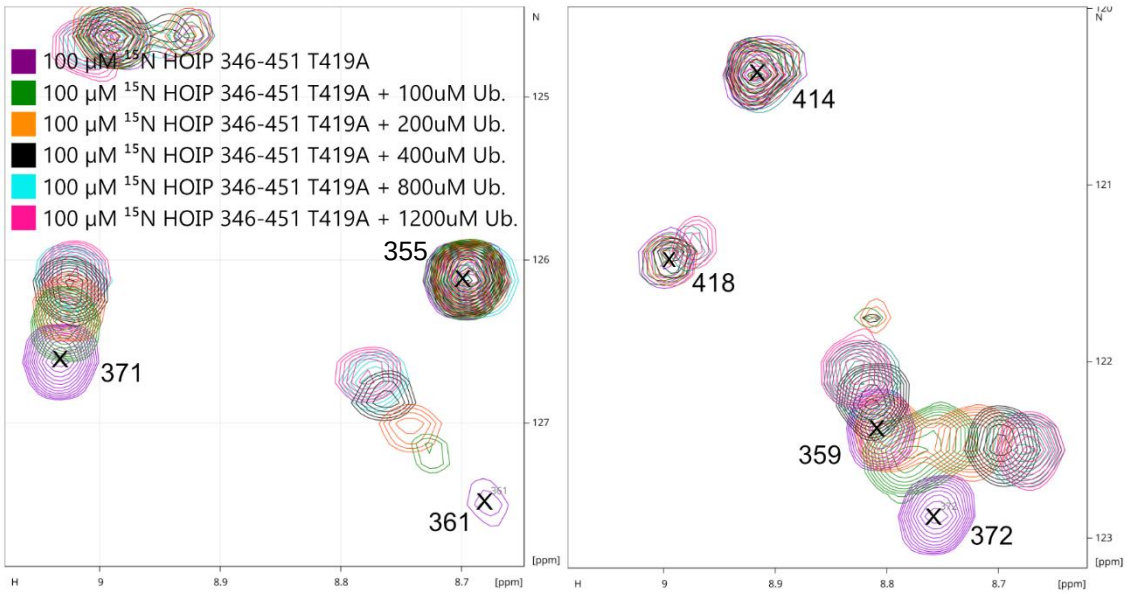


Figure 20: BEST-TROSY spectra of ^{15}N-labelled HOIP NZF1-NZF2 T419A (aa 346-451, purple) and HOIP NZF1-NZF2 T419A mixed with 1:0.5 molar excess (green), 1:1 molar excess (orange), 1:2 molar excess (black), 1:4 molar excess (turquoise), 1:6 molar excess monoubiquitin (pink), showing several peaks shifting upon ubiquitin addition. Close-up of spectral regions of interest, displaying the shifts of residues A355, F361 and S371 (Left) and C359, I372, Y414 and C418 (Right). The peak of residue F420 has changed its spectral position due to its proximity to the mutated residue T419A. Full spectra can be found in Supplementary Figure 8.

cause could be that a higher ubiquitin concentration was available for binding to NZF2, combined with the fact that NZF2 still did not reach saturation (**Figure 18** right), allowing its residues to shift further and even leading additional residues around the TF/Φ motif to shift significantly. Shifts also increased compared to the NZF1-NZF2 wild-type construct. The increase in shifts must arise from the inability of NZF1, which possibly has a higher affinity to monoubiquitin, to bind the monoubiquitin and remove it from the substrate pool of NZF2. While the total ubiquitin concentration was the same between the two titrations, the free concentration, which determines the shifts of NZF2, is now higher. Alternatively, NZF1 binding to ubiquitin could cause sterical clashes between ubiquitin moieties, again restricting NZF2's ability to bind to monoubiquitin fully. Overall, the experiment confirms that NZF2 can bind monoubiquitin on its own, but with a much lower affinity compared to NZF1.

The same phenomenon is not observed for the T419A mutant, where NZF1 is the one capable of binding ubiquitin. NZF1 residues shift similarly to the NZF1-NZF2 wild-type

construct, reaching saturation equally fast and at the same spectral position (**Figure 20**). The CSP values remain the same, with only one additional residue now having a significant shift. (**Figure 21** bottom). This illustrates that the ubiquitin-binding interface of NZF1 is unaltered by the inability of NZF2 to bind to ubiquitin, demonstrating that NZF1 and NZF2 serve as individual ubiquitin-binding domains. Additionally, NZF1 must have a higher affinity to monoubiquitin than NZF2, seeing as it is able to reach saturation at lower substrate concentrations and is not affected by NZF2, a binding site with lower affinity, binding to ubiquitin in the wild-type construct.

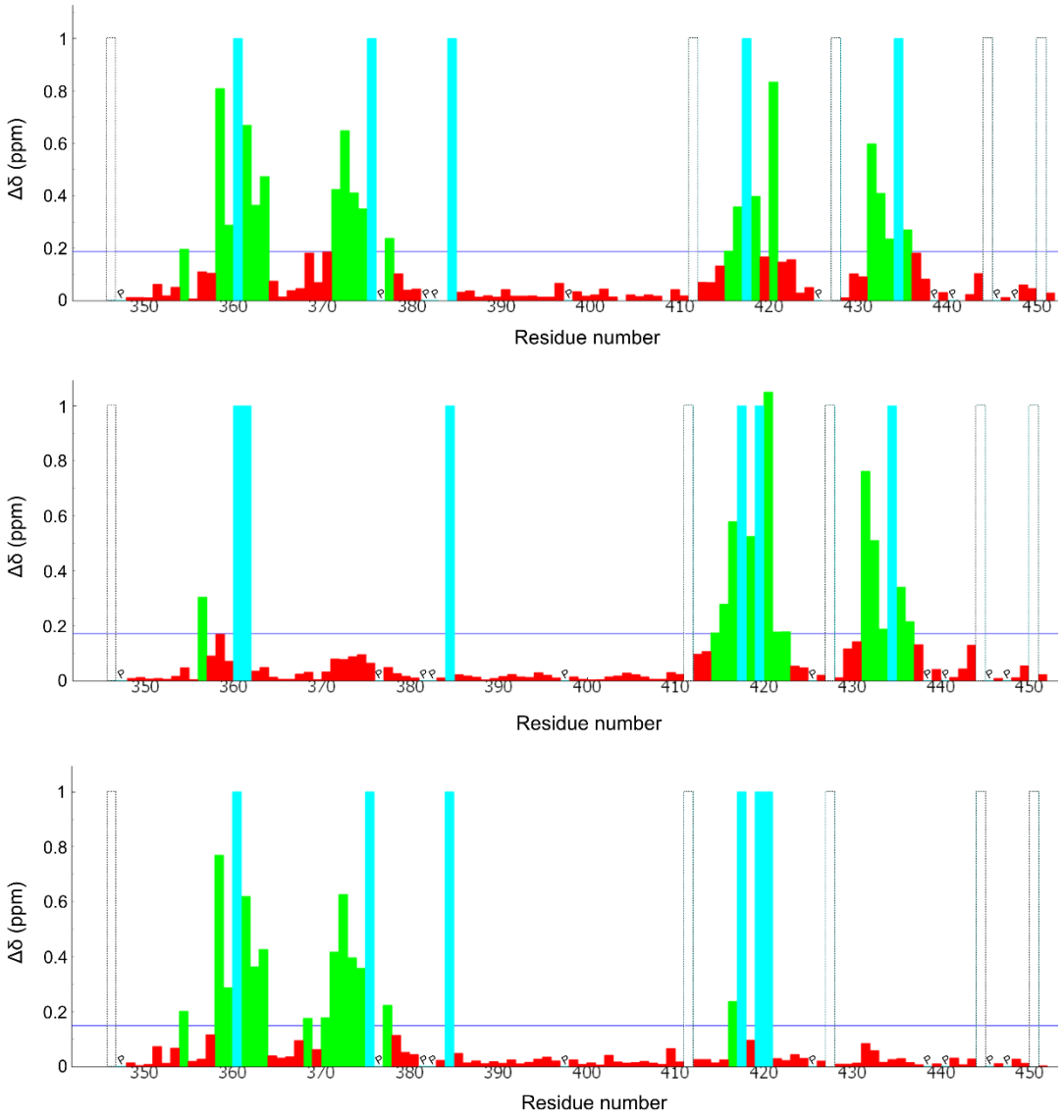


Figure 21: Chemical shift perturbation maps of HOIP NZF1-NZF2 wild-type (aa 346-451, top), HOIP NZF1-NZF2 T360A (aa 346-451, center) and HOIP NZF1-NZF2 T419A (aa 346-451, bottom), derived from their titrations with monoubiquitin as seen in Figures 17, 19 and 20, respectively. The cut-off for significant shifts was set as the standard deviation and illustrated as

a blue horizontal line. Peaks shifting significantly as defined by the cut-off are coloured in green, peaks not shifting coloured in red, peaks disappearing during the titration coloured in blue with shift value set at 1, not assigned peaks presented as transparent boxes and prolines indicated with a P.

3.6. NZF1 binds to monoubiquitin stronger than NZF2

Binding affinity is an important factor to determine the physiological significance of a binding effect and/or a protein's preferential binding partner. As a titrated binding experiment, NMR can be used to speculate or determine the binding affinity of interaction partners. However, a more accurate technique to determine binding affinities is ITC.

The K_d of NZF1 and NZF2 to monoubiquitin was measured and found to be very different between the two domains, far higher for NZF1 (K_d of 7 to 30 µM across repeats, average K_d 9.6 ± 1.1 µM) than for NZF2 (average K_d 228 ± 58.1 µM) (**Figure 22A**) (**Table 2**). NZF1 displays a high affinity, similar to ones measured in previous studies, while NZF2 generally corresponds to previously reported K_d values of UBDs to monoubiquitin [18, 33, 49]. Interestingly, the overall affinity of NZF1-NZF2 to monoubiquitin (average K_d of 65.9 ± 5.9 µM) is much closer NZF1 than to the average of NZF1 and NZF2 (that would be a K_d of over 100 µM), while a two binding site analysis of NZF1-NZF2 coincides to a larger extent with the values established for the individual domains (site 1: 20 µM, site 2: 208 µM). The stoichiometry values (N) of the NZF domains binding to ubiquitin also provide insight into the binding event. While NZF1 shows N values slightly higher than 1, NZF2 shows very low values and NZF1-NZF2 has values between 1 and 1.5. This corresponds to the model of NZF1 being the main binding site for monoubiquitin, while NZF2 contributes only partially due to its low affinity. It should be noted that the thermodynamic values for NZF2 have large error margins precisely due to the low affinity interaction, deeming determining its details and parameters difficult and barely within the limits of ITC.

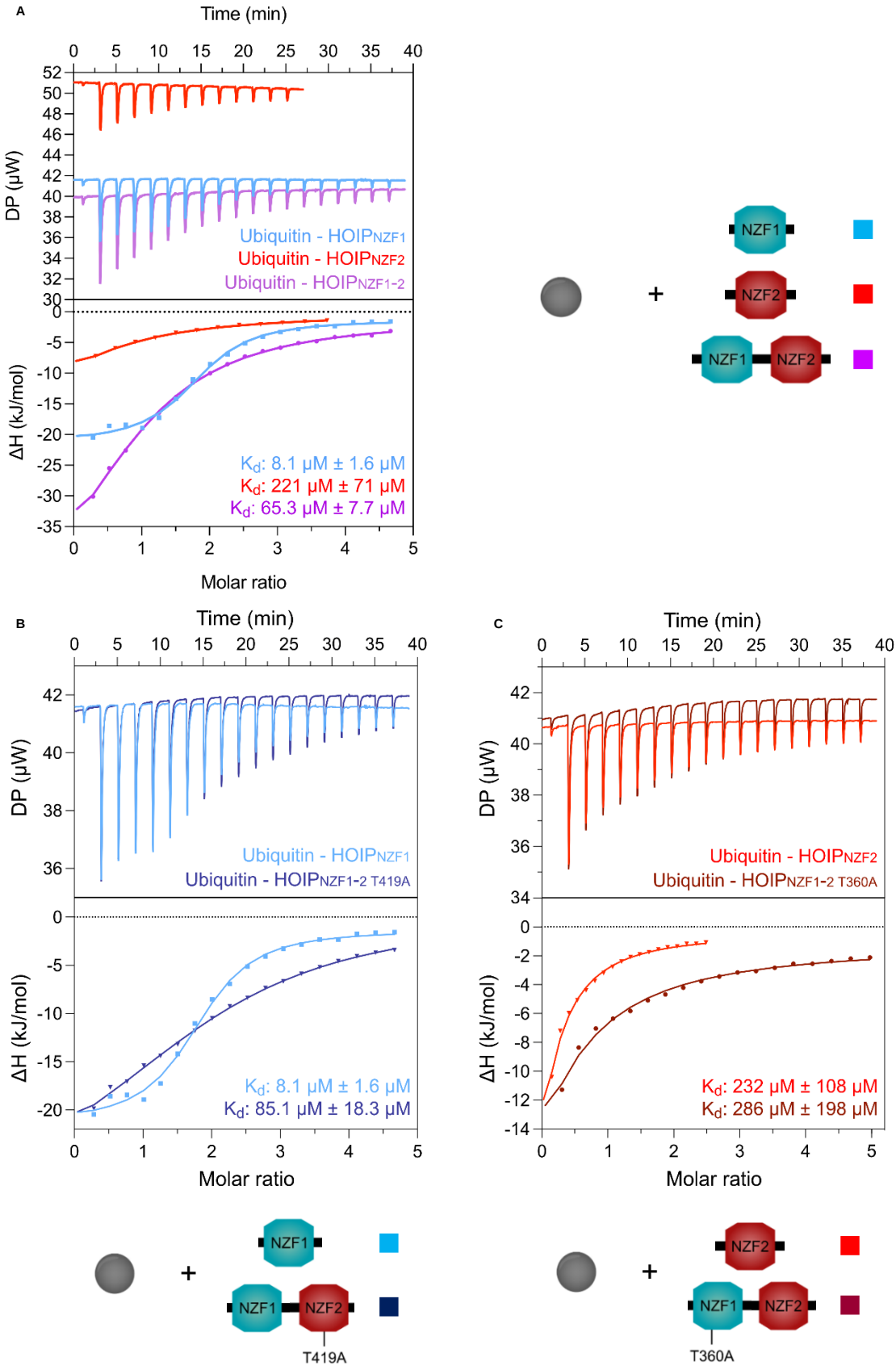


Figure 22: ITC titration curves and graphic illustration of the interaction of monoubiquitin with (A) HOIP NZF1 (aa 346-400, skyblue), NZF2 (aa 380-451, red) or NZF1-NZF2 wild-type (aa 346-451, purple traces), (B) HOIP NZF1 (aa 346-400, skyblue) or NZF1-NZF2 T419A (aa 346-451,

dark blue traces) and (C) HOIP NZF2 (aa 380-451, red) or NZF1-NZF2 T360A (aa 346-451, dark red traces). Two biological replicates were performed for NZF1-2, NZF1 and NZF2. For NZF1 the second biological replicate was performed twice as a technical replicate, resulting in three overall replicates.

Table 2: Thermodynamic parameters for the ITC titration curves of HOIP NZF1-NZF2 wild-type, HOIP NZF1, HOIP NZF1-NZF2 T419A, NZF2 and HOIP NZF1-NZF2 T360A binding to monoubiquitin. Two biological replicates were performed for NZF1-2, NZF1 and NZF2. For NZF1 the second biological replicate was performed twice as a technical replicate, resulting in three overall replicates. The first biological replicate for NZF1-2 was also analysed using sequential site analysis, resulting in thermodynamic values for the two calculated sites (1) and (2).

Syringe	**Cell**	**K_d (µM)**	**ΔH (kJ/mol)**	**-TΔS (kJ/mol)**	**ΔG (kJ/mol)**	**N (stoichiometry)**
Ub.	HOIP NZF1-2	66.7 ± 9.2	-31.2 ± 2.4	7.31	-23.9	1.47 ± 0.39
		65.3 ± 7.7	-56 ± 4.75	32.1	-23.9	1.04 ± 0.04
	HOIP NZF1-2 (Seq. site analysis)	(1) 22.2 ± 0.6	(1) -26.5 ± 0.2	(1) -0.09	-	-
		(2) 261 ± 6.7	(2) -37.5 ± 3.6	(2) 17		
Ub.	HOIP NZF1	35.4 ± 4.25	-27.6 ± 1.6	2.13	-25.4	1.17 ± 0.03
		8.1 ± 1.6	-20 ± 0.76	-9.12	-29.1	1.78 ± 0.04
		7.4 ± 1.6	-27.2 ± 1.19	-2.15	-29.3	1.41 ± 0.04
Ub.	HOIP NZF1-2 T419A	85.1 ± 18.3	-30.6 ± 3.32	7.4	-23.3	2.12 ± 0.08
Ub.	HOIP NZF2	221 ± 71	-24.0 ± 10.9	3.12	-20.9	0.69 ± 0.20
		232 ± 108	-335 ± 2970	314	-20.8	0.03 ± 0.24
Ub.	HOIP NZF1-2 T360A	286 ± 198	-335 ± 4360	315	-20.3	0.07 ± 0.84

To study whether NZF1 and NZF2 are independent or cooperative binding sites the affinity of the ubiquitin-binding mutants NZF1-NZF2 T360A and NZF1-NZF2 T419A to monoubiquitin was measured. NZF1-NZF2 T360A, where only NZF2 can bind ubiquitin, binds with an affinity and stoichiometry similar to that of NZF2 on its own (286 ± 198 µM, N of 0.06) (**Figure 22C**). Due to the large error of fit no direct conclusion can be drawn on the effect of the presence of NZF1 on NZF2 ubiquitin binding. However, the effect of the presence of NZF2 on NZF1 binding is apparent in measurements with NZF1-NZF2

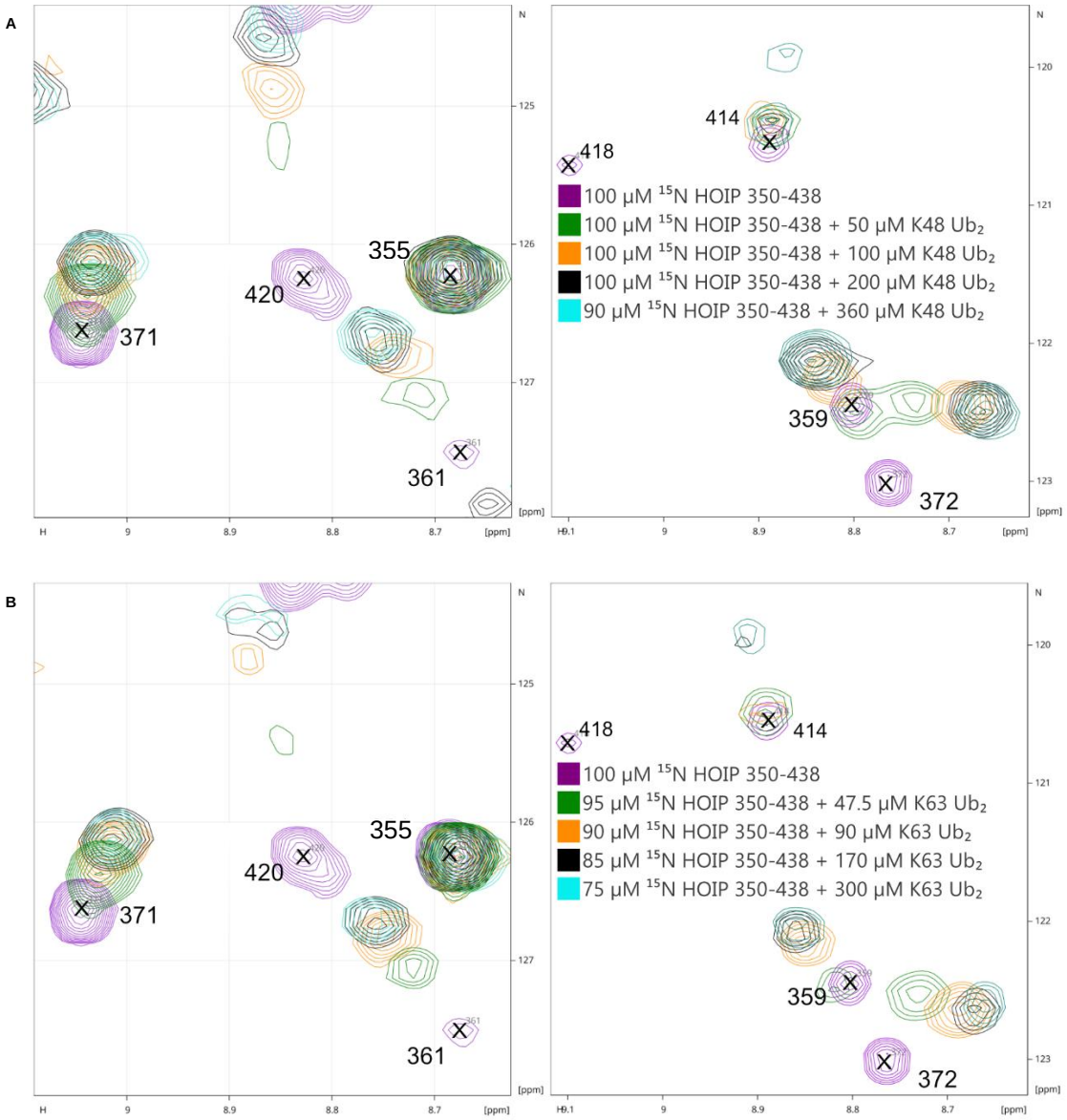
T419A. The construct, where only NZF1 binds to monoubiquitin, has an affinity up to 10 lower than NZF1 on its own (K_d 85 ± 18.3 μM) (**Figure 22B**). The presence of NZF2 in a state unable to bind or simply not bound to monoubiquitin therefore appears to reduce the affinity of NZF1 to monoubiquitin. However, this measurement was performed only once, disabling us from drawing a final conclusion.

3.7. NZF2 possesses an extended binding patch for K63-linked chains

Insight into the mechanism of NZF binding to monoubiquitin can help establish the details of their binding to ubiquitin moieties of ubiquitin chains. However, information on the interaction with the chains themselves is highly necessary, since they, and not monoubiquitin, are the designated substrate for recruitment to signaling complexes. To acquire amino acid-specific information on this binding, NMR titration series were completed for the NZF1-NZF2 (aa 350-438, for more information on this truncated construct see *Construct crystallization aimed to elucidate HOIP's specificity for K63-linked ubiquitin chains*) binding to K48- and to K63-linked diubiquitin. K63 binding was studied as the preferred binding partner of NZF1-NZF2, according to literature, while K48 chains were used as a control chain type which binds in a measurable manner, but not as tightly as K63 chains [77].

The titration series can be seen in **Figure 23** (A for K48, B for K63, **Supplementary Figure 9**). Due to the increased affinity of NZF1-NZF2 to diubiquitin compared to monoubiquitin, a lower final concentration was used. The binding leads to observable shifts which are saturated already at a 1:2 molar excess, as seen by the overlap between the black and turquoise spectra, which translates to a possibly higher affinity interaction. At first glance the shifts appear similar between the two chain types, with peaks reaching similar positions at the end of each titration series, albeit with slight differences in lower

concentrations of added diubiquitin. For example F420 shifts further in a 1:0.5 molar excess of K48 chains compared to K63 chains (green spectrum), but then reaches the same spectral position at 1:4 molar excess for both chain types (turquoise spectrum, **Figure 23A-B**, left, **Supplementary Figure 9**). Furthermore, a few peaks shifted in distinct directions upon addition of different chain types, indicating that they were interacting with each chain type differently. For example residue V430 shifted in different directions for K48- and K63-linked diubiquitin and only shifted significantly for the latter (**Figure 23C**).



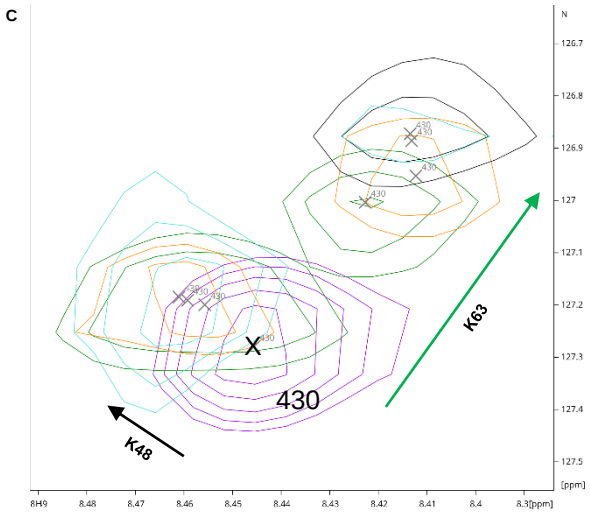


Figure 23: BEST-TROSY spectra of ^{15}N-labelled HOIP NZF1-NZF2 (aa 350-438, purple) and HOIP NZF1-NZF2 mixed with 1:0.5 molar excess (green), 1:1 molar excess (orange), 1:2 molar excess (black) and 1:4 molar excess diubiquitin (turquoise), with the titration of K48-linked diubiquitin in (A) and K63-linked diubiquitin in (B), showing several peaks shifting upon ubiquitin addition. Close-up of spectral regions of interest, displaying the shifts of residues A355, F361 and S371 and F420 (Left) and C359, I372, Y414 and C418 (Right). (C) Close-up of residue V430, which shows different chemical shift directions according to diubiquitin chain type. Full spectra can be found in Supplementary Figure 9.

Plotting the shifts on a CSP map offers finer details of the binding to each chain type (**Figure 24**, A for K48, B for K63). CSP values are overall similar for diubiquitin of both linkage types, with a maximum of approximately 0.8 for NZF1 and 1.5 for NZF2 residues. Shifts are stronger in NZF2 residues compared to NZF1 residues, although this does not inherently mean stronger or weaker binding, as explained previously. While NZF1 residues shift as strongly when bound to diubiquitin as to monoubiquitin, NZF2 residues shift almost twice as much. This could be caused by NZF1 binding to diubiquitin, which raises the local concentration of ubiquitin for NZF2 and brings it closer to a fully bound state in these experiments.

No additional NZF1 residues shift when bound to diubiquitin compared to monoubiquitin, meaning that its binding interface remains the same as the one observed in **Figure 15**. For NZF2 the effect of diubiquitin binding compared to monoubiquitin depends on the chain type. For K48-linked diubiquitin the only residue additional to the ones observed for monoubiquitin is G426. However, residues V412, W413 and V430 shift in the

presence of K63-linked chains, but not monoubiquitin, reestablishing its binding interface to ubiquitin chains. In addition to this difference between diubiquitin and monoubiquitin binding, the residues shifting and constituting the binding interface slightly change between K48 and K63 chains. Residues A355 and E362 of NZF1 and, more notably, V412, W413, T419 and V430 of NZF2 shift only in the presence of K63 chains, but not K48 (**Figure 24**). Overall, the K63 diubiquitin binding interface diverged more from the one for monoubiquitin compared to the K48 binding interface.

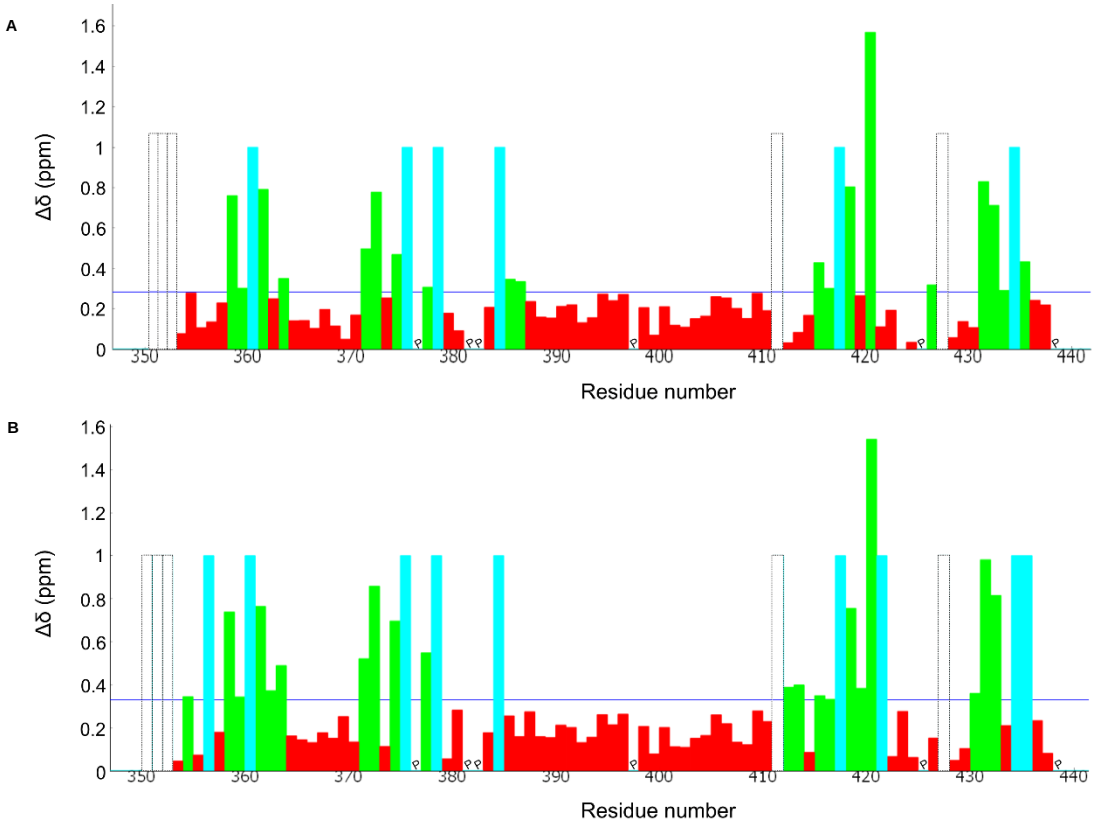
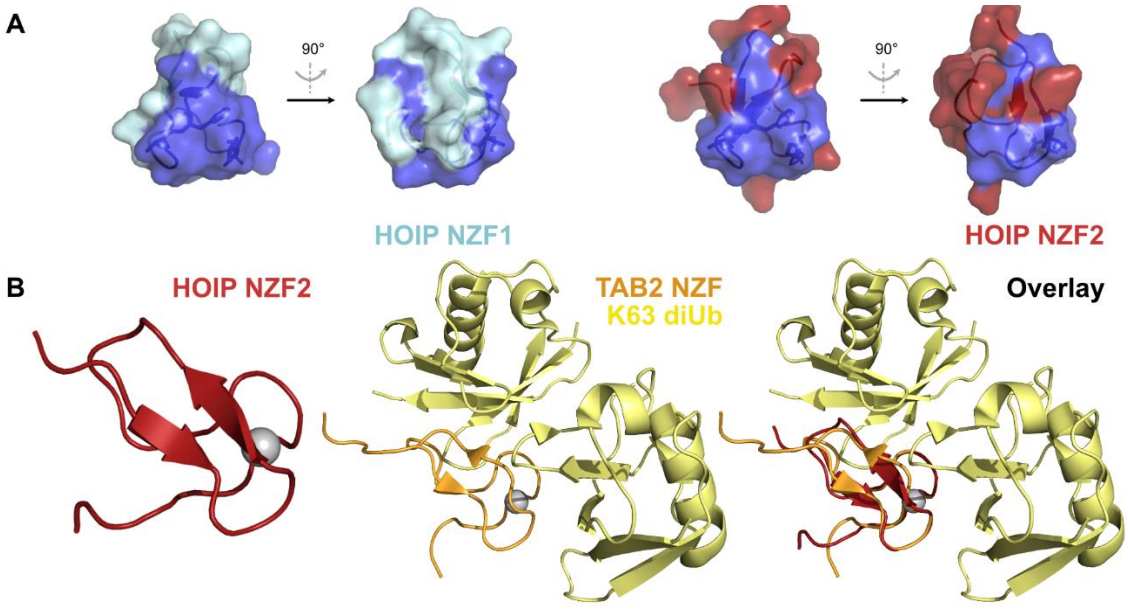


Figure 24: Chemical shift perturbation maps of HOIP NZF1-NZF2 (aa 350-438), derived from its titrations with K48-linked (A) and K63-linked diubiquitin (B) as seen in Figure 23. The cut-off for significant shifts was set as the standard deviation and illustrated as a blue horizontal line. Peaks shifting significantly as defined by the cut-off are coloured in green, peaks not shifting coloured in red, peaks disappearing during the titration coloured in blue with shift value set at 1, not assigned peaks presented as transparent boxes and prolines indicated with a P.

To visualize the newly established binding interface of each NZF with K63-linked diubiquitin, the observed shifts were mapped onto the crystal structure of NZF1. While the structure of NZF2 is unresolved, recent advances in protein structure simulation using the model AlphaFold have provided a structural prediction of all currently

annotated HOIP domains, including NZF2 [95]. As explained, the NZF1 binding interface and orientation relative to those of other NZF domains remains the same with diubiquitin as with monoubiquitin and can be seen in **Figure 16**. This indicates that NZF1 does not possess an extended binding patch even in titrations with polyubiquitin, indicating that it may lack an inherent mechanism for linkage specificity in binding. For NZF2 the binding patch to K63-linked diubiquitin was visualized onto the AlphaFold prediction. The interface is similar to the one of NZF1 and covered a slightly larger surface area (**Figure 25A**). To examine the binding interface for K63 chains specifically, NZF2 was compared to the TAB2 NZF domain, which is K63-specific. The NZF domains adopt similar folds (**Figure 25B**). While the canonical T419F420/M431 NZF motif contacts the distal ubiquitin of the diubiquitin, the binding patch is extended by residues V412 and W413 but forms no contacts with the proximal ubiquitin moiety (**Figure 25C**). This is in contrast to the binding interface of TAB2, which is elongated and facilitates binding to both the distal and the proximal ubiquitin (**Figure 25D**). The differences between HOIP NZF2 and TAB2 NZF binding to K63 diubiquitin therefore indicate that NZF2 could bind diubiquitin in a different orientation than the one observed for TAB2 due to the relative position of its extended binding patch to the canonical TF/Φ motif.



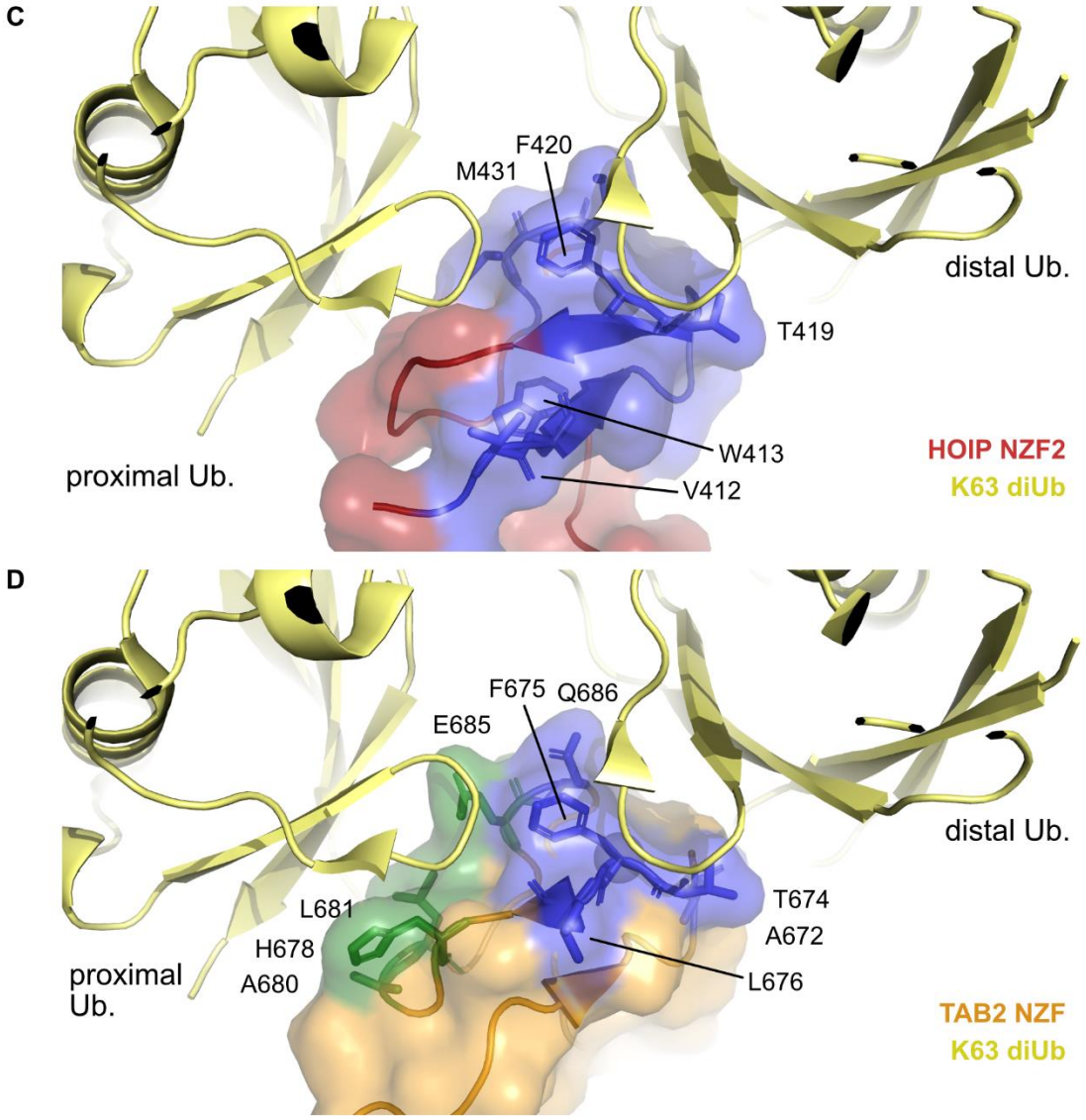


Figure 25: (A) Side-by-side comparison of the NZF1 (PDB: 4OWF, cyan, ubiquitin-binding patch established by NMR in blue) and NZF2 of HOIP (AlphaFold prediction, firebrick red, K63-linked diubiquitin-binding patch established by NMR in blue) in two orientations. The NZF ubiquitin binding pattern TF/Φ is shown as sticks. (B) Superposition on the NZF2 of HOIP (AlphaFold prediction, firebrick red) and the NZF of TAB2 bound to K63-linked diubiquitin (PDB: 2WWZ, NZF in orange, diubiquitin in gold), showing alignment of the NZF fold. (C) Simulation of the NZF2 of HOIP (AlphaFold prediction, firebrick red, K63-linked diubiquitin-binding patch established by NMR in blue) bound to K63-linked diubiquitin (PDB: 2WWZ, gold) showing alignment of the ubiquitin-binding patch with the distal ubiquitin moiety of the diubiquitin. The NZF ubiquitin binding pattern T419F420/M431 as well as residues V412 and W413 are shown as sticks. (D) Structure of the NZF of TAB2 bound to K63-linked diubiquitin (PDB: 2WWZ, NZF in orange, diubiquitin in gold), with the residues contributing to the distal (blue) and proximal (green) ubiquitin binding patches shown as sticks.

As seen in the interaction studies with monoubiquitin, it is vital to examine the binding of NZF domains both as individual and as tandem domains in order to understand their function in detail. The titrations with K48- and K63-linked diubiquitin were therefore

repeated for NZF1 and NZF2 as individual domains. NZF1 binds diubiquitin of both chain types and peaks shift at the lowest molar ratio studied (**Figure 26, Supplementary Figure 10**). Saturation is not reached by the end of either titration, seeing as the spectra for molar ratios NZF1:diubiquitin 1:2 (black) and 1:4 (turquoise) only overlap partially, which is in contrast with the saturation reached in the titrations of the NZF1-NZF2. This could indicate that NZF1-NZF2 has a higher affinity for diubiquitin than NZF1 individually, which agrees with the observation that NZF1 and NZF2 can only bind monoubiquitin individually and, therefore, possibly diubiquitin as cooperative domains.

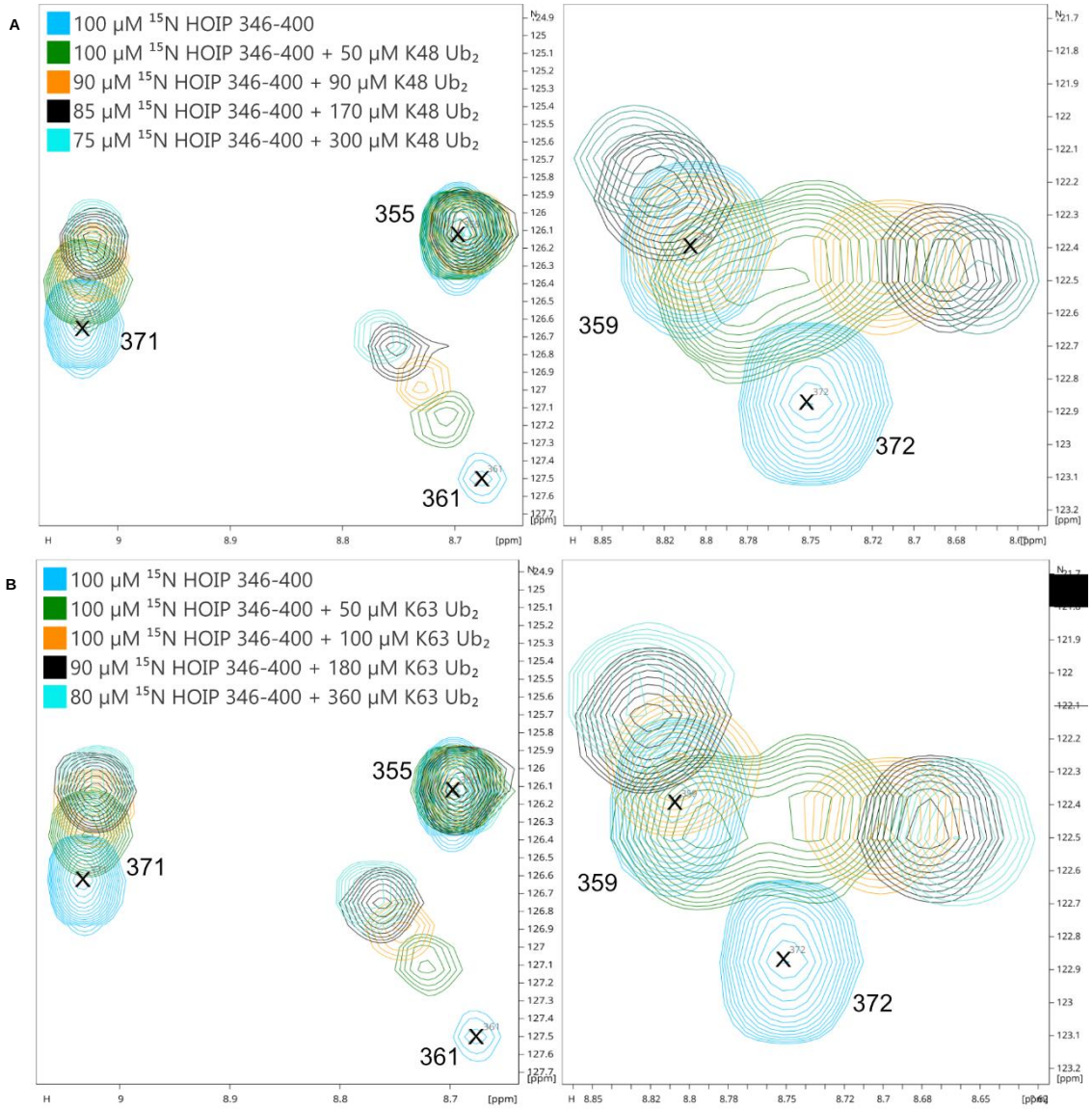


Figure 26: BEST-TROSY spectra of ^{15}N-labelled HOIP NZF1 (aa 346-400, skyblue) and HOIP NZF1 mixed with 1:0.5 molar excess (green), 1:1 molar excess (orange), 1:2 molar excess (black) and 1:4 molar excess diubiquitin (turquoise), with the titration of K48-linked diubiquitin in (A) and K63-linked diubiquitin in (B), showing several peaks shifting upon ubiquitin addition. Close-up of

spectral regions of interest, displaying the shifts of residues A355, F361 and S371 (Left) and C359 and I372 (Right). Full spectra can be found in Supplementary Figure 10.

CSP maps illustrate that NZF1 employs the same residues to bind diubiquitin of both linkage types, centered around the TF/Φ binding patch of ubiquitin-binding NZF domains (**Figure 27**). The NZF1 binding interface for diubiquitin is identical to the one previously established for monoubiquitin (**Figure 15**), confirming the observation arising from the NZF1-NZF2 diubiquitin titration that NZF1 preserves its monoubiquitin binding patch for binding diubiquitin moieties and probably does not possess an extended ubiquitin binding patch similar to linkage-specific NZF domains.

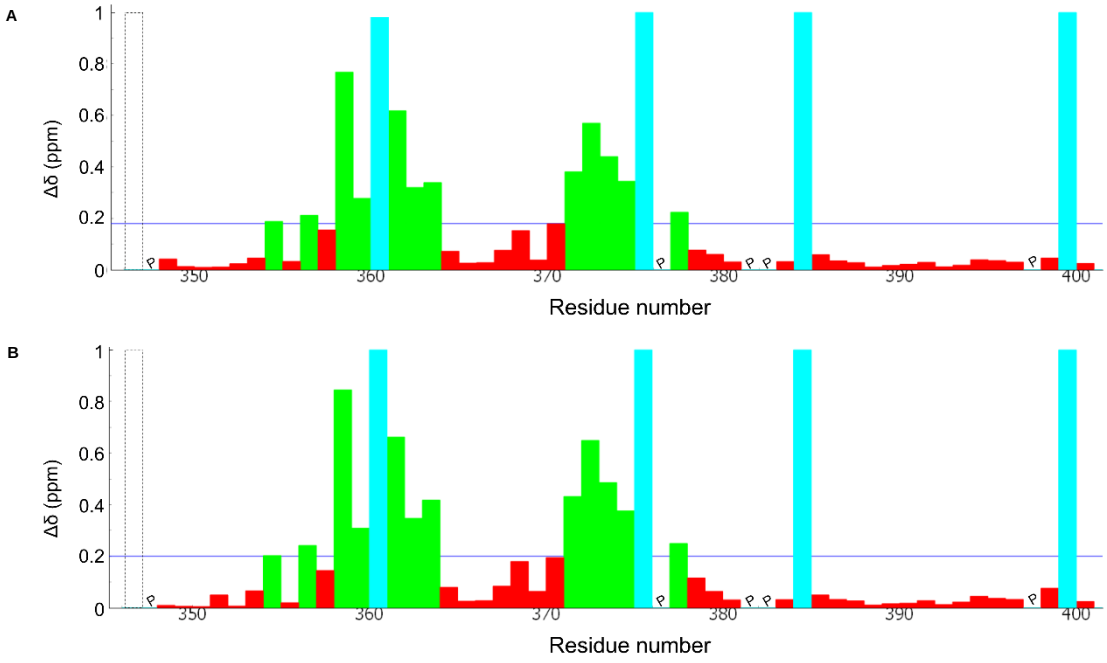


Figure 27: Chemical shift perturbation maps of HOIP NZF1 (aa 346-400), derived from its titrations with K48-linked (A) and K63-linked diubiquitin (B) as seen in Figure 26. The cut-off for significant shifts was set as the standard deviation and illustrated as a blue horizontal line. Peaks shifting significantly as defined by the cut-off are coloured in green, peaks not shifting coloured in red, peaks disappearing during the titration coloured in blue with shift value set at 1, not assigned peaks presented as transparent boxes and prolines indicated with a P.

NZF2 is able to bind diubiquitin of both linkage types, as shown in **Figure 28** (**Supplementary Figure 11**). The ubiquitin-binding residues do not reach saturation, which can be attributed to a low affinity to diubiquitin. Similarly to NZF1 this is in stark

contrast to the shifts observed for the NZF1-NZF2 and would indicate that the affinity of NZF2 to diubiquitin is higher in constructs where NZF1 also contributes to the binding.

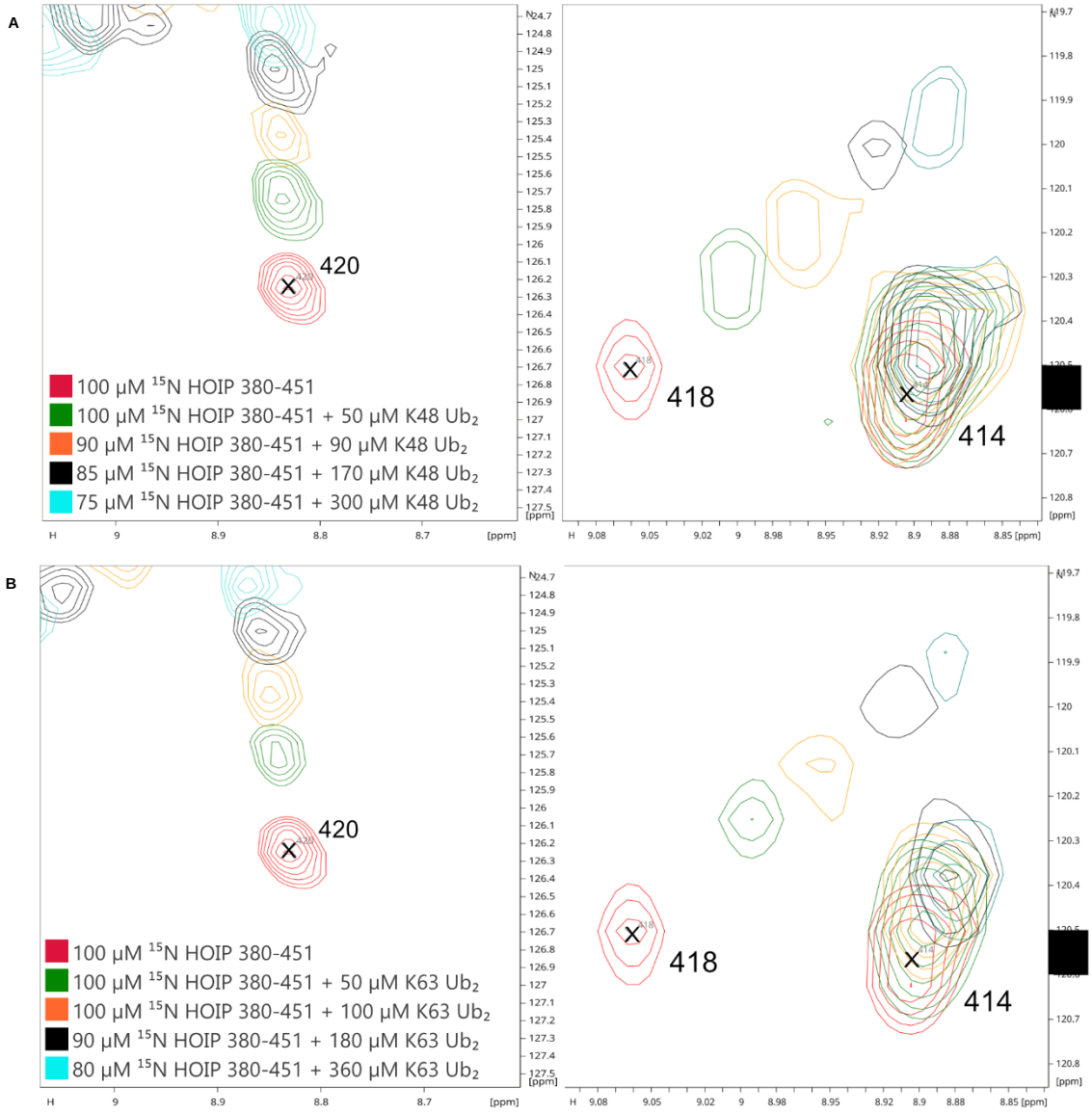


Figure 28: BEST-TROSY spectra of ^{15}N-labelled HOIP NZF2 (aa 380-451, red) and HOIP NZF2 mixed with 1:0.5 molar excess (green), 1:1 molar excess (orange), 1:2 molar excess (black) and 1:4 molar excess diubiquitin (turquoise), with the titration of K48-linked diubiquitin in (A) and K63-linked diubiquitin in (B), showing several peaks shifting upon ubiquitin addition. Close-up of spectral regions of interest, displaying the shift of residue F420 (Left) and Y414 and C418 (Right). Full spectra can be found in Supplementary Figure 11.

CSP map analysis of the binding events illuminates similarities but also differences in the binding characteristics of NZF2 with and without NZF1 (**Figure 29**). Residues shift stronger on average in the NZF1-NZF2, indicated by the maximum value of 1.5 ppm when NZF1 is present compared to 1.05 ppm here. NZF2 binds K48-linked diubiquitin in

a similar manner as an individual domain and in tandem with NZF1, however differences arise in regard to the K63 binding interface. Residues V412, W413, T419 and V430 do not shift significantly when NZF1 is not present. For V412 and W413 a possible explanation is the flexibility of the N-terminus of the NZF2 construct. The residues directly precede the linker region between NZF1 and NZF2, which is far more flexible than in NZF1-NZF2, since it is not constrained by the presence of a folded domain N-terminally, increasing the flexibility of the N-terminal residues V412 and W413 and impeding their interaction with diubiquitin. C-terminally residues R434, S436 and H443 shift only upon K63 binding to the NZF2 construct. This too could be an effect of construct design; the NZF1-NZF2 construct used for diubiquitin titrations includes amino acids 350-438, possibly increasing the flexibility of the C-terminus of the construct and hindering its interaction with diubiquitin. The NZF2 construct possesses an elongated C-terminus, possibly facilitating aa R434, S436 and H443 binding to K63 diubiquitin.

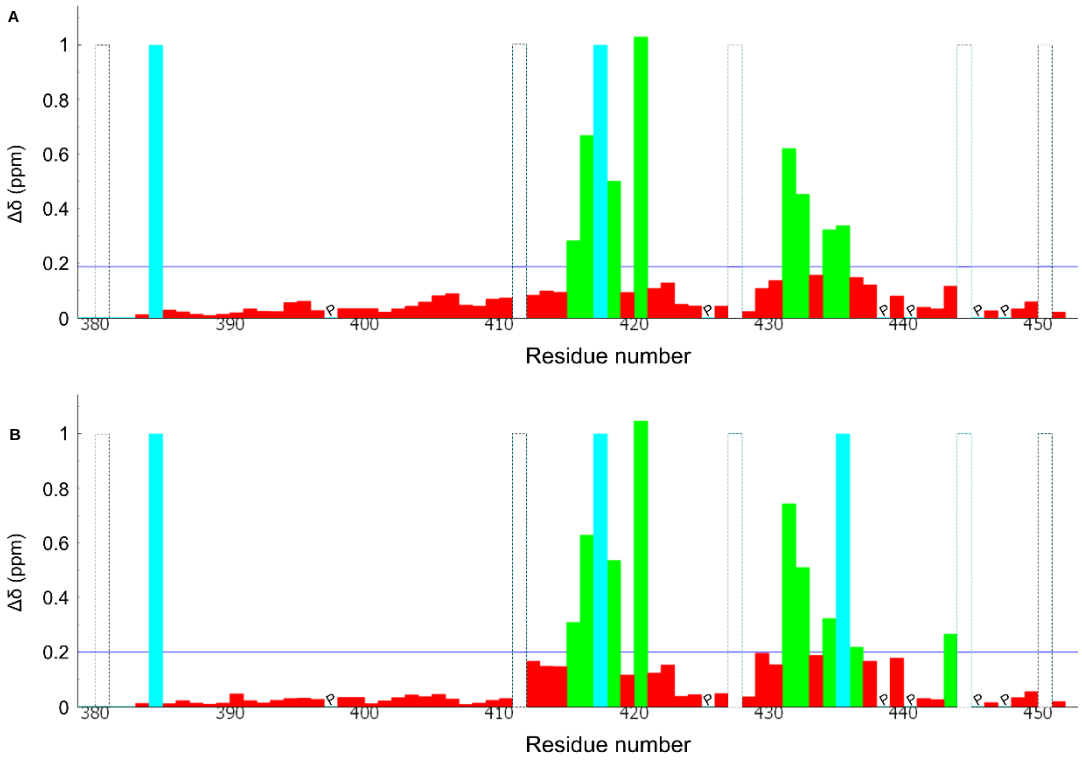
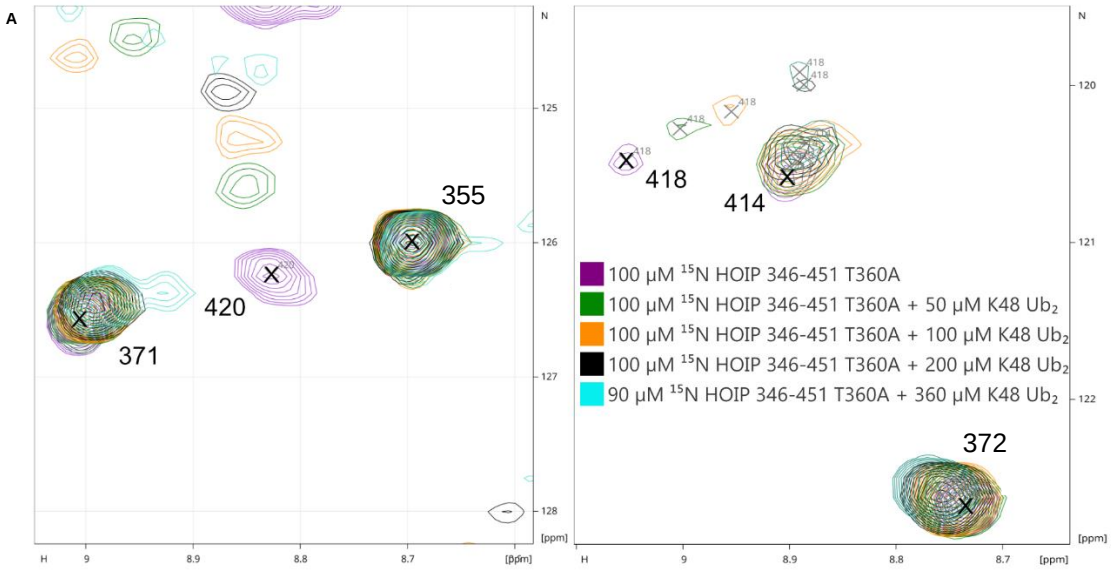


Figure 29: Chemical shift perturbation maps of HOIP NZF2 (aa 380-451), derived from its titrations with K48-linked (A) and K63-linked diubiquitin (B) as seen in Figure 28. The cut-off for significant shifts was set as the standard deviation and illustrated as a blue horizontal line. Peaks shifting significantly as defined by the cut-off are coloured in green, peaks not shifting coloured

in red, peaks disappearing during the titration coloured in blue with shift value set at 1, not assigned peaks presented as transparent boxes and prolines indicated with a P.

To delve further into the role of NZF2 residues in diubiquitin binding and study the interplay between NZF1 and NZF2 in regard to chain specificity, the titrations were repeated with the NZF1-NZF2 T360A mutant, in which only NZF2 is able to bind diubiquitin. The spectra appear similar to the titration of the same construct with monoubiquitin (**Figure 19**), in which NZF1 residues did not shift or shifted significantly less than in the wild-type (**Figure 30, Supplementary Figure 12**). A notable difference between NZF1-NZF2 wild-type and T360A spectra is that in the latter the shifts are not saturated at 1:2 molar excess of K63 diubiquitin (black spectrum) and continue shifting further at 1:4 molar excess (turquoise spectrum). A possible explanation would be that the mutated construct has a lower affinity for diubiquitin than the wild-type has, similarly to the NMR titration of diubiquitin to NZF2 and the observation from ITC that NZF1-NZF2 T360A binds monoubiquitin, and therefore possibly diubiquitin, much weaker than the wild-type. Additionally, abrogating NZF1 binding reverses the increase in local ubiquitin concentration observed in the NZF1-NZF2, affecting the shifts of NZF2 residues.



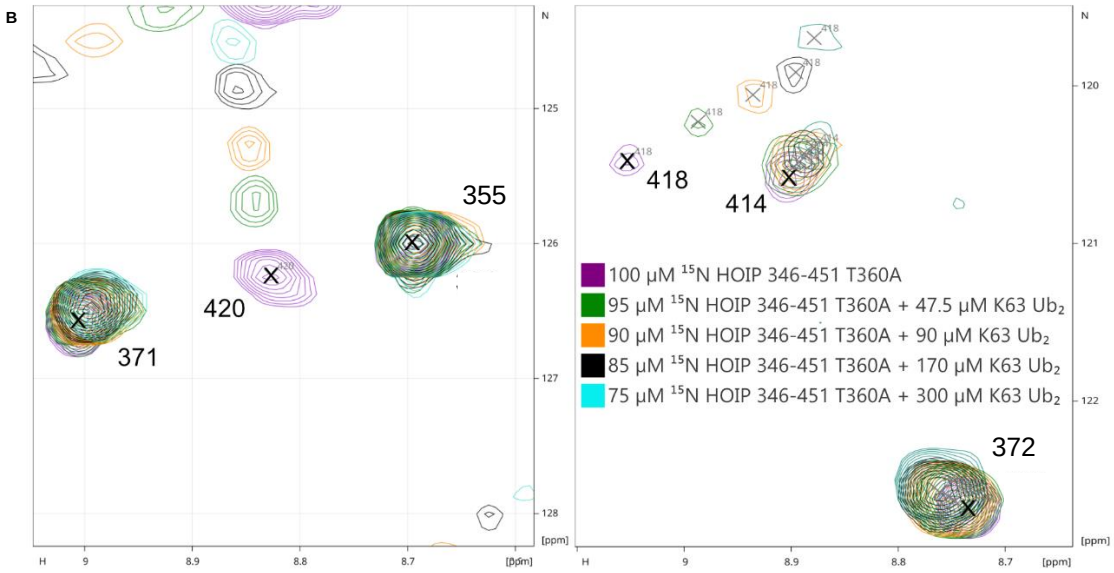


Figure 30: BEST-TROSY spectra of ^{15}N-labelled HOIP NZF1-NZF2 T360A (aa 346-451, purple) and HOIP NZF1-NZF2 mixed with 1:0.5 molar excess (green), 1:1 molar excess (orange), 1:2 molar excess (black) and 1:4 molar excess diubiquitin (turquoise), with the titration of K48-linked diubiquitin in (A) and K63-linked diubiquitin in (B), showing several peaks shifting upon ubiquitin addition. Close-up of spectral regions of interest, displaying the shifts of residues A355, S371 and F420 (Left) and I372, Y414 and C418 (Right). The peaks of residues C359 and F361 have changed their spectral positions due to their proximity to the mutated residue T360A. Full spectra can be found in Supplementary Figure 12.

The shifted residues were analysed in a CSP map (**Figure 31**, A for K48, B for K63 chains). As with monoubiquitin nearly no NZF1 residues shifted upon diubiquitin addition. NZF2 residues shift slightly less strongly than in the wild-type NZF1-NZF2 construct (wild-type: 1.5 ppm, here: 1.2 ppm), although this could be due to the aforementioned different affinities to diubiquitin and the decrease in the local concentration of ubiquitin compared to the wild-type. The shifts generally follow the pattern seen in the NZF1-NZF2 wild-type construct. Additionally, residues C429 and I439 shifted only in the mutant titrations, however an increase in the total number of residues interacting with ubiquitin between the wild-type and the NZF1 non-binding mutant T360A was also observed for monoubiquitin (**Figure 21**) and could be subject to the flexibility of ubiquitin binding to NZF2. Interestingly, the shifts in residues V412 and W413 remain even when NZF1 is mutated, meaning that the extended ubiquitin binding pocket of NZF2 shown in **Figure 31** is independent of NZF1 binding to ubiquitin and could allow NZF2 to possess diubiquitin linkage specificity like other described NZF domains. This further supports

the hypothesis that residues V412 and W413 did not shift in the titration of NZF2 with K63-linked diubiquitin due to the increased flexibility of the linker region.

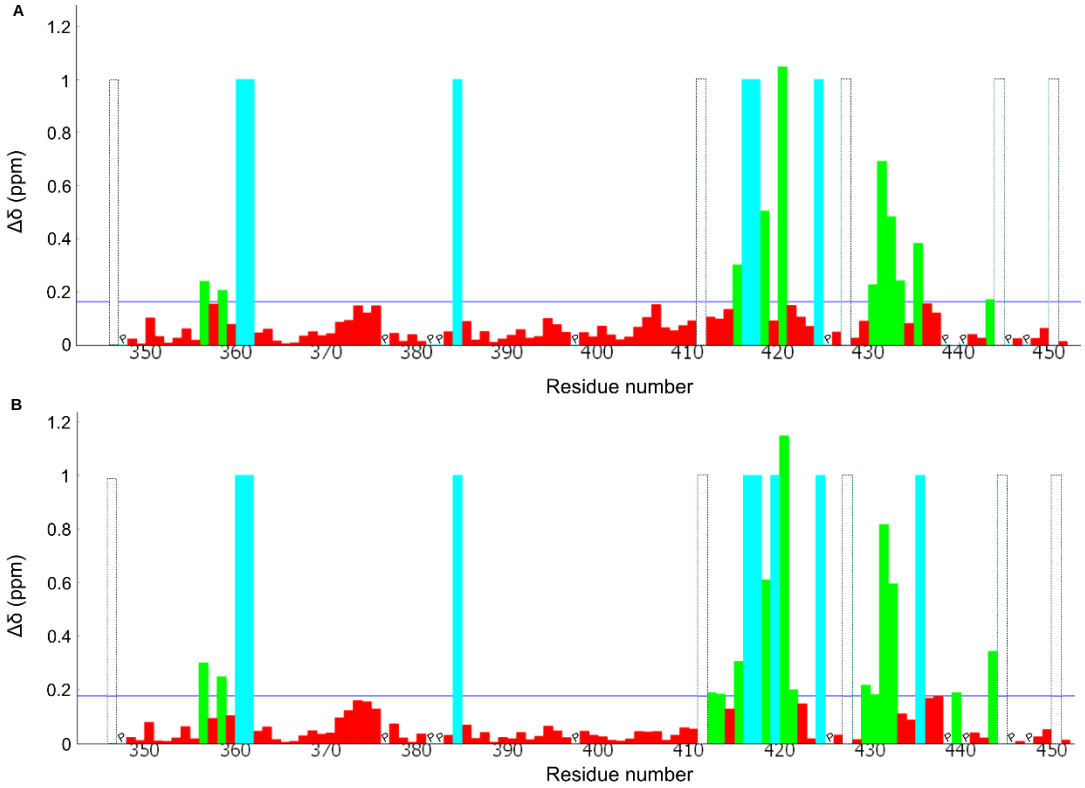


Figure 31: Chemical shift perturbation maps of HOIP NZF1-NZF2 T360A (aa 346-451), derived from its titrations with K48-linked (A) and K63-linked diubiquitin (B) as seen in Figure 25. The cut-off for significant shifts was set as the standard deviation and illustrated as a blue horizontal line. Peaks shifting significantly as defined by the cut-off are coloured in green, peaks not shifting coloured in red, peaks disappearing during the titration coloured in blue with shift value set at 1, not assigned peaks presented as transparent boxes and prolines indicated with a P.

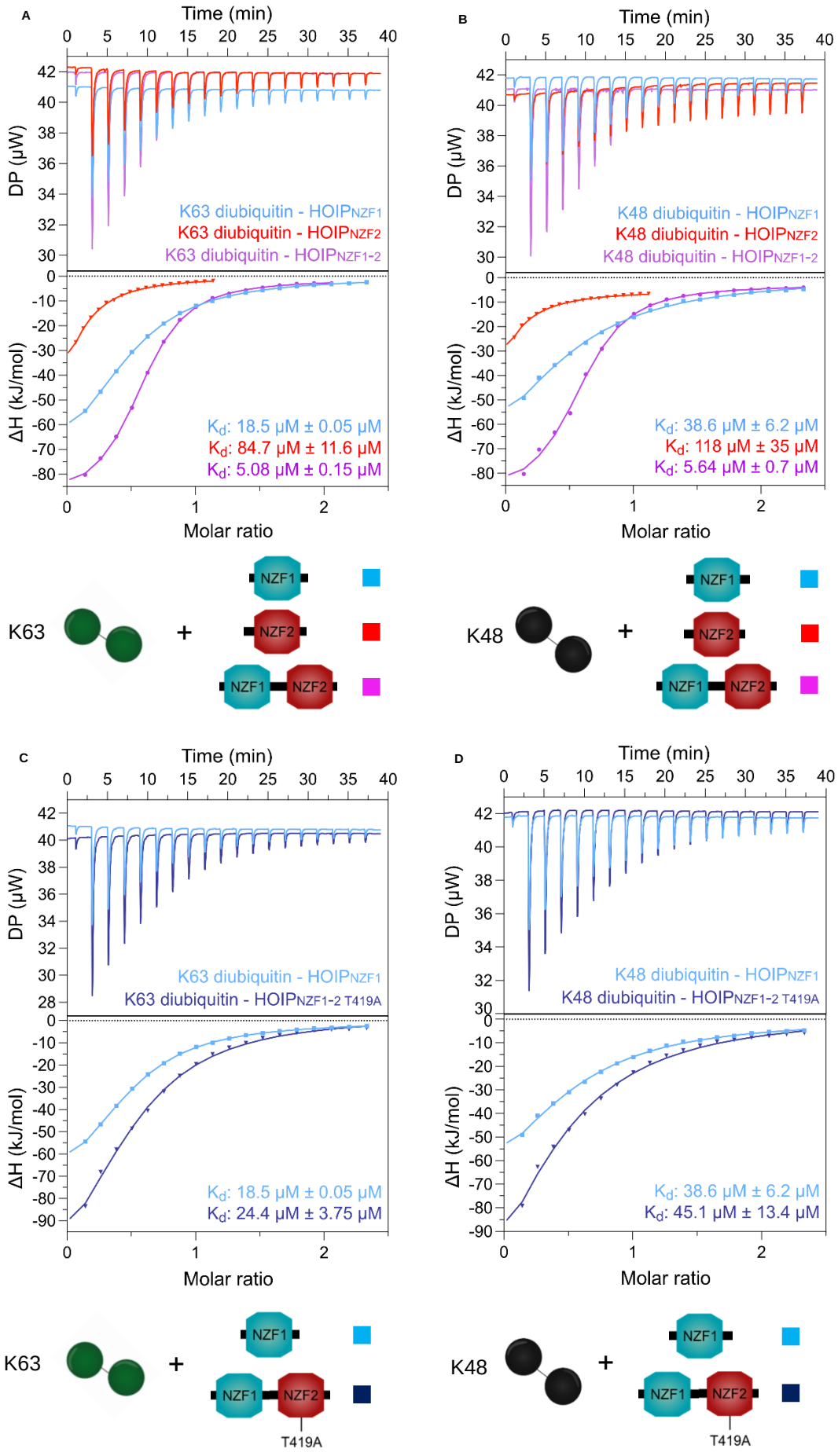
3.8. NZF1 binds ubiquitin chains tighter than NZF2 and the HOIP N-terminus shows specificity for K63 chains

Establishing the binding affinity between NZF1 and NZF2 and diubiquitin of different linkage types is a crucial step in determining HOIP's chain specificity and therefore its recruitment. To confirm the observations from NMR, the interactions of each NZF, as well as the NZF1-NZF2 construct, with K48- and K63-linked diubiquitin were studied with ITC. The K_d values of NZF1-NZF2 wild-type and T360A have been described previously

and, although they show the same trend in terms of chain preference, are now shown to be higher than in the study from 2017 (**Table 3**) [77].

NZF1 shows a clear preference for K63-linked diubiquitin (average K_d of 18.6 ± 0.5 μM) over K48-linked diubiquitin (average K_d of 40.1 ± 5.0 μM) (**Figure 32A-B**), binding both with a stoichiometry of approximately 0.5, meaning a ratio of one NZF1 binding to two diubiquitin molecules. Interestingly enough, its affinity to K63 chains is in the realm of the one observed for monoubiquitin. This effect is reverse in the NZF1-NZF2 T419A construct. Here affinity to monoubiquitin is much lower than for NZF1 on its own (see *NZF1 binds to monoubiquitin stronger than NZF2*), but the construct binds to diubiquitin comparably to NZF1 (**Figure 32C-D**). The elongation of the construct to include NZF2, therefore affects NZF1 monoubiquitin, but not diubiquitin binding, or its chain preference. As with monoubiquitin, the low affinity interactions of NZF2 led to wide error margins, but the results still clearly indicated that NZF2 has a preference for K63 over K48 chains. The resulting K_d values are higher than the ones calculated for monoubiquitin, but stoichiometry remained low, less than 0.1. As with NZF1, the NZF1-NZF2 T360A construct was used to assess the contribution of NZF1 to NZF2 binding and specificity. It possesses affinities similar to the ones of NZF2 on its own, confirming that the presence of NZF1 does not inherently affect the interaction of NZF2 with ubiquitin (**Figure 32E-F**). The measurements involving NZF2 and NZF1-NZF2 T360A must, however, be repeated, since the values inferred from data with such high error margins and low stoichiometry cannot be interpreted reliably.

In HOIP NZF1 and NZF2 are not found isolated from one another and must therefore be studied together in terms of establishing the protein's chain specificity. NZF1-NZF2 has a higher affinity for K63 over K48 chains, with K_d values up to 10 times higher than the ones for monoubiquitin binding. The calculated K_d values for each chain type are up to four times higher than the ones of NZF1 or NZF2 on their own, indicating that NZF1 and NZF2 bind diubiquitin cooperatively, leading to this higher overall affinity for NZF1-NZF2 (**Figure 32A-B**).


A
Time (min)
DP (µW)
K63 diubiquitin - HOIPNZF1
K63 diubiquitin - HOIPNZF2
K63 diubiquitin - HOIPNZF1-2
ΔH (kJ/mol)
Kd: 18.5 µM ± 0.05 µM
Kd: 84.7 µM ± 11.6 µM
Kd: 5.08 µM ± 0.15 µM
Molar ratio
B
Time (min)
DP (µW)
K48 diubiquitin - HOIPNZF1
K48 diubiquitin - HOIPNZF2
K48 diubiquitin - HOIPNZF1-2
ΔH (kJ/mol)
Kd: 38.6 µM ± 6.2 µM
Kd: 118 µM ± 35 µM
Kd: 5.64 µM ± 0.7 µM
Molar ratio
K63
NZF1
NZF2
NZF1 NZF2
K48
NZF1
NZF2
NZF1 NZF2
C
Time (min)
DP (µW)
K63 diubiquitin - HOIPNZF1
K63 diubiquitin - HOIPNZF1-2 T419A
ΔH (kJ/mol)
Kd: 18.5 µM ± 0.05 µM
Kd: 24.4 µM ± 3.75 µM
Molar ratio
K63
NZF1
NZF1 NZF2
T419A
D
Time (min)
DP (µW)
K48 diubiquitin - HOIPNZF1
K48 diubiquitin - HOIPNZF1-2 T419A
ΔH (kJ/mol)
Kd: 38.6 µM ± 6.2 µM
Kd: 45.1 µM ± 13.4 µM
Molar ratio
K48
NZF1
NZF1 NZF2
T419A

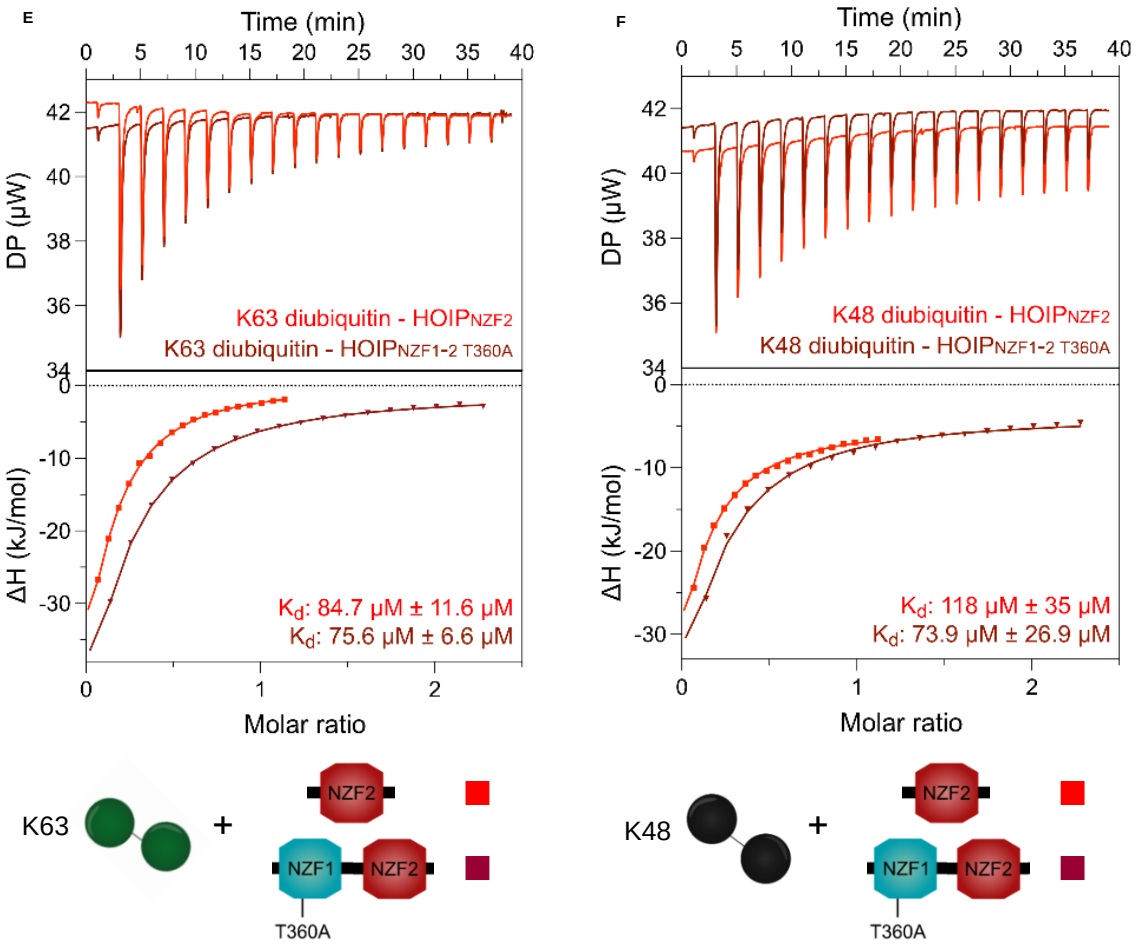


Figure 32: ITC titration curves and graphic illustration of the interaction of HOIP NZF1 (aa 346-400, skyblue), NZF2 (aa 380-451, red) or NZF1-NZF2 wild-type (aa 346-451, purple traces) with K63 diubiquitin (A) or K48 diubiquitin (B), HOIP NZF1 (aa 346-400, skyblue) or NZF1-NZF2 T419A (aa 346-451, dark blue traces) with K63 diubiquitin (C) or K48 diubiquitin (D) and HOIP NZF2 (aa 380-451, red) or NZF1-NZF2 T360A (aa 346-451, dark red traces) with K63 diubiquitin (E) or K48 diubiquitin (F). Two biological replicates were performed for NZF1-2 and NZF1.

Table 3: Thermodynamic parameters for the ITC titration curves of HOIP NZF1, HOIP NZF1-NZF2 T419A, NZF2, HOIP NZF1-NZF2 T360A and HOIP NZF1-NZF2 wild-type, binding to K48- and K63-linked diubiquitin. Two biological replicates were performed for NZF1-2 and NZF1.

Syringe	Cell	K_d (µM)	ΔH (kJ/mol)	-TΔS (kJ/mol)	ΔG (kJ/mol)	N (stoichiometry)
K48 Ub_2	HOIP NZF1	42.8 ± 8.3	-106 ± 47	81.4	-25	0.38 ± 0.14
		38.6 ± 6.2	-103 ± 13.5	77.8	-25.2	0.51 ± 0.03
K63 Ub_2	HOIP NZF1	30.8 ± 5.9	-104 ± 39	78.2	-25.8	0.35 ± 0.11
		18.5 ± 0.05	-88.3 ± 1.22	61.3	-27	0.47 ± 0.03
K48 Ub_2	HOIP NZF2	118 ± 35	-335 ± 937	313	-22.4	0.03 ± 0.08

K63 Ub_2	HOIP NZF2	84.7 ± 11.6	-125 ± 38.7	102	-23.3	0.1 ± 0.02
K48 Ub_2	HOIP NZF1-2	8.49 ± 0.68 5.64 ± 0.7	-59.4 ± 1.4 -87.4 ± 2.6	30.4 57.5	-29 -30	0.75 ± 0.01 0.55 ± 0.01
K63 Ub_2	HOIP NZF1-2	5.81 ± 1.32 5.08 ± 0.15	-61.5 ± 4.5 -90.3 ± 0.7	31.6 60	-29.9 -30.2	0.82 ± 0.04 0.57 ± 0.02
K48 Ub_2	HOIP NZF1-2 T419A	45.1 ± 13.4	-208 ± 66.2	183	-24.8	0.4 ± 0.08
K63 Ub_2	HOIP NZF1-2 T419A	24.4 ± 3.75	-148 ± 14.4	122	-26.4	0.5 ± 0.02
K48 Ub_2	HOIP NZF1-2 T360A	73.9 ± 26.9	-335 ± 1000	311	-23.5	0.04 ± 0.131
K63 Ub_2	HOIP NZF1-2 T360A	75.6 ± 6.56	-335 ± 186	311	-23.5	0.06 ± 0.03

3.9. Construct crystallization aimed to elucidate HOIP's specificity for K63-linked ubiquitin chains

Affinity studies, complemented by NMR experiments, help biophysically characterize a protein interaction, establish its specificity and form an overview of the binding process. In the study of NZF domains crystal structures of the domains bound to mono- or polyubiquitin have provided snapshots of the fine details of the binding mechanism and of the root of the specificity of each NZF, thereby allowing for the formation of a holistic picture when combined with biophysical data. In order to fully characterize the binding of NZF1-NZF2 to ubiquitin chains, I aimed to obtain a crystal structure of the complex of NZF1-NZF2 with K63-linked di- or triubiquitin.

The NZF1-NZF2 construct used to characterize monoubiquitin binding and test the

interaction with binding partners (aa 346-451) was known from previous crystallization attempts to not yield crystals. Trimming the flexible ends of the construct, which includes parts of the linker regions between NZF0 and NZF1 N-terminally and NZF2 and UBA1 C-terminally, would greatly reduce global flexibility and favour compact crystal formation. In order to determine which residues constituted part of these linkers a heteronuclear NOE (HetNOE) spectrum of ^{15}N-labelled HOIP NZF1-NZF2 (aa 346-451) was collected. HetNOE experiments provide information on how rigid or flexible an amino acid is by studying how every individual ^{1}H-^{15}N vector tumbles in solution compared to the construct's overall tumbling [96, 97]. The HetNOE is influenced by motions that are faster (ps) than the overall tumbling time (ns). More flexible regions reorient more rapidly, corresponding to a lower HetNOE value, while rigid amino acid sequences, such as folded domains, maintain their structure and tumble with the overall rotational correlation time [86]. As seen in **Figure 33**, the NZF1 and NZF2 domains possess higher HetNOE values (> ~0.5) compared to the linker domain between them as well as the termini. This allows for a clearer annotation of the domains as follows: NZF1 (aa 350-379), NZF1-NZF2 linker (aa 380-409) and NZF2 (aa 410-444), with the linker region appearing more flexible than the domains, although not as flexible as the construct's termini.

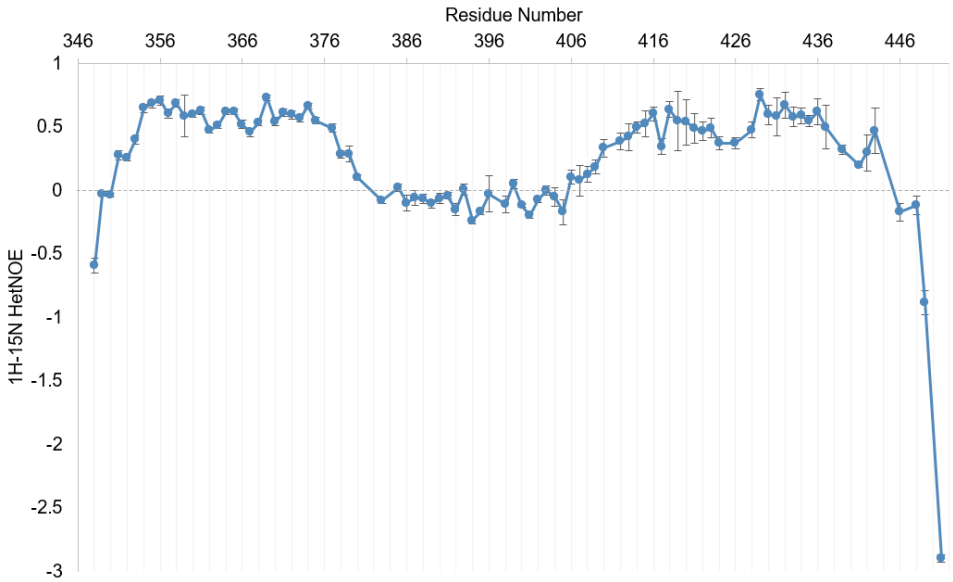


Figure 33: ^{1}H-^{15}N HetNOE values for HOIP NZF1-NZF2 (aa 346-451), with the standard deviation of individual values indicated as bars. Prolines and other not assigned residues Q411, W427, A444 and S450 not indicated.

After determining these more flexible residues, a new NZF1-NZF2 construct was designed (NZF1-NZF2*, aa 350-438), which omitted the N-terminal residues 346-350, the C-terminal residues of NZF2 438-444, due to their flexibility relative to the rest of the domain, and the subsequent linker region 445-451. To ensure that shortening the ends of the construct did not affect its fold it was produced ^{15}N-labelled and its ^{1}H-^{15}N BEST-TROSY spectrum was collected and compared to that of the previous construct (HOIP NZF1-NZF2, aa 346-451). The two spectra largely overlap, with the exceptions of the shortened termini, which were not present for NZF1-NZF2* (e.g. residue 448 in **Figure 34**), and the new N-terminus of NZF1-NZF2*, which could not be detected (**Figure 34**, **Supplementary Figure 13**).

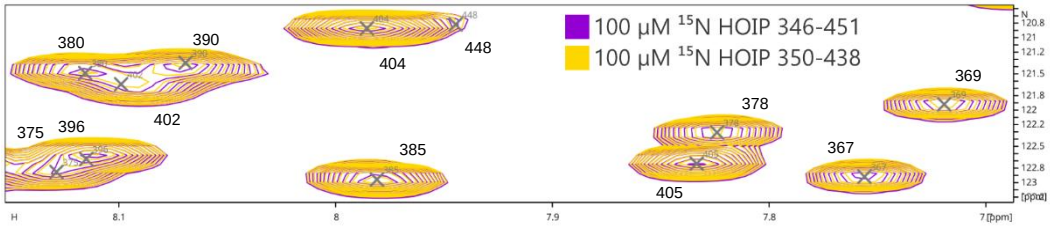


Figure 34: BEST-TROSY spectra of ^{15}N-labelled HOIP NZF1-NZF2 (aa 346-451, purple) and the truncated construct HOIP NZF1-NZF2* (aa 350-438, gold), with the backbone assigned residues of the longer construct displayed. Full spectra can be found in Supplementary Figure 13.

It was therefore concluded that the new construct preserves the NZF folds of the previous construct, which was proven to bind to ubiquitin chains with an established specificity, and could be used for crystallization. An SDS-PAGE analysis of the SEC fractions of NZF1-NZF2*, K63-linked diubiquitin and K63 triubiquitin used for crystallization screens can be seen in **Figure 35**, with the used fractions indicated at the top. The expected molecular weight of the NZF1-NZF2* construct is 9.7kDa and runs slightly lower here. However, the ^{15}N-labelled construct possessed all amino acids of the construct and ran at the same height, meaning this is not a degraded form and in fact the full construct. K63-linked ubiquitin chains run at the expected molecular weight as described in literature [83]. K63-linked diubiquitin tends to form aggregates when in high concentrations, causing the higher molecular weight bands seen here.

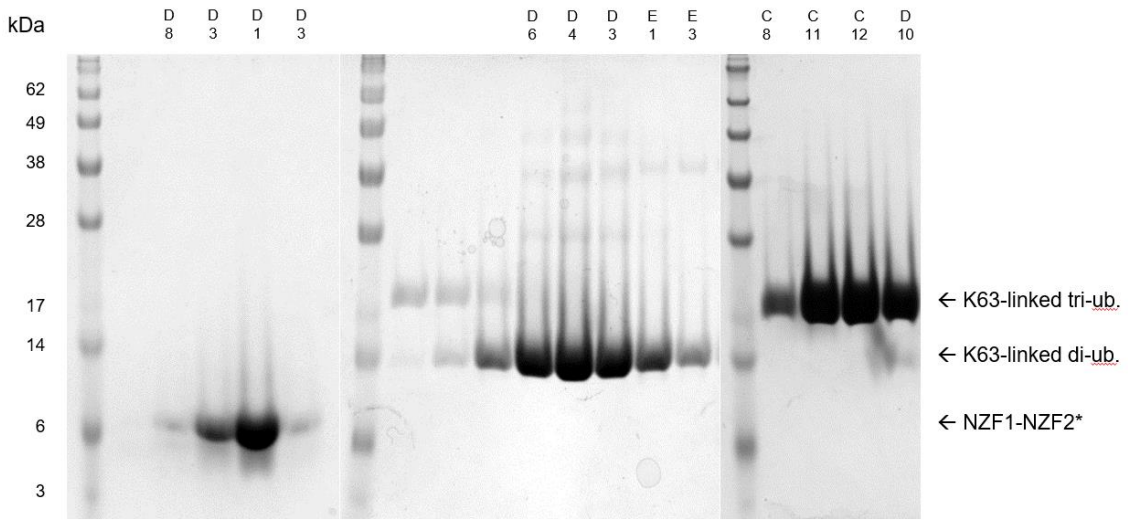


Figure 35: Coomassie-stained SDS-PAGE analysis of the proteins used for crystallization. From left to right: HOIP NZF1-NZF2 (aa 350-438), K63-linked diubiquitin, K63-linked triubiquitin.

NZF1-NZF2* was mixed in a 1:1.2 molar excess with K63-linked diubiquitin or, separately, with K63-linked triubiquitin and concentrated to 16mg/mL and 15mg/mL, respectively. These complexes were used directly for an initial screen, where the complex was mixed 1:1 with the precipitant and which produced a variety of hits in the form of spherulites, after 5 days in conditions containing sulfate salts, and needle-like crystals, after two weeks when sodium and potassium phosphate were present. Fine cubic crystals also formed quickly in zinc-containing conditions (**Figure 36A**); however they were identified as crystals of ubiquitin in complex with zinc ions. Refinement screens were set up centered around the hits of the initial screens. They were set up for both diubiquitin and triubiquitin in a 1:1 mix with the precipitant and separately for the diubiquitin complex in a 2:1 and 1:2 mixture with the precipitant. Similarly to the initial hits, numerous spherulites formed in the sulfate conditions of both di- and triubiquitin complexes and some needle-like crystals formed in conditions with phosphates, although the diubiquitin complex yielded overall better results and was selected to continue the crystallization efforts. The spherulites of the NZF1-NZF2·K63-linked diubiquitin complex were harvested, crushed and used for microseeding the complex in new conditions in a 1:1:0.5 proportion between precipitant, complex and microseeding

complex. This new screen offered a multitude of interesting crystals in various forms, including larger, uniform crystals (**Figure 36B-C**), some of which will be used for data collection at the Diamond Light Source.

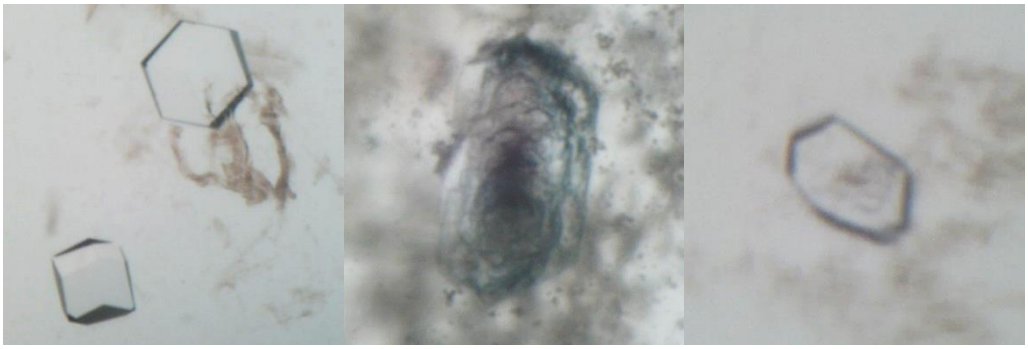


Figure 36: (A) Exemplary image of ubiquitin crystals, typically adopting cubic forms in zinc-containing conditions. (B, C) Uniform crystals appearing in conditions using microseeding.

3.10. Phosphorylation in S383 does not significantly affect polyubiquitin binding

S383 is located in the linker region between NZF1 and NZF2 and is conserved among mammals. It was identified as a phosphorylation site but no physiological function or the kinase responsible have yet been described for this post-translational modification [81]. Phosphorylation is known to modulate ubiquitin binding or even the specificity of enzymes of the ubiquitin code, and the positioning of this site between two UBDs makes it an interesting candidate as a regulator of ubiquitin binding by HOIP [48].

Rather than searching for the kinase responsible for this phosphorylation and phosphorylating the construct in vitro, a phosphomimetic approach was employed. To mimic the structure of phosphoserine S383 was mutated to a glutamic acid, which possesses a similar charge and chemical structure (S383E) [98]. The effect of this mutation was evaluated by ITC, in which the affinity of the wild-type and S383E constructs to K63- and K48-linked diubiquitin was measured. As shown in **Figure 37** the two constructs display similar binding to each diubiquitin type, with a slightly higher

affinity to K63 over K48 chains (**Table 4**). No significant difference was observed between the wild-type and the mutant.

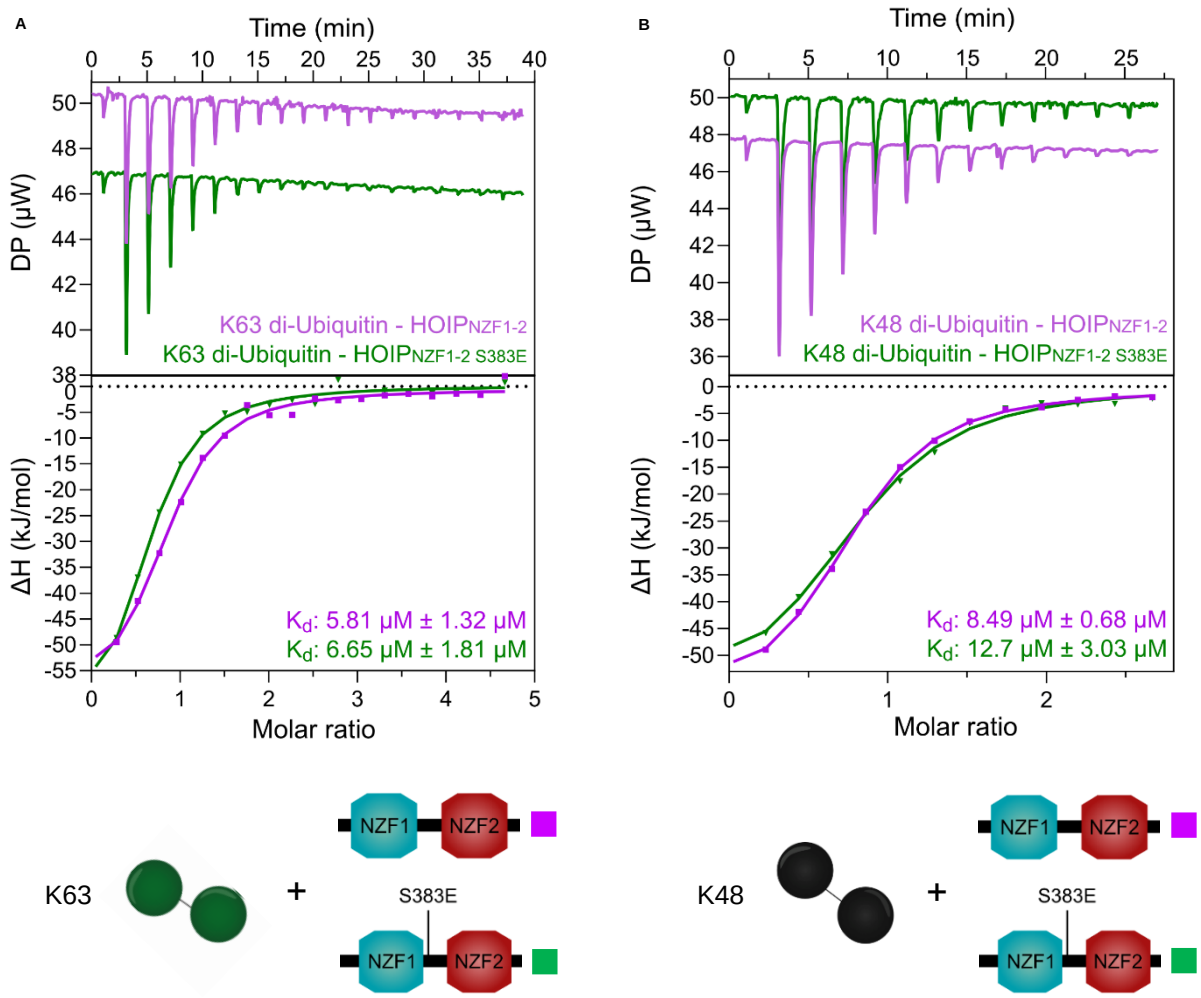


Figure 37: ITC titration curves and graphic illustration of the interaction between HOIP NZF1-NZF2 wild-type (aa 346-451, purple traces) or HOIP NZF1-NZF2 S383E (aa 346-451, green traces) with K63-linked diubiquitin (A) and K48-linked diubiquitin (B). Two biological replicates were performed for NZF1-2.

Table 4: Thermodynamic parameters for the ITC titration curves of HOIP NZF1-NZF2 wild-type and S383E (aa 346-451) binding to K63- and K48-linked diubiquitin. Two biological replicates were performed for NZF1-2.

Syringe	**Cell**	**K_d (µM)**	**ΔH (kJ/mol)**	**-TΔS (kJ/mol)**	**ΔG (kJ/mol)**	**N (stoichiometry)**
K48 Ub_2	HOIP NZF1-2	8.49 ± 0.68 5.64 ± 0.7	-59.4 ± 1.4 -87.4 ± 2.6	30.4 57.5	-29 -30	0.75 ± 0.01 0.55 ± 0.01

K48 Ub_2	HOIP NZF1-2 S383E	12.7 ± 3.0	-59.9 ± 5.0	31.9	-28	0.80 ± 0.02
K63 Ub_2	HOIP NZF1-2	5.81 ± 1.32 5.08 ± 0.15	-61.5 ± 4.5 -90.3 ± 0.7	31.6 60	-29.9 -30.2	0.82 ± 0.04 0.57 ± 0.02
K63 Ub_2	HOIP NZF1-2 S383E	6.65 ± 1.81	-70.0 ± 8.1	40.4	-29.6	0.62 ± 0.05

3.11. HOIP's oligomerization is controlled by the B-box domain and does not influence ubiquitin chain affinity

HOIP has been hypothesized to be a dimer in cells, with oligomerization facilitated by its B-box domain [53]. Adjacent to the B-box are the UBDs NZF1 and NZF2, indicating that in a dimeric form four UBDs would be in proximity, possibly influencing the ubiquitin-binding abilities of the dimer. This set of domains could possess a binding affinity higher than the monomer and furthermore stabilize the interaction with longer chains, which are LUBAC's substrates for recruitment to inflammatory signaling complexes. In order to test this hypothesis the binding of the zinc-finger region of HOIP to longer chains must be measured and compared between the wild-type, a monomeric mutant and the NZF1-NZF2 alone.

A crystal structure of the B-box domain revealed its ability to form homodimers in solution (Elliott Lab, unpublished). Residue L219 is vital in the formation of the dimeric interface. To test whether the B-box is the only domain in the N-terminus necessary for dimer formation, point mutants of the zinc finger region of HOIP were generated where L219 was mutated to more (L219I) or less hydrophobic (L219D, L219R, L219Y) amino acids, in order to observe effects on the dimer interface. The molar mass of the constructs was then measured by SEC-MALS, using two different concentrations per construct (**Figure**

38, **Table 5**). Slight contaminations of 13kDa were observed for both concentrations of the L219R construct, which has a mass of 25kDa. Since the contaminant's molecular weight and mass fraction was the same for both concentrations it is possible that it stems from the purification of the construct, most probably from a degraded form previously not separated on the size exclusion column.

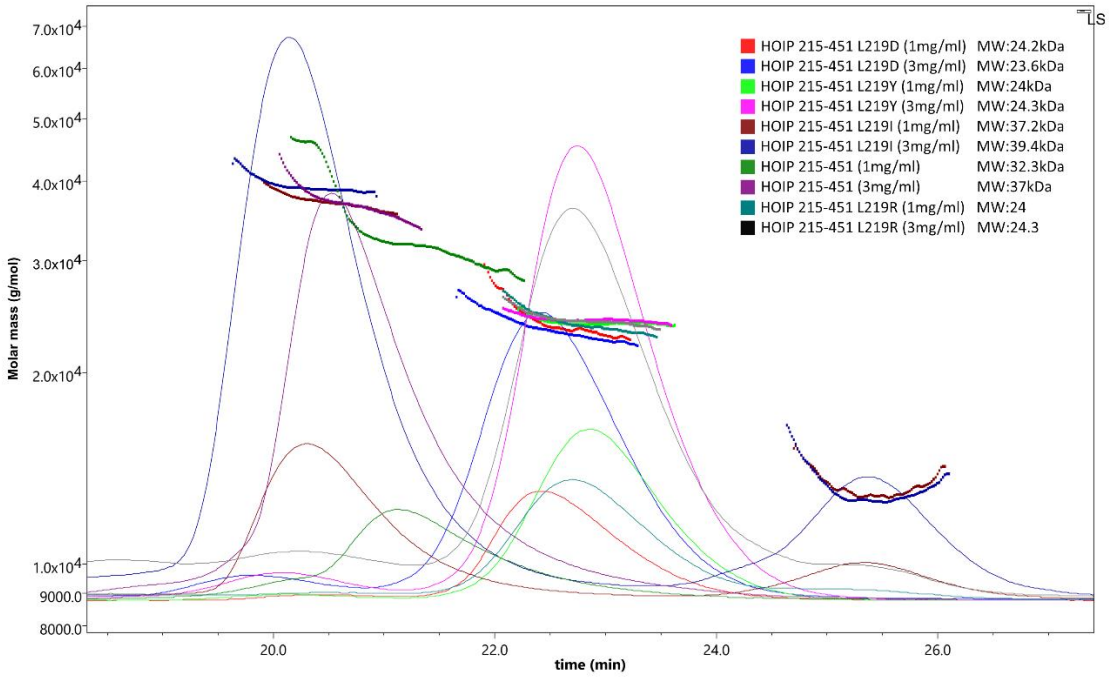


Figure 38: SEC-MALS analysis of HOIP's zinc finger domains and their mutants L219D, L219I, L219R, L219Y on a Superdex 75 column. The observed molecular weight is noted next to each construct, with an average deviation of 0.45%. A contaminant of lower molecular weight (13kDa) was present in the HOIP 215-451 L219I construct.

All five samples show homogenous elution profiles for the two concentrations used. The wild-type construct shows the largest difference in molar mass between the two concentrations, namely a shift of 5kDa. The L219D, L219Y and L219R mutants elute as a monomer with a molar mass of 24kDa for both concentrations. The wild-type and L219I mutant show a mono-dimer exchange state at a low concentration (32.3kDa and 37kDa, respectively) with both of them shifting to higher molar mass in higher concentrations (37kDa and 39.4kDa, respectively). No mutation clearly favoured the formation of only dimers, although L219I leads to the population with the overall highest molar mass. Due to their oligomerization profiles, the L219D, L219R or L219Y mutants were deemed as

monomeric mutants to be used interchangeably to study the effects of oligomerization

Table 5: Calculated molar masses of the HOIP B-box-NZF0-NZF1-NZF2 wild-type and mutant constructs. Although all constructs share the same theoretical molecular weight (MWt), their observed molecular weight infers their oligomeric state in solution.

Construct	Monomer MWt (kDa)	Dimer MWt (kDa)	Observed MW (kDa)	Oligomeric state
B-box-NZF domains	24.89	49.78	32.3 – 37	Monomer-dimer exchange
B-box-NZF domains L219I			37.2 – 39.4	Monomer-dimer exchange
B-box-NZF domains L219D			23.6 – 24.2	Monomer
B-box-NZF domains L219R			24 – 24.3	Monomer
B-box-NZF domains L219Y			24 – 24.3	Monomer

and L219I was the dimeric control, since it leads to a higher molar mass in lower concentrations compared to the wild-type.

ITC was used to measure the effects of oligomerization to ubiquitin chain affinity. Longer K63-linked ubiquitin chains were used, with upwards of six ubiquitin moieties per chain. The wild-type zinc finger region was compared to the monomeric mutant L219R as well as a construct of NZF1-NZF2 alone (**Figure 39**). The stoichiometry of the constructs to ubiquitin chains confirms the oligomerization profile, since the wild-type is in a monomer-dimer exchange and has a higher stoichiometry than the L219R, while NZF1-NZF2 also shows a higher stoichiometry due to numerous constructs binding to one longer chain. All of them showed similar affinities to K63 chains with K_d values ranging between 7 and

10 µM (**Table 6**). Overall no effect of oligomerization in regard to the interaction with long K63-linked polyubiquitin could be observed.

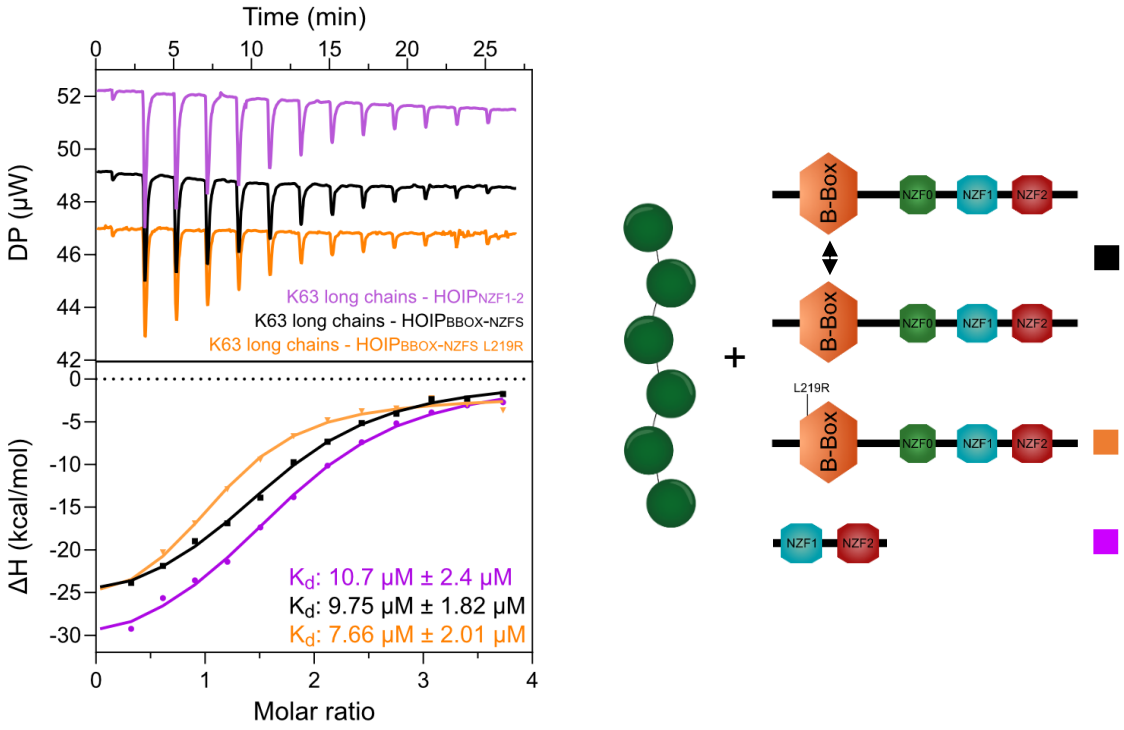


Figure 39: ITC titration curves and graphic illustration of the interaction between HOIP NZF1-NZF2 wild-type (aa 346-451, purple traces), HOIP B-box-NZF0-NZF1-NZF2 wild-type (aa 215-451, black traces) and HOIP B-box-NZF0-NZF1-NZF2 L219R (aa 215-451, orange traces) with long K63-linked polyubiquitin chains.

Table 6: Thermodynamic parameters for the ITC titration curves of HOIP NZF1-NZF2 wild-type, HOIP B-box-NZF0-NZF1-NZF2 wild-type and HOIP B-box-NZF0-NZF1-NZF2 L219R binding to long K63-linked ubiquitin chains.

Syringe	Cell	K_d (µM)	ΔH (kJ/mol)	-TΔS (kJ/mol)	ΔG (kJ/mol)	N (stoichiometry)
K63 Ub_{6+}	HOIP B-box-NZF domains	9.75 ± 1.82	-28.4 ± 1.6	-0.256	-28.6	1.58 ± 0.04
K63 Ub_{6+}	HOIP B-box-NZF domains L219R	7.66 ± 2.01	-26.8 ± 2.2	-2.44	-29.2	1.09 ± 0.04
K63 Ub_{6+}	HOIP NZF1-2	10.7 ± 2.4	-34.3 ± 2.4	5.89	-28.4	1.71 ± 0.06

3.12. The ubiquitin-binding patch of NZF1 overlaps partially with its NEMO binding interface, hindering binding to monoubiquitin

The zinc finger region of HOIP fulfills numerous functions for LUBAC signaling. Apart from ubiquitin chains, the B-box and NZF domains have been known to interact with various signaling partners of the complex, found both upstream and downstream of LUBAC recruitment to inflammatory or xenophagic complexes (*see 1.12. HOIP's zinc finger domains as a potential recruitment center for LUBAC*). Since many of these interactions were established through co-immunoprecipitation assays, it is vital to confirm if they are direct interactions between HOIP and its signaling partners. Upon determining these direct interaction partners, the preference between binding to them versus binding to ubiquitin chains, if the domain is a UBD, must be determined to infer how the zinc finger region balances signaling partner interaction and recruitment.

NZF1 possesses a dual function for HOIP. Firstly, it binds ubiquitin chains to facilitate recruitment to signaling complexes, since its T360A mutant abolishes recruitment to the TNF signaling complex. Secondly, it binds to NEMO, a downstream effector of the pathway, thereby facilitating signaling, inflammation and anti-apoptosis [76]. Immunoprecipitation assays found that NZF1 can fulfill both of its roles simultaneously, claiming that ubiquitin binding and NEMO binding do not influence or counter each other [76]. However, no biophysical data is available regarding this to this date, and we deemed it necessary to complement our findings on ubiquitin binding with the effect of NEMO binding, in order to gain an in-depth perspective into the role of NZF1 in the interaction with ubiquitin chains.

To study this phenomenon the interaction surface of NZF1 and NEMO was established using an NMR titration series. NEMO's CoZi domain is a coiled coil domain and its elongated structure causes anisotropic tumbling in solution, leading its signal, or the

signal of any protein bound it, to experience line broadening. This serves as a characteristic sign of coiled-coil domain binding in 2D NMR and can be seen along the titration series, where the peaks shift far less than with other interaction partners (e.g. ubiquitin), but become increasingly weaker (**Figure 40A**, see green spectrum compared to skyblue in circled peaks). The shifts can be tracked with a CSP map, which shows a broad interface for NEMO binding to NZF1 (**Figure 43**, top). Due to how weak the shifts are, a cut-off value of 1.5 times the standard deviation, rather than simply the standard deviation, was used, in order to avoid false positive shifts.

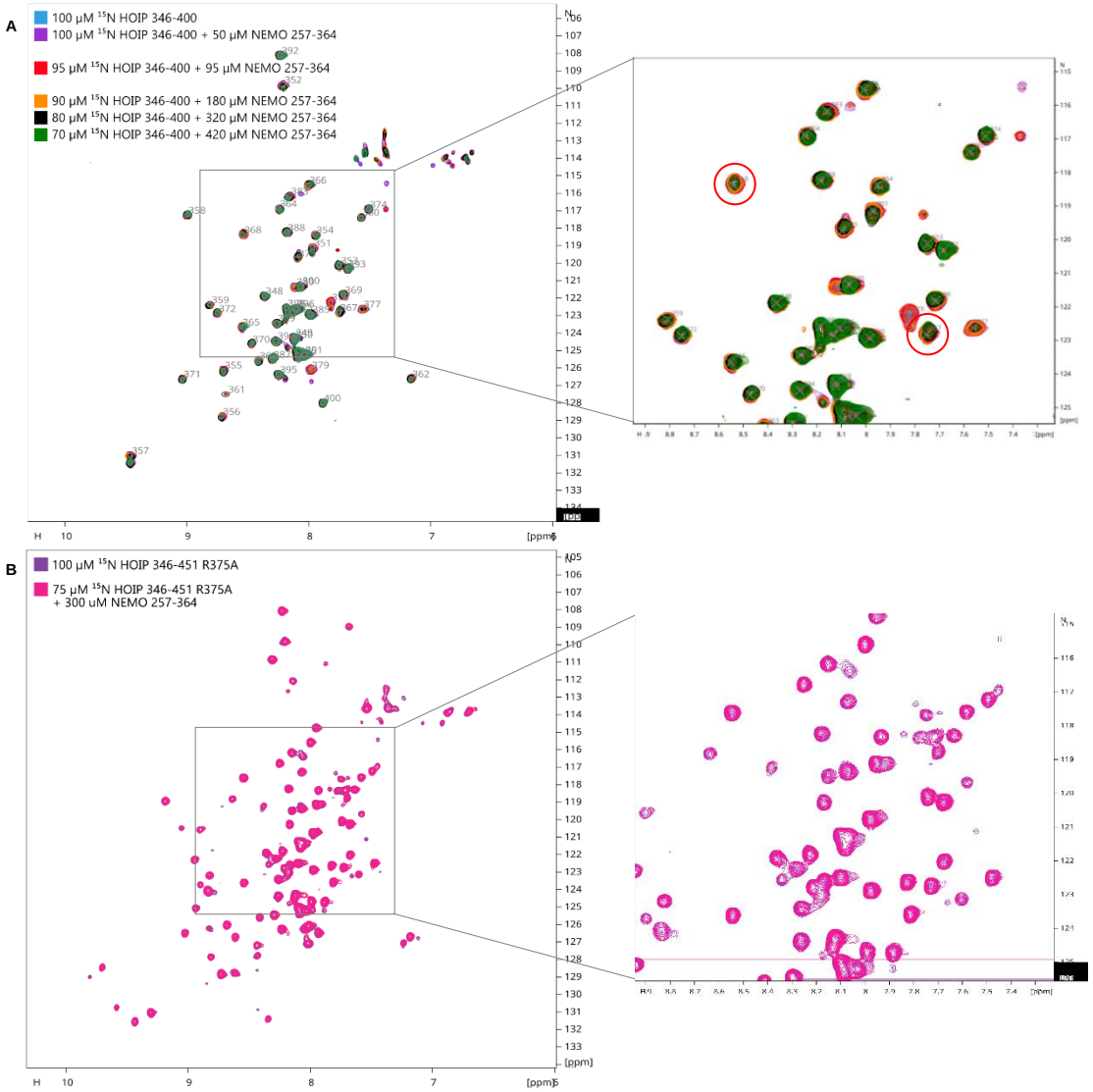


Figure 40: (A) (Left) BEST-TROSY spectra of ^{15}N-labelled HOIP NZF1 (aa 346-400, skyblue) and HOIP NZF1 mixed with 1:0.5 molar excess (purple), 1:1 molar excess (red), 1:2 molar excess (orange), 1:4 molar excess (black), 1:6 molar excess NEMO CoZi domain (aa 257-364) (green), showing several peaks broadening and disappearing during the titration. (Right) Close-up of a spectral region of interest, illustrating the peak broadening and signal loss upon binding to NEMO, with two residues shifting significantly (aa 368, 267) emphasized in red circles. (B) (Left) BEST-

TROSY spectra of ^{15}N-labelled HOIP NZF1-NZF2 R375A (aa 346-451, purple) and mixed with 1:4 molar excess NEMO CoZi domain (aa 257-364, pink), showing no peak shifting or broadening upon NEMO addition. (Right) Close-up of the same region of interest as in (A), showing that previously broadening and shifting residues are now unaffected by the addition of NEMO.

To confirm our model of NEMO binding to NZF1, the mutant NZF1-NZF2 R375A (aa 346-451) was designed. R375 is a vital residue of the NZF1·NEMO interface, as established through the crystal structure of the complex (PDB: 4OWF) [76]. Indeed, no peak broadening or shifting is observed upon mixing with a 1:4 molar excess of NEMO (**Figure 40B**), confirming that such effects on peak location and intensity are binding-dependent and can be used as a measure for the interaction. The NMR spectra of the R375A construct show a change in the positions of the amino acid peaks, indicating a partial change in the fold of the construct (**Figure 41**, left, **Supplementary Figure 14**). While still able to bind monoubiquitin, it was unable to do so to the extent of the wild-type construct (**Figure 41**, right, **Supplementary Figure 14**), raising questions about the interplay of NEMO and ubiquitin binding for NZF1.

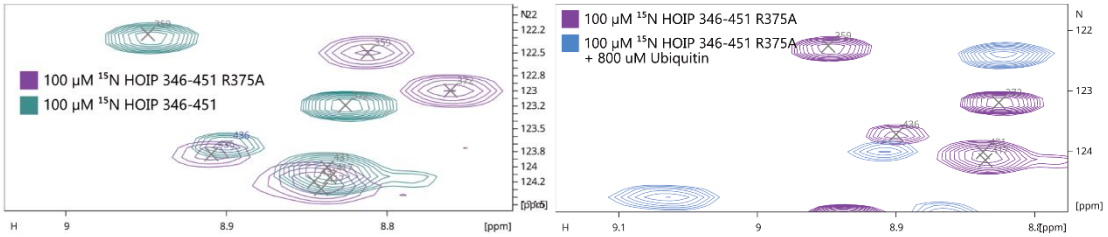


Figure 41: (Left) BEST-TROSY spectra of ^{15}N-labelled HOIP NZF1-NZF2 R375A (aa 346-451, purple) and HOIP NZF1-NZF2 (aa 346-451, cyan), showing several peaks shifting due to the mutation inserted in the construct. (Right) BEST-TROSY spectra of ^{15}N-labelled HOIP NZF1-NZF2 R375A (aa 346-451, purple) and mixed with 1:4 molar excess monoubiquitin (skyblue), showing several peaks shifting upon ubiquitin addition, albeit not as strongly as in the wild-type construct in Figure 17. Full spectra can be found in Supplementary Figure 14.

To determine whether NEMO binding affects monoubiquitin binding, at the end of the NEMO titration the sample was mixed with increasing concentrations of monoubiquitin. Previously observed shifts for monoubiquitin can be seen (**Figure 42**), while the peaks remain weak and broad, indicating that NEMO is still bound to the construct. The shifts caused by the addition of ubiquitin, as seen in **Figure 43**, correspond to the

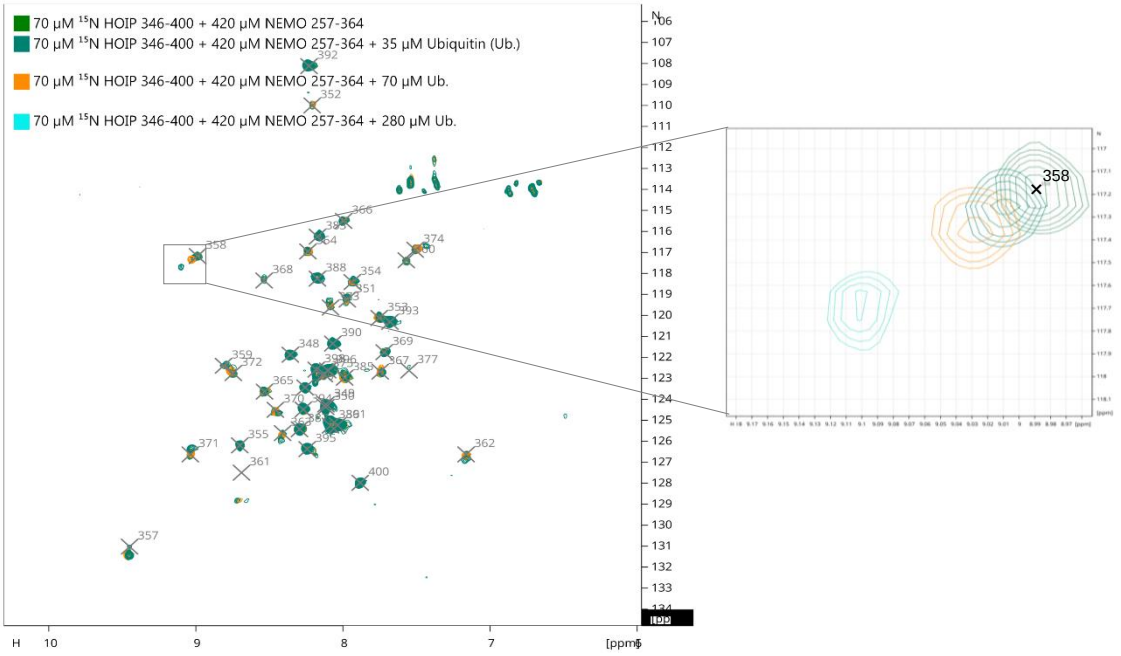


Figure 42: (Left) BEST-TROSY spectra of ^{15}N-labelled HOIP NZF1 (aa 346-400) mixed with 1:6 excess NEMO CoZi domain (aa 257-364) (green) and HOIP NZF1·NEMO CoZi mixed with 1:0.5 molar excess (cyan), 1:1 molar excess (orange) and 1:4 molar excess monoubiquitin (turquoise), showing several peaks shifting upon ubiquitin addition. (Right) Close-up of a spectral region of interest, displaying the shifts of residue S383.

ubiquitin-binding motif previously observed for NZF1 (**Figure 15**), but show weaker CSPs when NEMO is present.

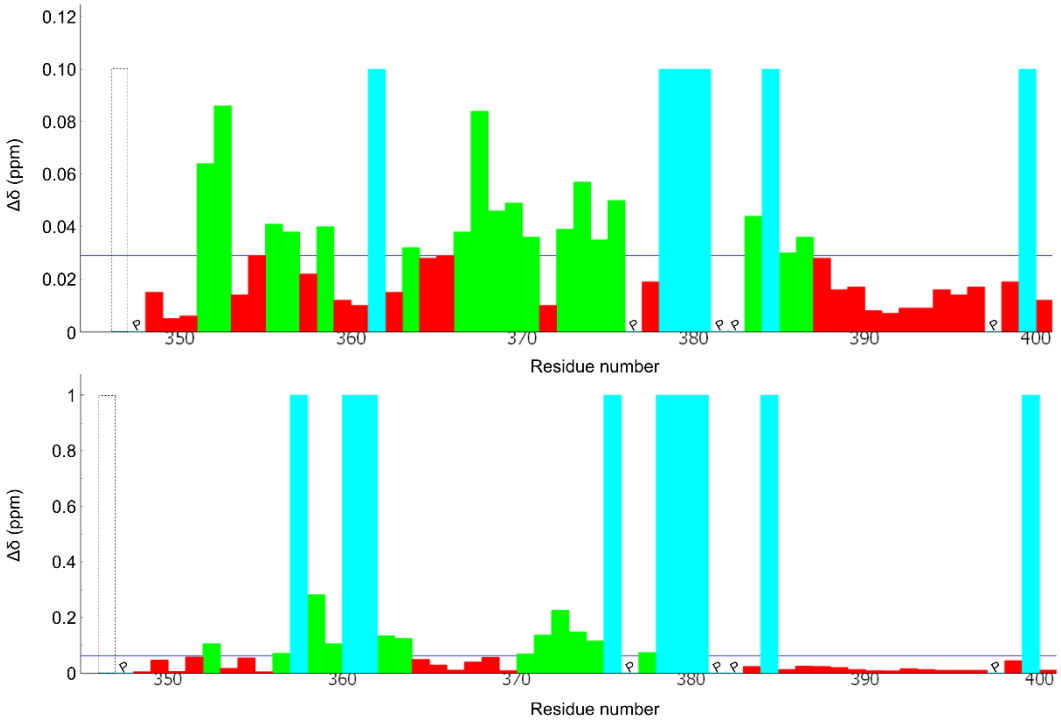


Figure 43: Chemical shift perturbation maps of HOIP NZF1 (aa 346-400), derived from its titration with NEMO CoZi domain (aa 257-364, top) and subsequently with monoubiquitin (bottom) as

seen in Figures 40A and 42, respectively. The cut-off for significant shifts was set as the standard deviation (bottom) and 1.5x the standard deviation (top) due to the small shift values upon NEMO binding and was illustrated as a blue horizontal line. Peaks shifting significantly as defined by the cut-off are coloured in green, peaks not shifting coloured in red, peaks disappearing during the titration coloured in blue with shift value set at 1 (bottom) and 0.1 (top), not assigned peaks presented as transparent boxes and prolines indicated with a P.

To elucidate the reason why NZF1 cannot bind fully to ubiquitin while bound to NEMO, the interaction surfaces were mapped onto the available NZF1·NEMO structure (PDB: 4OWF, **Figure 44A**). The NZF1·NEMO interaction surface calculated by NMR overlaps with the binding patch that results from the crystal structure (orange). The ubiquitin-binding patch (blue) correlates with the conserved NZF·Ub interface, as described in the chapter *NZF1 and NZF2 both bind monoubiquitin via their TF/Φ motif.* Interestingly, there is an overlap between the two patches, highlighted here in green, which encompasses a large part of both interaction surfaces and includes vital residue R375. By mapping the conservation of NZF1 onto its structure, it is clear that the NEMO interface is more highly conserved than the one used for ubiquitin binding (**Figure 44B**), indicating that one binding event may take place preferentially over the other.

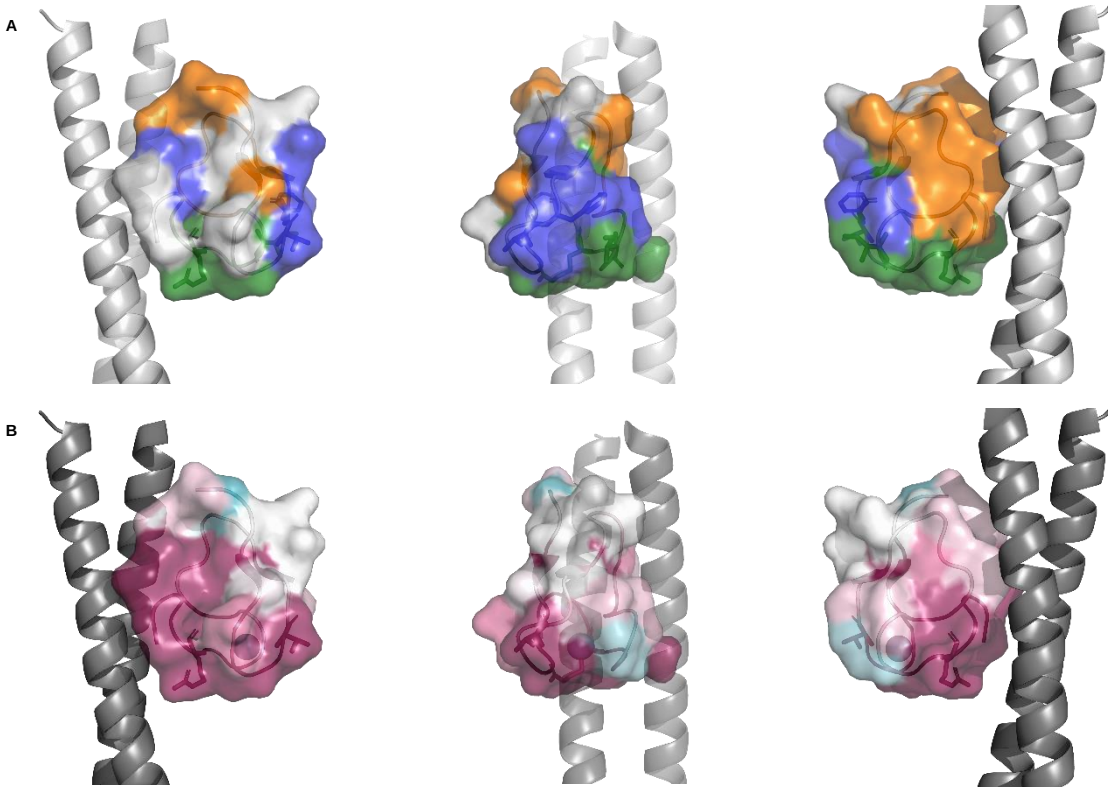


Figure 44: (A) Crystal structure of HOIP NZF1 with NEMO CoZi domain (PDB: 4OWF, surface and cartoon in gray), with the ubiquitin-binding patch of NZF1 established by NMR in blue, the NEMO binding patch in orange and their overlap in green. The residues T360, F361 and R375, vital for ubiquitin and NEMO binding respectively, are shown as sticks. (B) Crystal structure of HOIP NZF1 with NEMO CoZi domain (PDB: 4OWF, cartoon in dark grey), with the surface of HOIP NZF1 coloured according to its sequence conservation using ClustalW (raspberry: highly conserved, pink: conserved, light blue: partially conserved, white: not conserved). The residues T360 and R375, vital for ubiquitin and NEMO binding respectively, are shown as sticks.

To confirm the effect of this overlap on ubiquitin binding, the affinity of the R375A mutant to monoubiquitin was compared to the one of the wild-type via ITC. As expected, NZF1-NZF2 R375A has a lower affinity to monoubiquitin than NZF1-NZF2 wild-type, although binding to monoubiquitin is not abolished in the mutant (**Figure 45, Table 7**). This confirms that R375 is a residue vital for NEMO binding and significant for ubiquitin binding and illustrates that the overlap in the binding patches of NZF1 affects its binding to each interaction partner.

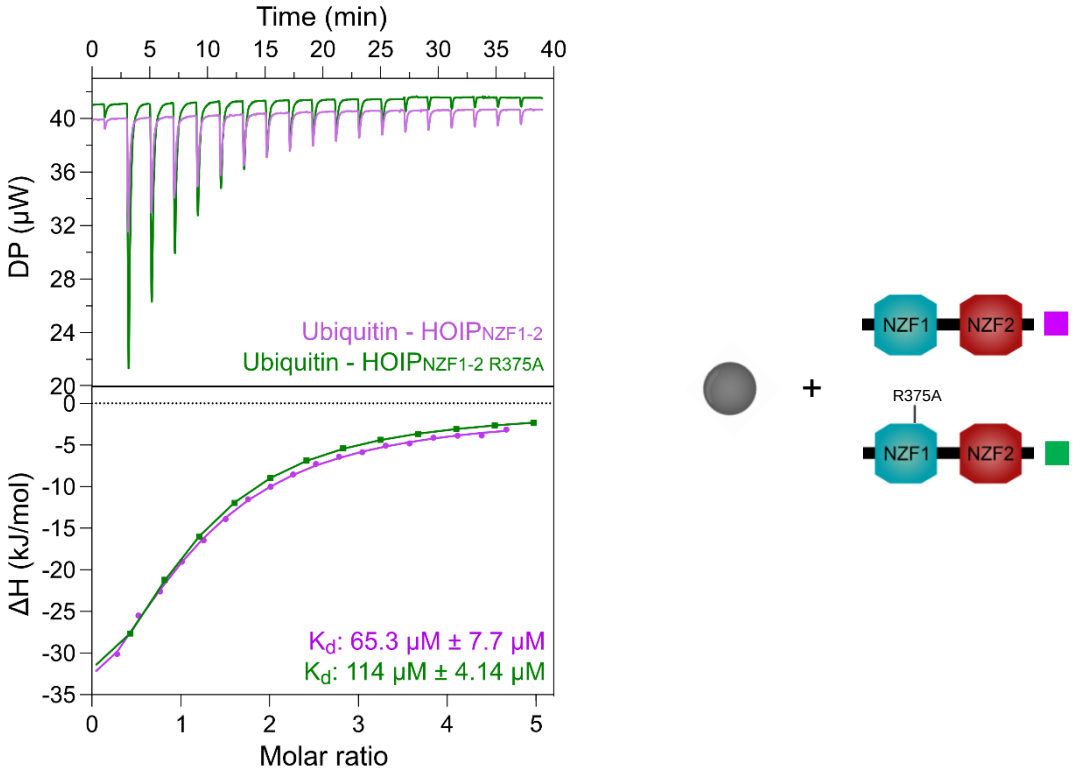


Figure 45: Thermodynamic parameters for the ITC titration curves of HOIP NZF1-NZF2 wild-type, and HOIP NZF1-NZF2 R375A binding to monoubiquitin. Two biological replicates were performed for NZF1-2.

Table 7: Thermodynamic parameters for the ITC titration curves of HOIP NZF1-NZF2 wild-type and HOIP NZF1-NZF2 R375A binding to monoubiquitin. Two biological replicates were performed for NZF1-2.

Syringe	Cell	K_d (μM)	ΔH (kJ/mol)	-TΔS (kJ/mol)	ΔG (kJ/mol)	N (stoichiometry)
Ub.	HOIP NZF1-2	42.8 ± 8.3 65.3 ± 7.7	-31.2 ± 2.4 -56 ± 4.75	7.31 32.1	-23.9 -23.9	1.47 ± 0.39 1.04 ± 0.04
Ub.	HOIP NZF1-2 R375A	114 ± 4.14	-56.3 ± 1.58	33.7	-22.5	0.945 ± 0.01

Lastly, to ensure that NZF1 is the only domain in HOIP that interacts with NEMO, ^{15}N-labelled HOIP NZF0 (aa 280-340) and NZF2 (aa 380-451) were mixed with 1:4 molar excess of NEMO CoZi domain to determine an interaction. No peak shifting or broadening is observed (**Figure 46**, **Supplementary Figure 15**), except for slight shifts for NZF0 that are, however, not accompanied by line broadening characteristic for NEMO binding. This confirms that NZF1 is the only domain in HOIP responsible for a direct interaction with NEMO.

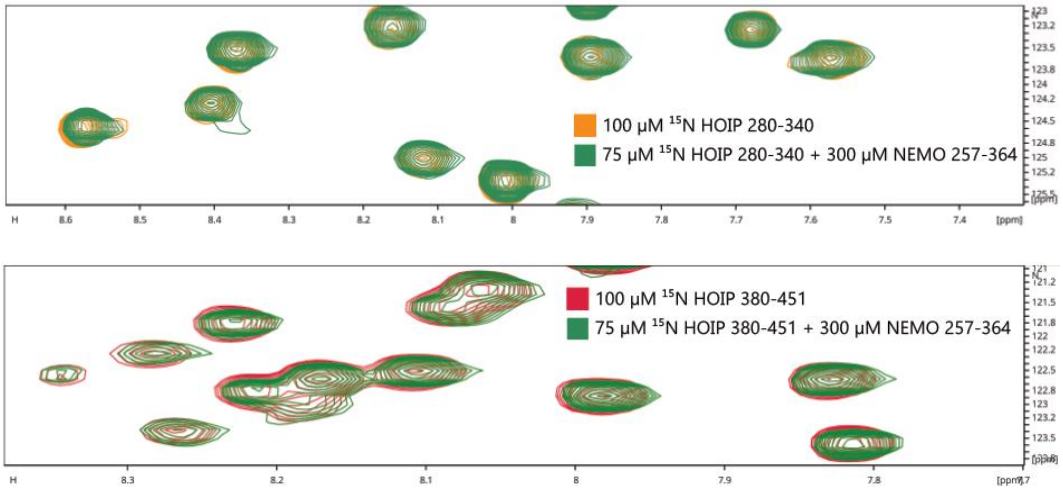


Figure 46: (Top) BEST-TROSY spectra of ^{15}N-labelled HOIP NZF0 (aa 280-340, orange) and mixed with 1:4 molar excess NEMO CoZi domain (aa 257-364, green), showing no peak shifting or line broadening upon NEMO addition. (Bottom) BEST-TROSY spectra of ^{15}N-labelled HOIP NZF2 (aa 380-451, red) and mixed with 1:4 molar excess NEMO CoZi domain (aa 257-364, red), showing no peak shifting or broadening upon NEMO addition. Full spectra can be found in Supplementary Figure 15.

3.13. Other signaling partners do not bind directly to the HOIP N-terminus

The HOIP N-terminus (including its PUB, B-box and NZF domains) has been credited as the sight for various interactions with signaling partners. Few of these interactions have been shown to be direct through crystallography or biophysical techniques. Similarly to the study of the NZF1-NEMO interaction, these previously described interactions were studied with NMR in order to identify further direct interactions and their possible effect on ubiquitin chain recruitment.

The B-box has been ill described until now, but was found to interact with a component of the T cell receptor pathway, CARMA1 [78]. ^{15}N-labelled HOIP B-box-NZF0-NZF1-NZF2 construct (aa 215-451) was mixed in 1:1 molar ratio with CARMA1 (aa 673-1028) to observe possible chemical shifts and therefore a direct interaction. No peaks shift, indicating no direct interaction between the B-box and CARMA1 (**Figure 47**, **Supplementary Figure 16**).

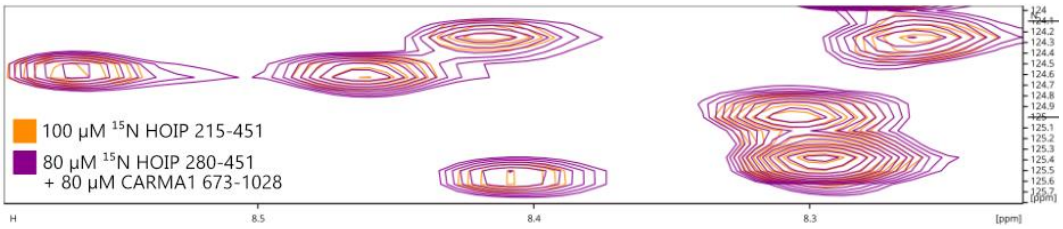


Figure 47: BEST-TROSY spectra of ^{15}N-labelled HOIP B-box-NZF0-NZF1-NZF2 construct (aa 215-451, orange), mixed with 1:1 molar excess CARMA1 (aa 673-1028, purple), showing no peak shifting upon addition. Full spectra can be found in Supplementary Figure 16.

Two proteins widely involved with inflammatory signaling and hypothesized to bind directly to HOIP are TRAF6 and NDP52. TRAF6 is an E3 ligase which is postulated to create the chains HOIP is recruited to in some inflammatory cascades [99]. However, no direct interaction between the two proteins has been shown. To test this hypothesis

^{15}N-labelled HOIP PUB (aa 1-184), NZF0 (aa 280-340), NZF1 (aa 346-400) and NZF2 (aa 346-451) and ^{13}C-^{15}N-labelled HOIP B-box (aa 195-291) spectra were collected and the samples were mixed in 1:4 molar excess with the TRAF6 RING and Zf domains (aa 50-279). No residues shift, indicating no direct interaction or very weak binding to TRAF6 in the HOIP N-terminus (**Figure 48**, **Supplementary Figure 17**).

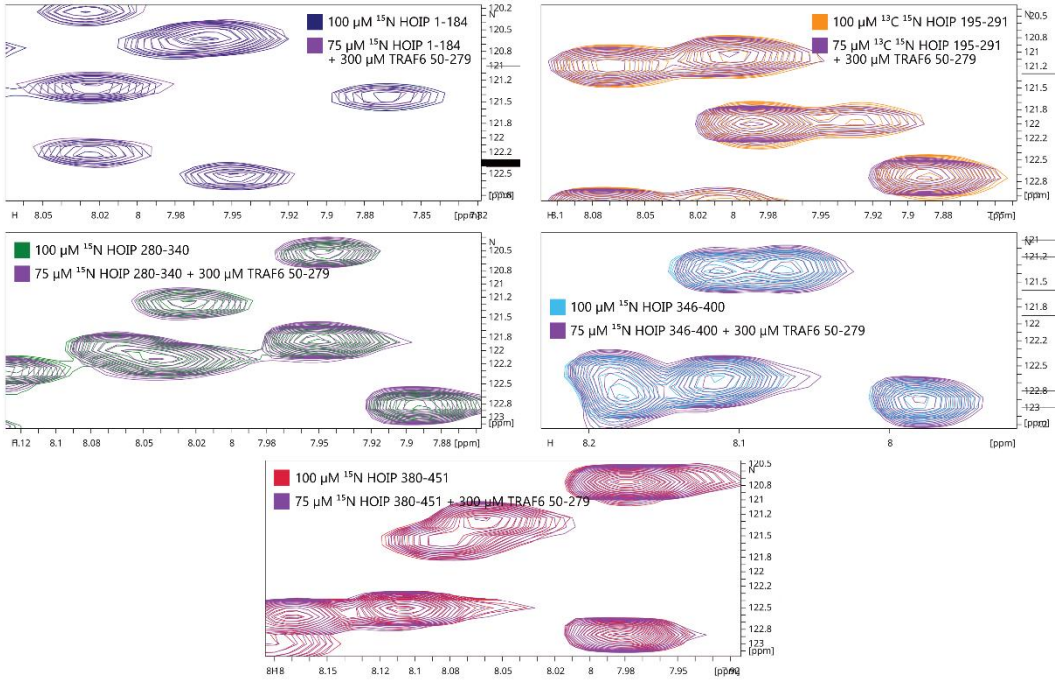


Figure 48: BEST-TROSY spectra of ^{15}N-labelled HOIP PUB domain (aa 1-184, top left, dark blue), B-box (aa 195-291, top right, orange), NF0 (aa 280-340, green, center left), NZF1 (aa 346-451, center right, skyblue) and NZF2 (aa 380-451, bottom, red) on their own and mixed with 1:4 molar excess TRAF6 RING and Zf domains (aa 50-279, red), showing no peak shifting upon addition. Full spectra can be found in Supplementary Figure 17.

NDP52 serves as an autophagy receptor and therefore displays signaling crosstalk with LUBAC. Recently two domains of NDP52, its SKIP carboxyl homology (SKICH) and Ubiquitin-binding zinc finger (UBZ) domain, were found to bind to HOIP's zinc finger and UBA domains [100]. To confirm whether this is a direct or indirect interaction, ^{15}N-labelled HOIP PUB (aa 1-184), NZF0 (aa 280-340), NZF1 (aa 346-400) and NZF2 (aa 346-451) and ^{13}C ^{15}N-labelled HOIP B-box (aa 195-291) were mixed in 1:2 molar excess with NDP52 SKICH domain (aa 17-132) and, in a separate measurement, with NDP52 UBZ domain (aa 388-446). The spectrum remains the same as in the unbound construct and shows that HOIP does not bind directly to NDP52 via its N-terminus in less than a 1:2

excess (**Figures 49** and **50**, **Supplementary Figures 18** and **19**, for SKICH and UBZ domains, respectively).

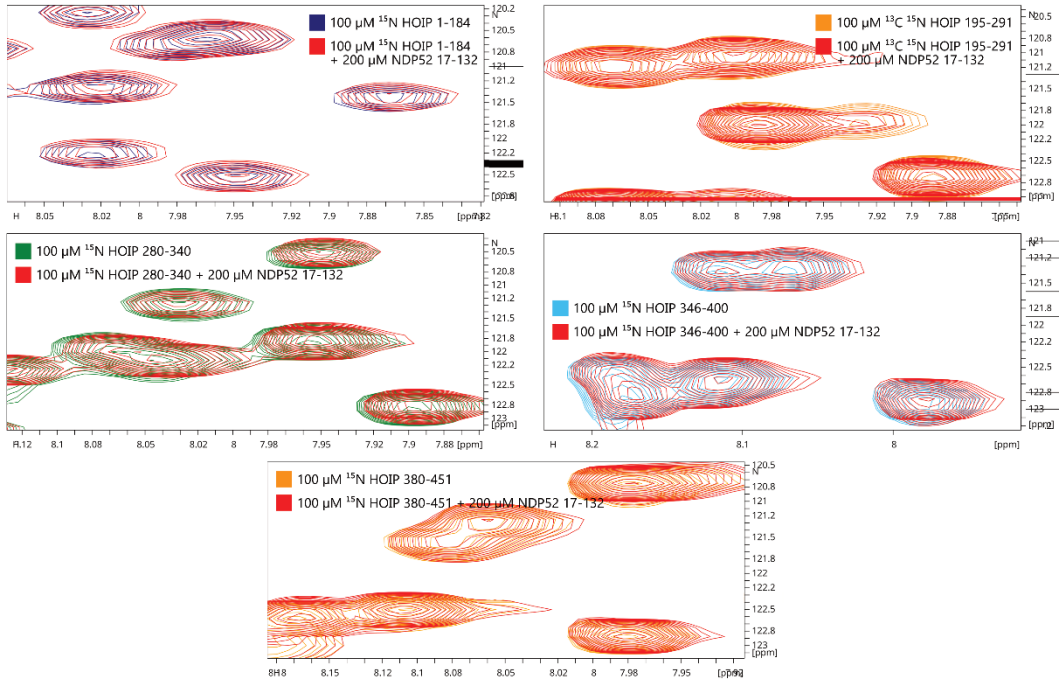


Figure 49: BEST-TROSY spectra of ^{15}N-labelled HOIP PUB domain (aa 1-184, top left, dark blue), B-box (aa 195-291, top right, orange), NF0 (aa 280-340, green, center left), NZF1 (aa 346-451, center right, skyblue) and NZF2 (aa 380-451, bottom, orange) on their own and mixed with 1:2 molar excess NDP52 SKICH domain (aa 17-132, red), showing no peak shifting upon addition. Full spectra can be found in Supplementary Figure 18.

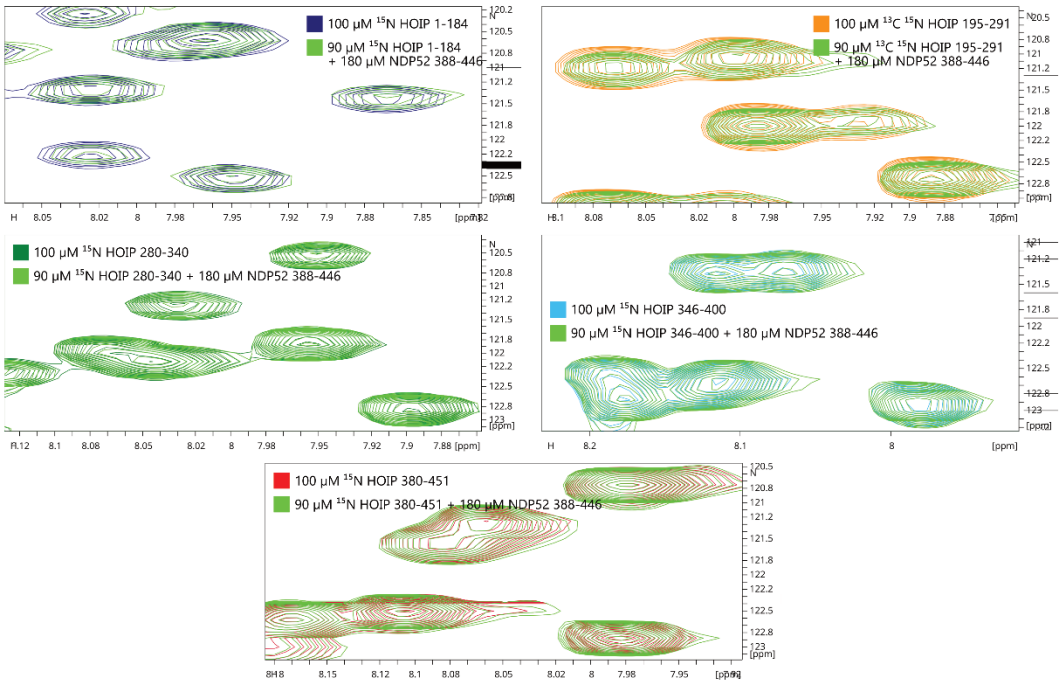


Figure 50: BEST-TROSY spectra of ^{15}N-labelled HOIP PUB domain (aa 1-184, top left, dark blue), B-box (aa 195-291, top right, orange), NF0 (aa 280-340, green, center left), NZF1 (aa 346-451, center right, skyblue) and NZF2 (aa 380-451, bottom, red) on their own and mixed with 1:2 molar

excess NDP52 UBZ domain (aa 388-446, lime), showing no peak shifting upon addition. Full spectra can be found in Supplementary Figure 19.

As described earlier in this thesis, UBAN domains are commonly found in proteins involved with inflammation, including NEMO, ABINs and OPTN, and have all been found to bind to ubiquitin chains [101]. This leads to the question of whether there is a conserved binding mode between NZF domains and UBAN domains, much like the one between NZF domains and ubiquitin or UBAN domains and linear ubiquitin. To test this the interaction between HOIP's NZF0 (aa 280-340) and NZF1 (aa 346-400) with the UBAN domain of ABIN2 was studied, in which ^{15}N-labelled NZF0 (aa 280-340) and NZF1 (aa 346-400) were mixed with an equal molar amount of ABIN2 (aa 252-344) to observe peak shifts or broadening. No such effect is seen (**Figure 51**, **Supplementary Figure 20**), concluding that NZF0 and NZF1 do not build a complex with ABIN2 via its UBAN domain in the given molar proportion.

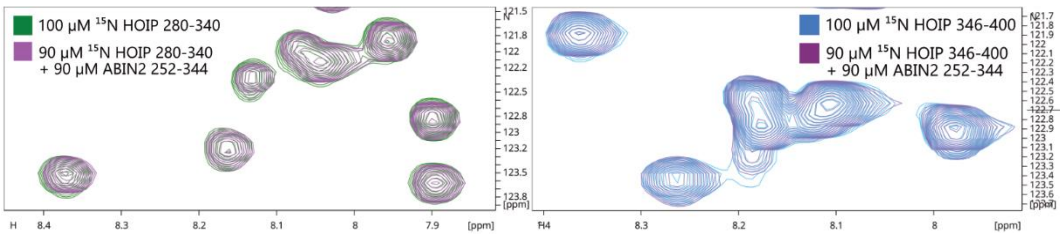


Figure 51: (Left) BEST-TROSY spectra of ^{15}N-labelled HOIP NZF0 (aa 280-340, green) mixed with 1:1 excess ABIN2 UBAN domain (aa 252-344, lilac), showing an overlap between the spectra. (Right) BEST-TROSY spectra of ^{15}N-labelled HOIP NZF1 (aa 346-400, blue) mixed with 1:1 excess ABIN2 UBAN domain (aa 252-344, purple), showing an overlap between the spectra. Full spectra can be found in Supplementary Figure 20.

The last studied interaction partner has been confirmed to interact directly with HOIP over a decade ago and is SHARPIN, the accessory subunit of LUBAC. Early studies of the HOIP-SHARPIN interaction claimed that NZF2 mediated the interaction, but recent crystallographic structures of HOIP's UBA bound to SHARPIN's UBL disprove this [44, 47]. To confirm that the UBA domain is the only one responsible for this interaction, ^{15}N-labelled NZF0 (aa 280-340) and NZF1-NZF2 (aa 346-451) were mixed with SHARPIN UBL in a 1:4 molar excess (aa 167-309) and compared with the domain

spectra on their own. No peaks shift (**Figure 52**, **Supplementary Figure 21**), showing that there is no direct interaction between SHARPIN's UBL domain and HOIP's NZF domains, including NZF2.

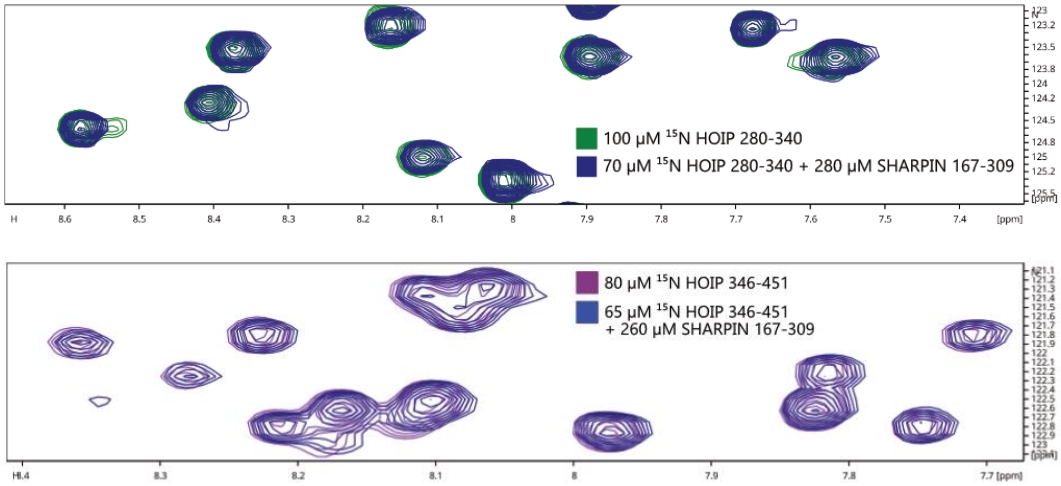


Figure 52: BEST-TROSY spectra of ^{15}N-labelled HOIP NZF0 (aa 280-340, top, green) and NZF1-NZF2 (aa 346-451, bottom, lilac) alone and mixed with 1:4 excess SHARPIN UBL domain (aa 167-309, dark blue), showing no shifts upon SHARPIN addition. Full spectra can be found in Supplementary Figure 21.

In summary, no interaction partners, whether proven or hypothesized, interact directly with HOIP's N-terminal domains at the concentrations used in each experiment. While these interactions were previously mapped on specific domains in HOIP (e.g. CARMA1 interacting with the B-box), they had not been studied using purified proteins but rather co-immunoprecipitation methods. By utilizing NMR as a sensitive method for protein interaction we can confirm that these interactions are not direct and they were therefore not further studied in terms of their effect on ubiquitin binding. As they are indirect it will be vital to determine the proteins that facilitate them, for example with CARMA1 or NDP52. Lastly, these experiments will need to be continued if more direct interaction partners for the zinc finger region of HOIP are discovered in the future.

4. Discussion

The recruitment of LUBAC is necessary for inflammatory complexes to activate NF-κB and prevent cell death. This study demonstrates how multiple domains of HOIP cooperate in order to drive LUBAC recruitment to pre-existing K63 chains on receptor complexes, providing insight into the assembly of complexes of the innate immune system as well as a novel mechanism of how tandem NZF domains achieve linkage-specificity.

HOIP NZF1 has so far been considered the domain responsible for HOIP's association with signaling complexes due to its ability to bind polyubiquitin [35]. Here it is shown that both NZF1 and NZF2 of HOIP bind monoubiquitin via a conserved TF/Φ motif, as determined by NMR titrations, with the motif being common amongst ubiquitin-binding NZF domains [49]. NZF1 binds monoubiquitin with a dissociation constant of 7 to 30 μM, more than five times higher than previously described NZF domains [44, 72]. NZF2, on the other hand, interacts with monoubiquitin with a lower affinity (K_d > 150 μM). The low affinity and stoichiometry of all measurements of NZF2 prohibit our making any statistically significant statements regarding its binding abilities based on ITC measurements alone. However, the findings are complemented by the NMR titration experiments, in which NZF1 residues reach saturation while NZF2 residues do not, making the difference in binding affinities apparent. These findings counter current theory on the characteristics of ubiquitin-binding NZF domains. It has been postulated that the NZF binding to monoubiquitin depends on the polarity of the residue Φ of the NZF TF/Φ ubiquitin-binding pattern, with only domains possessing a hydrophobic residue and therefore a 'complete' binding patch able to bind with a physiologically relevant affinity [20]. This is not the case for HOIP NZF1 and NZF2. Both domains possess a hydrophobic residue in the Φ position (I372 for NZF1 and M431 for NZF2)

and yet only NZF1 shows a high affinity, leading us to rethink this model of NZF-monoubiquitin interactions.

This thesis shows further that NZF1 and NZF2 work synergistically to establish linkage specificity in HOIP's ubiquitin chain interactions. NZF1 binds to K63-linked diubiquitin with high affinity, comparable to its affinity for monoubiquitin, and has a lower affinity for K48-linked diubiquitin. The values established here correspond well to those reported previously [44]. The binding patch is centered on the TF/Φ motif and shows no variation or extension compared to the one for monoubiquitin binding, leaving the question of how NZF1 binds the proximal ubiquitin moiety of the K63 diubiquitin and achieves linkage specificity open. Interpreting the data for the specificity of NZF2 proves difficult due to the aforementioned weak binding it shows in ITC measurements. NZF2 has a far higher affinity for diubiquitin than for monoubiquitin and preferentially binds K63 chains. While this preference was previously observed for an NZF1-NZF2 T360A construct, where only NZF2 can bind ubiquitin, the dissociation constants observed in the 2017 study were twice as high as here [77]. The complementation of these findings with NMR measurements leads to a clearer illustration of how NZF2 achieves K63 specificity. The TF/Φ monoubiquitin binding patch is extended to include V412 and W413 when bound to K63 but not K48 diubiquitin, possibly orienting the distal and proximal ubiquitin so that only K63 chains can interact with the binding patch. It should be noted that overlaying the predicted structure of NZF2 with the crystal structure of the NZF domains of TAB2/3 bound to K63 diubiquitin does not lead the K63 diubiquitin binding patch of NZF2 to align with that of TAB2/3, meaning that it must bind diubiquitin at a different angle or possibly through a different mechanism than the one previously observed for these NZF domains.

Tandem NZF domains, as found in HOIP and in TRABID, must be studied as a singular region in terms of their binding abilities in order to elucidate the ubiquitin binding of the protein as a whole. Constructs comprising both NZF1 and NZF2 have a high affinity for diubiquitin, nearly four times higher than observed for NZF1 and for NZF2 alone, and

display a preference for K63 over K48 chains. In NZF1-NZF2 T419A constructs, where NZF2 is unable to bind ubiquitin, this increase in the affinity to diubiquitin is not observed. As it was mentioned for NZF1-NZF2 T360A, previously reported values for the K_d constants of NZF1-NZF2 and diubiquitin display the same chain preference, but are higher in the 2017 report [77]. This overall increase in affinity between the individual and tandem NZF domains is interpreted to mean that NZF2 binding contributes cooperatively in the ability of the tandem NZF domains to bind K63-linked chains, raising the affinity in comparison to that of NZF1. Both NZF1 and NZF2 are therefore needed for HOIP to be able to bind polyubiquitin to its full extent.

The effect of NZF2 on the binding abilities of NZF1 is not only additive for diubiquitin binding, but also diminishing for monoubiquitin binding. NZF1 has a similar affinity for monoubiquitin as for K63-linked diubiquitin, complemented by the observation that NZF1 employs the same binding patch when binding to mono- and diubiquitin. In light of NZF1 not having a solidified mechanism for specificity between mono- and polyubiquitin, it could be the presence of NZF2 that regulates this specificity. In constructs encompassing both NZF domains affinity to monoubiquitin is greatly reduced. This is also the case when NZF1 and NZF2 are both present but only NZF1 binds ubiquitin, meaning that the decreased affinity is apparently due to the presence of NZF2. The incoherent biophysical parameters of these measurements (e.g. stoichiometry increasing two-fold between NZF1-NZF2 and NZF1-NZF2 T419A) do not allow us to make conclusive statements on the matter, but this data provides an interesting starting point on what is possibly the dual role of NZF2 in HOIP's recruitment to ubiquitin chains. NZF2 may contribute to binding to polyubiquitin while regulating the interaction of NZF1 with monoubiquitin. Refining the model of NZF1 and NZF2 as a synergetic binding unit in HOIP would elaborate on the role of tandem NZF domains in immunity and provide a novel mechanism for the regulation of recruitment to signaling complexes.

NZF1, apart from contributing to HOIP's recruitment to inflammatory complexes, facilitates its interaction with the downstream signaling effector NEMO. Immunoprecipitation studies had indicated that NZF1 binding to NEMO and to monoubiquitin are uncoupled events, each employing a different interface on NZF1 centered around R375 for NEMO binding and the TF/Φ patch for ubiquitin binding [76]. Here it is shown that NZF1 can bind both proteins simultaneously, but albeit not to the full possible extent, due to an overlap between the NEMO and ubiquitin binding patch. It is not unimaginable that, while NZF1 is bound to NEMO, the residues of the interface overlap are rendered unavailable to ubiquitin and therefore reduce its binding. The interaction with downstream signaling effectors therefore affects, although it does not dictate or abolish, ubiquitin binding. Through mutational studies it is shown that alterations in the interface overlap reduce the affinity of NZF1 to monoubiquitin, although the same mutant R375A was previously shown to not diminish HOIP recruitment to the TNF-RSC, bringing the physiological significance of the finding in question [76]. While NZF1 is hereby confirmed to interact with NEMO UBAN, it does not interact with ABIN2 UBAN in a 1:1 molar ratio. Determining the differences between ABIN2 UBAN and NEMO UBAN would therefore illustrate the structural elements that may hinder or promote their binding to NZF1. These findings can be extended to other proteins containing UBAN domains, such as OPTN, to conclude whether NZF-UBAN interactions are universal and present a conserved binding patch, equivalent to the TF/Φ patch for ubiquitin binding. Because UBAN domains are known to be regulated by phosphorylation in their binding to M1 chains, studying the effect of phosphorylation on their binding to NZF domains is of interest in characterizing this binding event further [48].

The contribution of the B-box and NZF0 to HOIP's zinc finger region and to the recruitment of LUBAC remain an enigma, although significant insight has been gained in the characterization of these conserved domains and the function of the B-box. NZF0 is identified as an NZF domain that does not bind ubiquitin, while B-box is a B-box type

I that controls HOIP's oligomerization. In vitro experiments reveal that the zinc region of HOIP is in a monomer-dimer exchange, with mutations in vital residue L219 abolishing dimerization. The oligomeric state of the zinc finger region does not influence its affinity to K63 chains and is therefore unlikely to play a role in the recruitment of LUBAC to inflammatory complexes through this mechanism. However, oligomerization may be implicated in other functions of HOIP, such as the interaction with DUBs, as observed previously [53]. Therefore, although no effect on binding has been shown in vitro it should not be ruled out that there may be an in vivo effect of the B-box. The insights gained from this thesis as to the behaviour of the B-box-NZF region and the characterization of point mutations that either disrupt ubiquitin binding or dimerization can confidently be incorporated into mutant HOIP variants for cellular assays. Such assays should center around the recruitment of LUBAC and LUBAC-mediated NF-κB signaling and may yet reveal an importance of this region. Furthermore, novel interaction partners can be studied using the techniques and models laid out in this thesis.

5. Limitations of the study

A number of findings of this thesis must be studied further in order to solidify them and employ them in the model of HOIP's recruitment to signaling complexes.

The first and most striking is the inexactness of the ITC data collected for the NZF2 and NZF1-NZF2 T360A constructs. The poor fits stem from the low affinity of the constructs for substrates such as monoubiquitin, requiring multiple repeats to solidify them or possibly the employment of a complementary technique, such as surface plasmon resonance, to reproduce them. Secondly, further insight is needed into how NZF1 and NZF2 achieve linkage specificity. While a crystal structure of the NZF1-NZF2·K63 Ub_2 complex would undoubtedly provide insight, alternative strategies can be used to complement such a structure. One example would be to study the flexibility of the construct in the presence and absence of diubiquitin via HetNOE measurements, in

order to study the effect of binding to the flexibility of the linker region between the two domains. Additionally, the extended K63 chain binding interface of NZF2 can be investigated further by mutating residues V412 and W413 to observe whether the domain preserves its preference for K63 chains.

The NMR measurements of the interactions of HOIP with its signaling partners are also limited in their interpretation. Some binding events are studied in low concentrations of the potential binding partner. The cause is the low concentration of some interaction partners (e.g. ABIN2 UBAN, NDP52, CARMA1). Since some low affinity interactions require high substrate concentrations to be detectable as chemical shifts in NMR titration series, further studies focusing on these binding events should include repetitions using higher final concentrations to solidify the finding that HOIP does not interact with the substrate. The proteins studied as potential binding partners can also be expanded to include, for example, more proteins with UBAN motifs, such as OPTN.

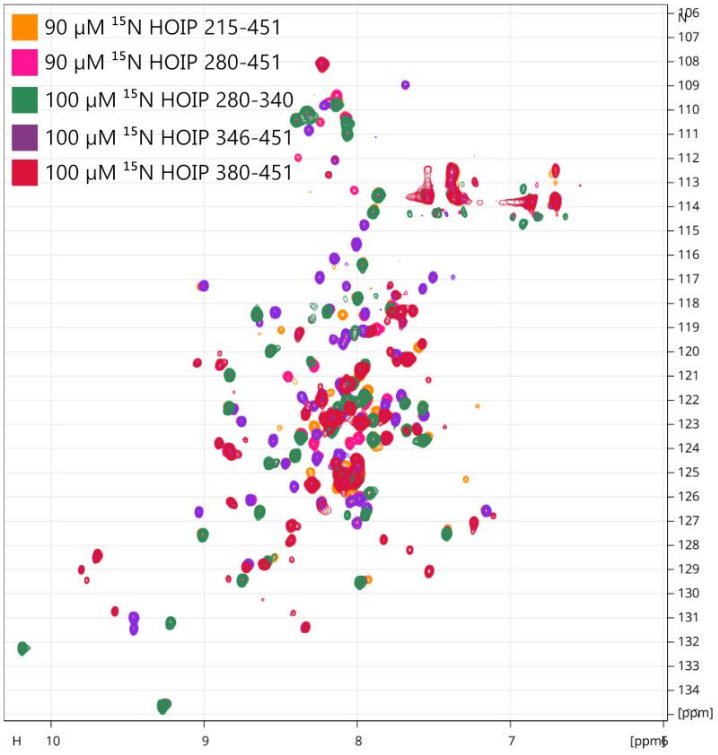
Lastly, it must be emphasized that the biophysical and biochemical characterization of proteins provides detail to the mechanisms they employ to fulfill their functions, but these functions must be confirmed by in vivo studies. The reason is that receptor complexes provide unique signaling conditions that can favor or inhibit interactions or provide alternative, complementary mechanisms, leading significant in vitro results to not produce a significant effect in vivo or vice versa. The findings of this study and the mutations employed and characterized in vitro must therefore be corroborated by in vivo experiments, preferably by mutating full-length HOIP and assessing the mutation's effect on its recruitment to the TNF-RSC via pulldown and immunoprecipitation studies.

6. Concluding remarks

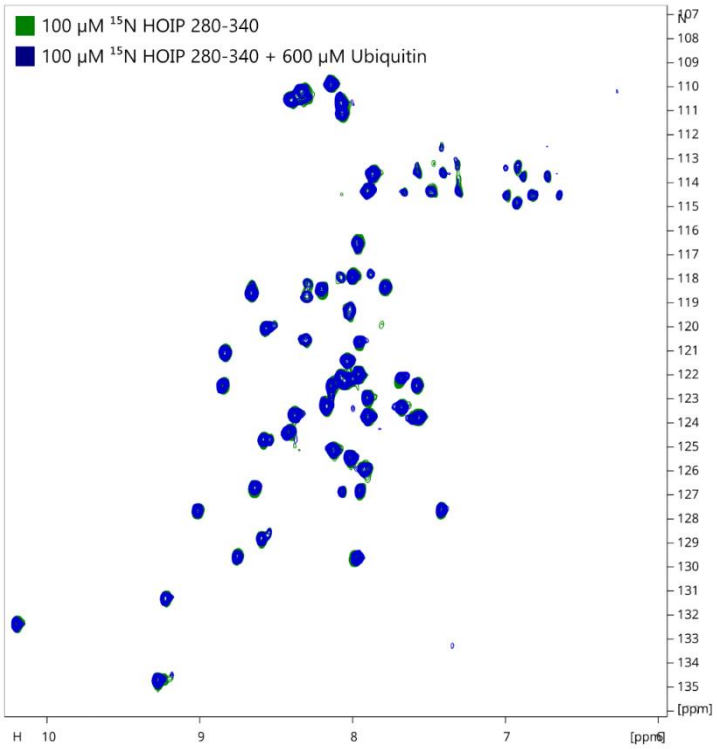
In this thesis the role of the tandem domains of HOIP in LUBAC's recruitment to inflammatory complexes is studied, with a focus on the newly discovered ability of NZF2 to bind K63 chains. The collaboration of NZF1 with NZF2 to drive polyubiquitin binding

by HOIP is determined via biophysical and structural studies. Additionally, HOIP's interaction with downstream signaling partners is found to affect, but not abolish, LUBAC's recruitment. These findings solidify our understanding of not only how inflammatory signaling complexes are assembled, but provides a novel model of how NZF domains may collaboratively determine ubiquitin chain specificity and affinity in proteins of the innate immune system.

Appendix



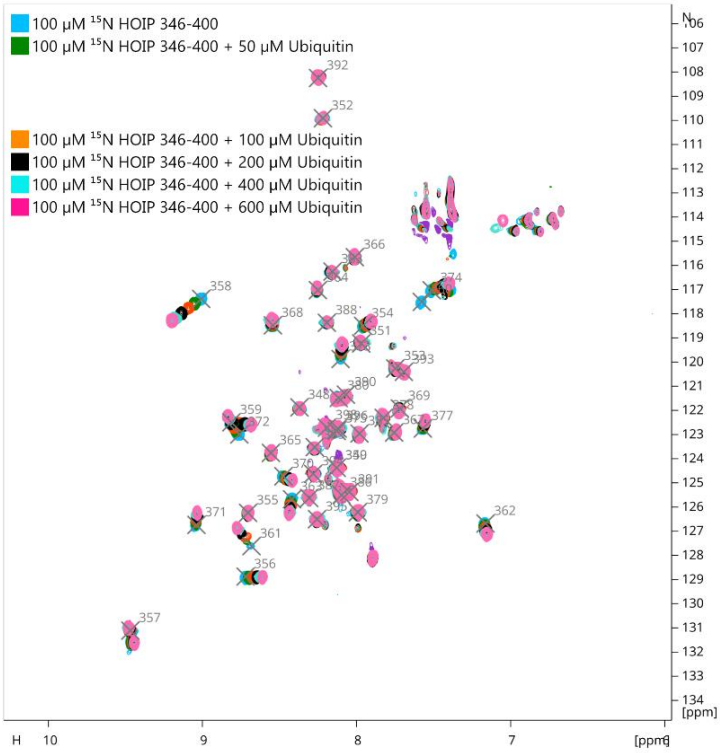
Supplementary Figure 1: BEST-TROSY spectra of ^{15}N-labelled HOIP constructs B-box-Zf-NZF1-NZF2 (aa 215-451, orange), Zf-NZF1-NZF2 (aa 280-451, pink), Zf (aa 280-340, green), NZF1-NZF2 (aa 346-451, purple) and NZF2 (aa 380-451, red), showing overlapping peaks for spectra with overlapping regions.



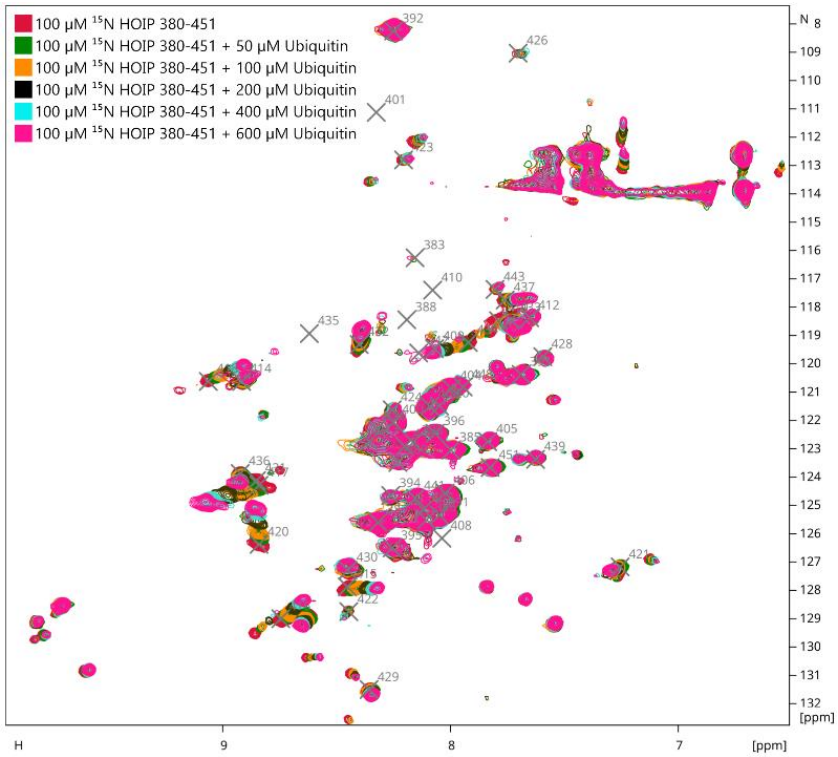
Supplementary Figure 2: BEST-TROSY spectra of ^{15}N-labelled HOIP NZF0 (aa 280-340, green) mixed with 1:6 molar excess monoubiquitin (blue), showing an overlap of the two spectra.



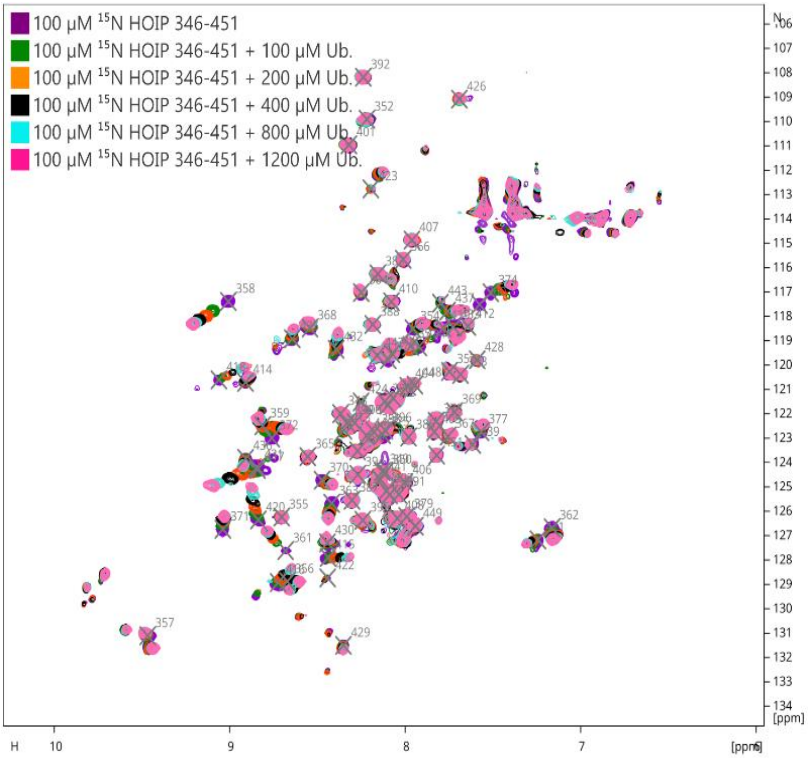
Supplementary Figure 3: BEST-TROSY spectra of ^{13}C-^{15}N-labelled HOIP NZF1-NZF2 (aa 346-451, purple), showing nearly all resonances backbone assigned to the corresponding amino acid of the sequence.



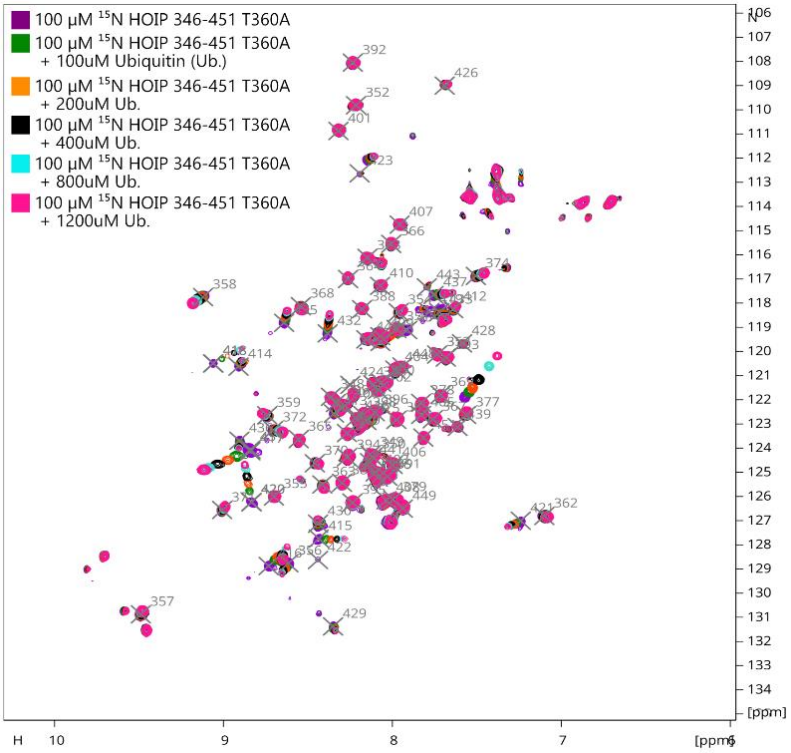
Supplementary Figure 4: BEST-TROSY spectra of ^{15}N-labelled HOIP NZF1 (aa 346-400, skyblue) and HOIP NZF1 mixed with 1:0.5 molar excess (green), 1:1 molar excess (orange), 1:2 molar excess (black), 1:4 molar excess (turquoise), 1:6 molar excess monoubiquitin (pink), showing several peaks shifting upon ubiquitin addition.



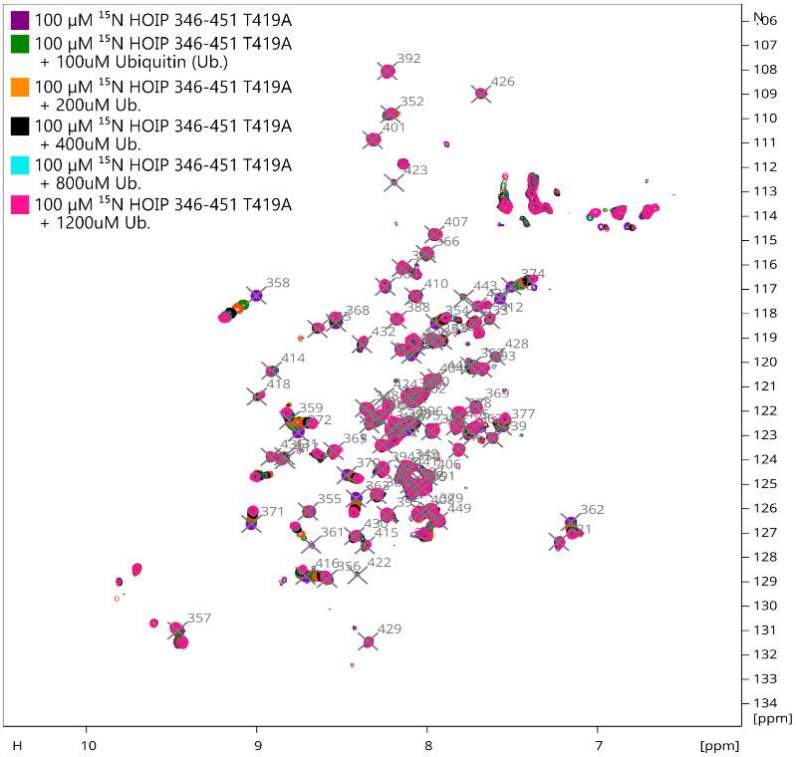
Supplementary Figure 5: BEST-TROSY spectra of ^{15}N-labelled HOIP NZF2 (aa 380-451, crimson) and HOIP NZF2 mixed with 1:0.5 molar excess (green), 1:1 molar excess (orange), 1:2 molar excess (black), 1:4 molar excess (turquoise), 1:6 molar excess monoubiquitin (pink), showing several peaks shifting upon ubiquitin addition.



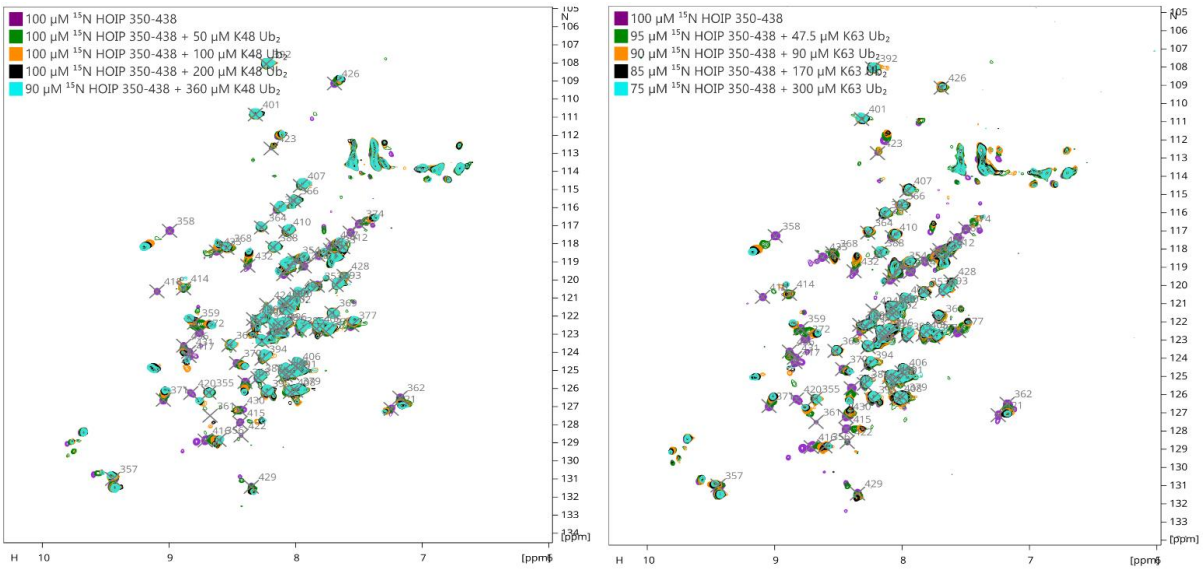
Supplementary Figure 6: BEST-TROSY spectra of ^{15}N-labelled HOIP NZF1-NZF2 (aa 346-451, purple) and HOIP NZF1-NZF2 mixed with 1:0.5 molar excess (green), 1:1 molar excess (orange), 1:2 molar excess (black), 1:4 molar excess (turquoise), 1:6 molar excess monoubiquitin per binding site (pink), showing several peaks shifting upon ubiquitin addition.



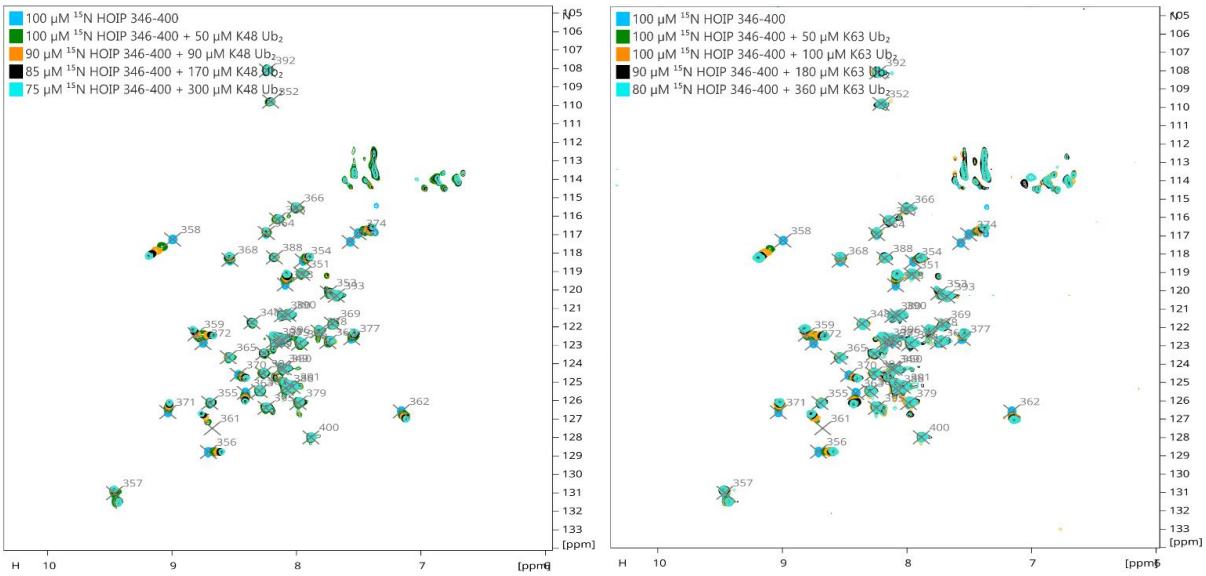
Supplementary Figure 7: BEST-TROSY spectra of ^{15}N-labelled HOIP NZF1-NZF2 T360A (aa 346-451, purple) and HOIP NZF1-NZF2 T360A mixed with 1:0.5 molar excess (green), 1:1 molar excess (orange), 1:2 molar excess (black), 1:4 molar excess (turquoise), 1:6 molar excess monoubiquitin (pink), showing several peaks shifting upon ubiquitin addition.



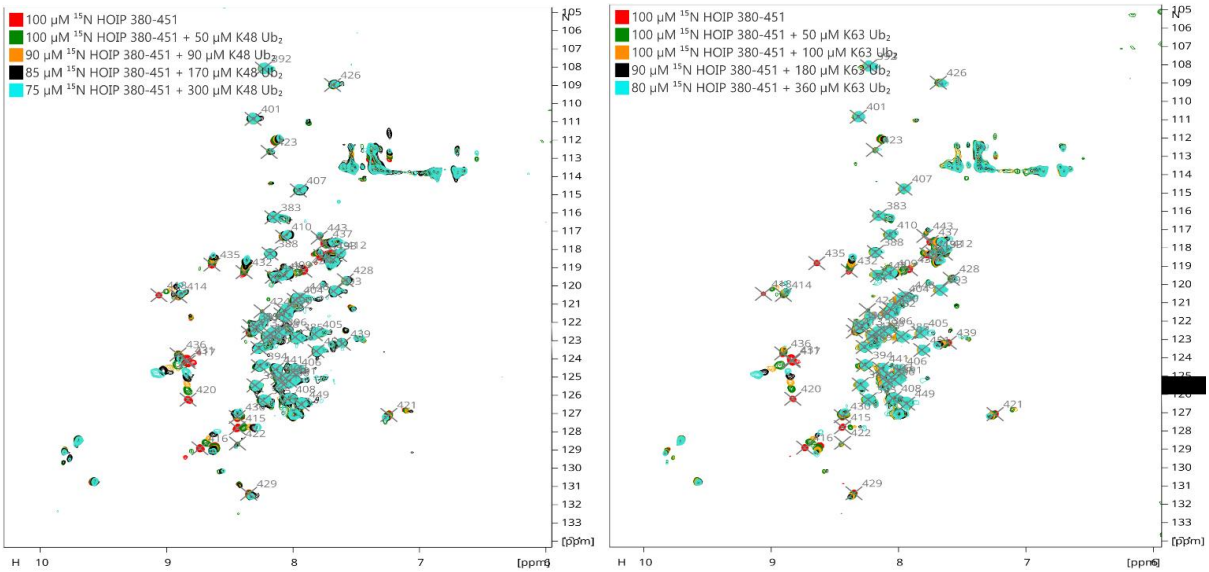
Supplementary Figure 8: BEST-TROSY spectra of ^{15}N-labelled HOIP NZF1-NZF2 T419A (aa 346-451, purple) and HOIP NZF1-NZF2 T419A mixed with 1:0.5 molar excess (green), 1:1 molar excess (orange), 1:2 molar excess (black), 1:4 molar excess (turquoise), 1:6 molar excess monoubiquitin (pink), showing several peaks shifting upon ubiquitin addition.



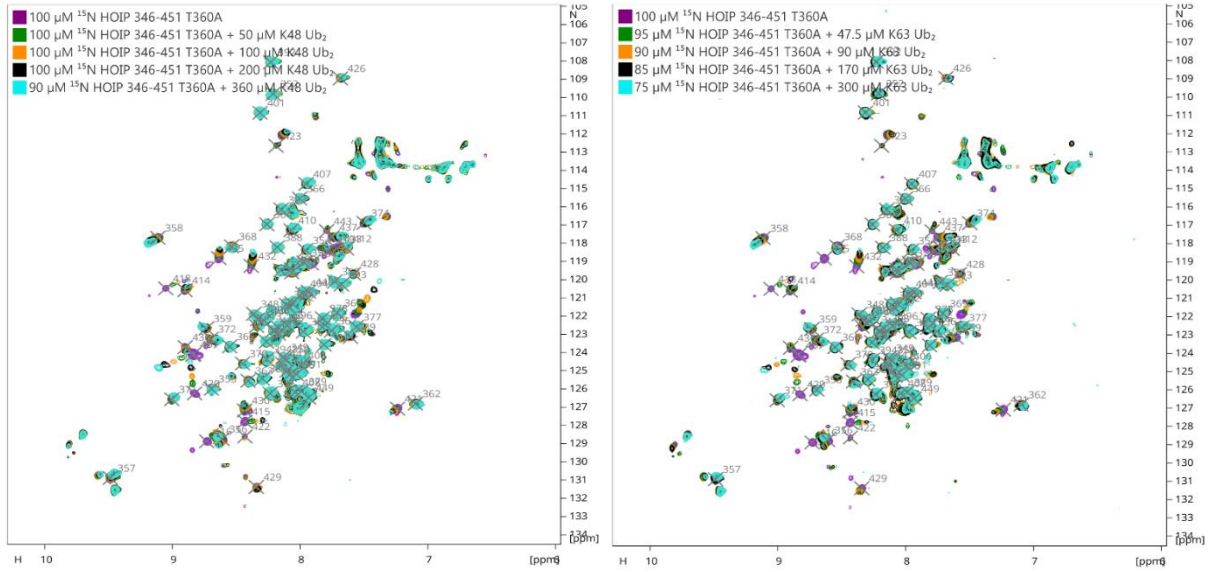
Supplementary Figure 9: BEST-TROSY spectra of ^{15}N-labelled HOIP NZF1-NZF2 (aa 350-438, purple) and HOIP NZF1-NZF2 mixed with 1:0.5 molar excess (green), 1:1 molar excess (orange), 1:2 molar excess (black) and 1:4 molar excess diubiquitin (turquoise), with the titration of K48-linked diubiquitin (Left) and K63-linked diubiquitin (Right), showing several peaks shifting upon ubiquitin addition.



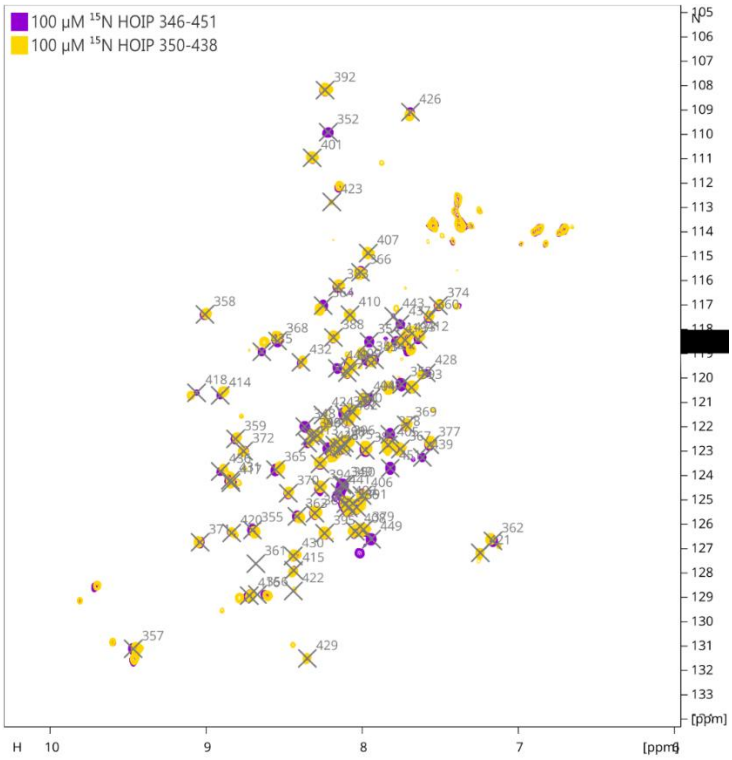
Supplementary Figure 10: BEST-TROSY spectra of ^{15}N-labelled HOIP NZF1 (aa 346-400, skyblue) and HOIP NZF1 mixed with 1:0.5 molar excess (green), 1:1 molar excess (orange), 1:2 molar excess (black) and 1:4 molar excess diubiquitin (turquoise), with the titration of K48-linked diubiquitin (Left) and K63-linked diubiquitin (Right), showing several peaks shifting upon ubiquitin addition.



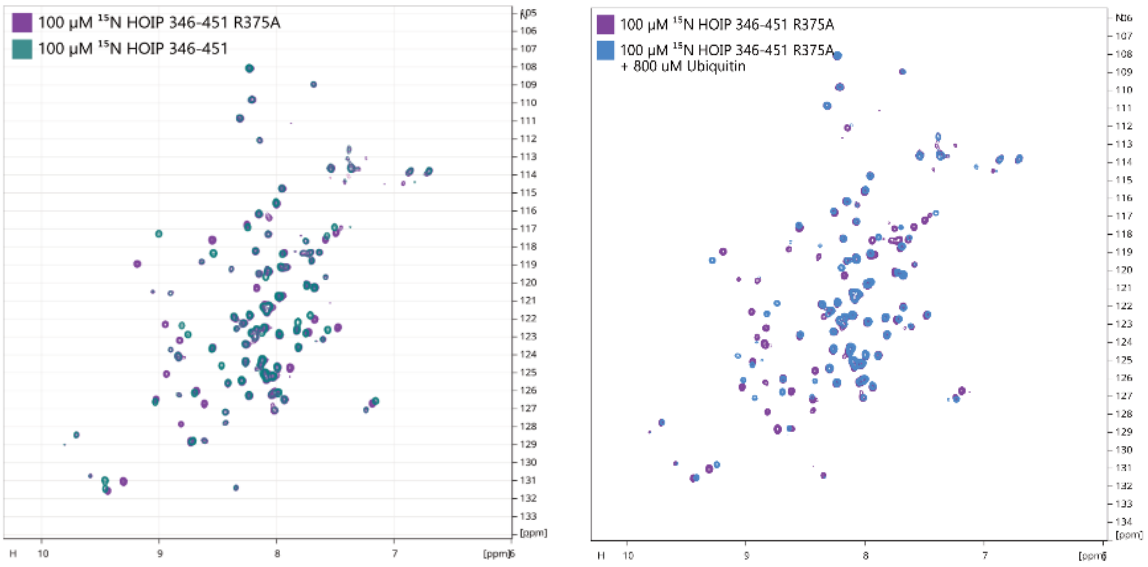
Supplementary Figure 11: BEST-TROSY spectra of ^{15}N-labelled HOIP NZF2 (aa 380-451, red) and HOIP NZF2 mixed with 1:0.5 molar excess (green), 1:1 molar excess (orange), 1:2 molar excess (black) and 1:4 molar excess diubiquitin (turquoise), with the titration of K48-linked diubiquitin (Left) and K63-linked diubiquitin (Right), showing several peaks shifting upon ubiquitin addition.



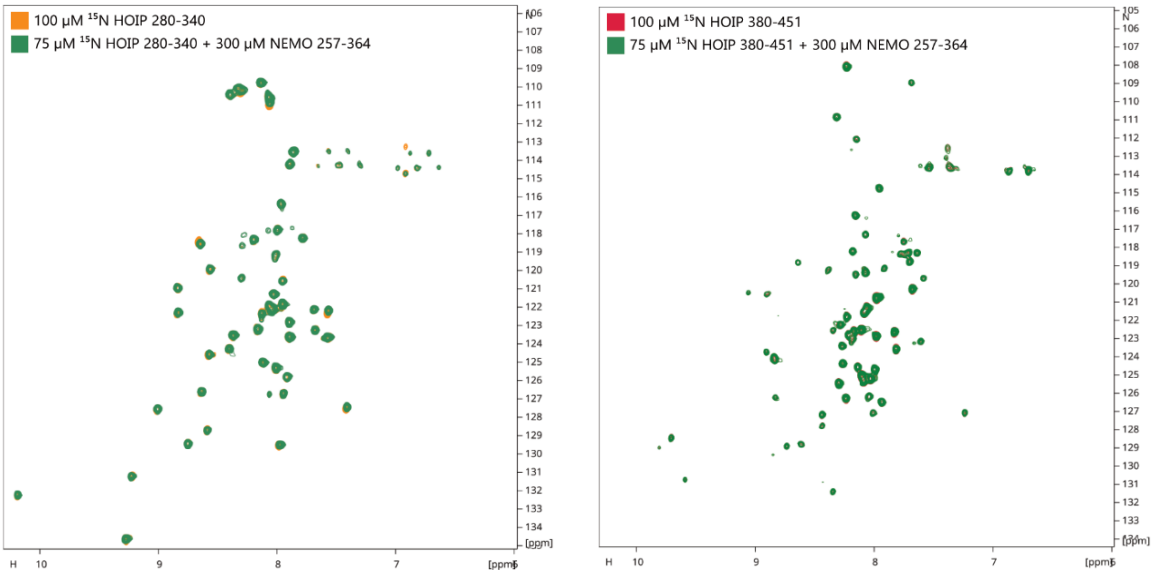
Supplementary Figure 12: BEST-TROSY spectra of ^{15}N-labelled HOIP NZF1-NZF2 T360A (aa 346-451, purple) and HOIP NZF1-NZF2 mixed with 1:0.5 molar excess (green), 1:1 molar excess (orange), 1:2 molar excess (black) and 1:4 molar excess diubiquitin (turquoise), with the titration of K48-linked diubiquitin (Left) and K63-linked diubiquitin (Right), showing several peaks shifting upon ubiquitin addition.



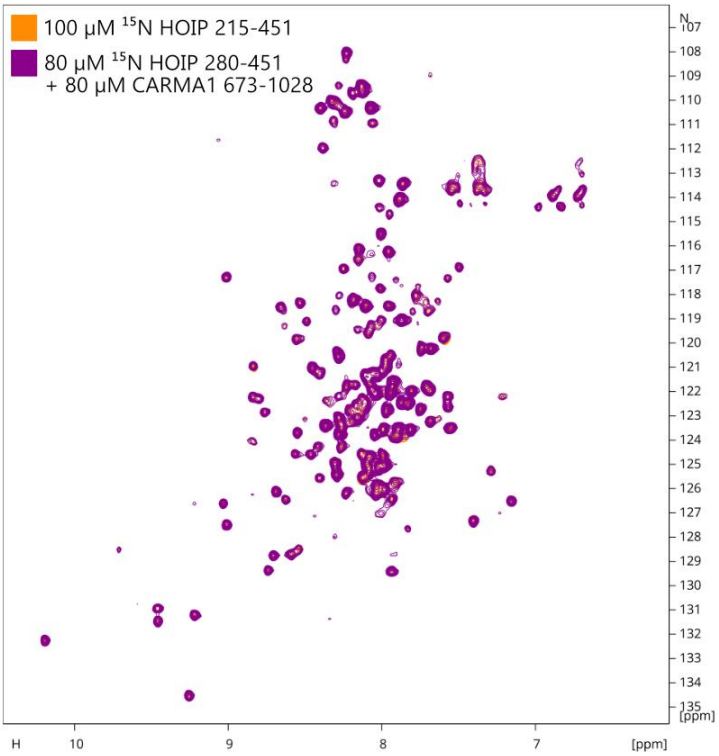
Supplementary Figure 13: BEST-TROSY spectra of ^{15}N-labelled HOIP NZF1-NZF2 (aa 346-451, purple) and the truncated construct HOIP NZF1-NZF2* (aa 350-438, gold), with the backbone assigned residues of the longer construct displayed.



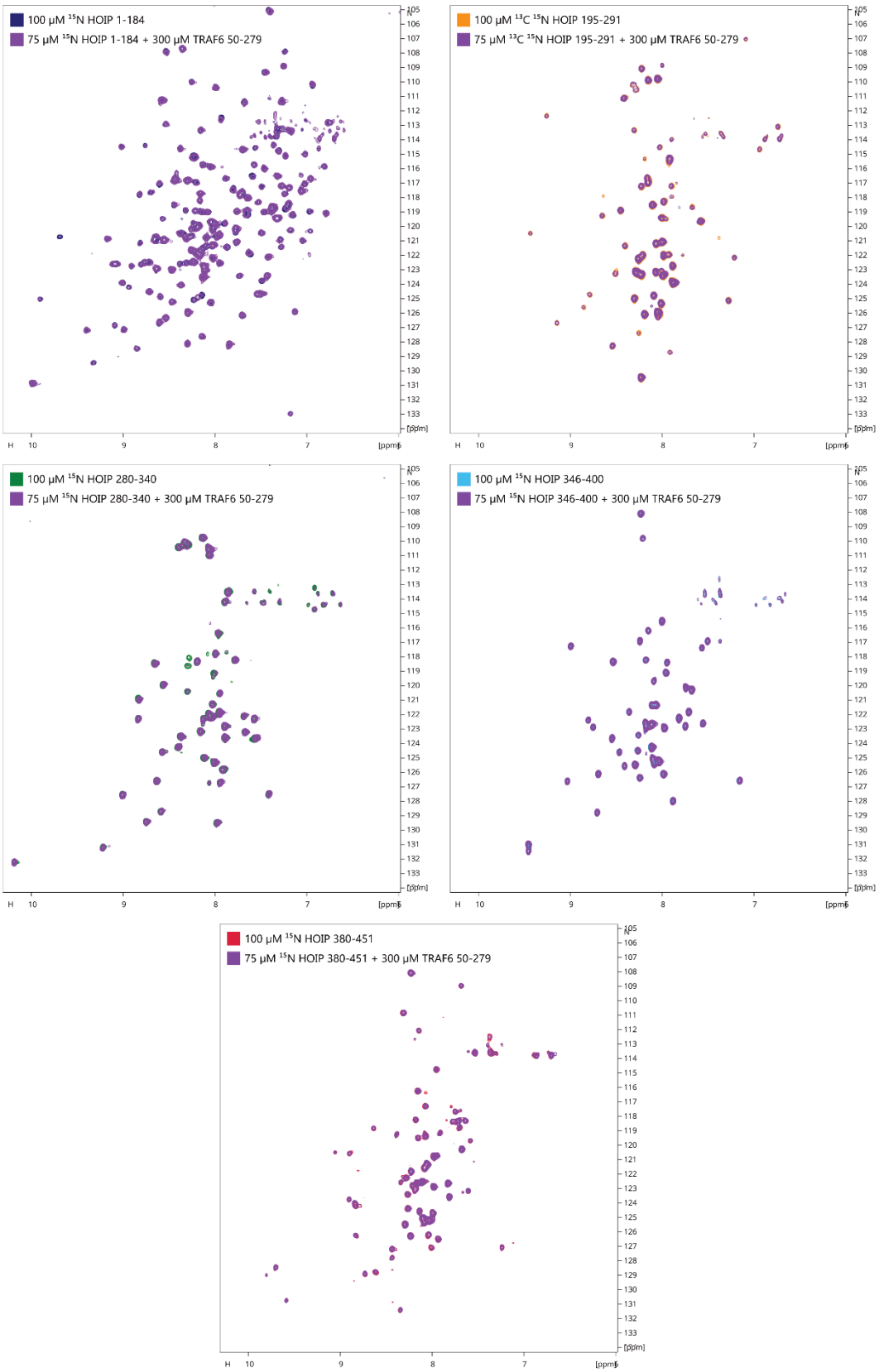
Supplementary Figure 14: (Left) BEST-TROSY spectra of ^{15}N-labelled HOIP NZF1-NZF2 R375A (aa 346-451, purple) and HOIP NZF1-NZF2 (aa 346-451, cyan), showing several peaks shifting due to the mutation inserted in the construct. (Right) BEST-TROSY spectra of ^{15}N-labelled HOIP NZF1-NZF2 R375A (aa 346-451, purple) and mixed with 1:4 molar excess monoubiquitin (skyblue), showing several peaks shifting upon ubiquitin addition, albeit not as strongly as in the wild-type construct in Figure 13 and Supplementary Figure 4.



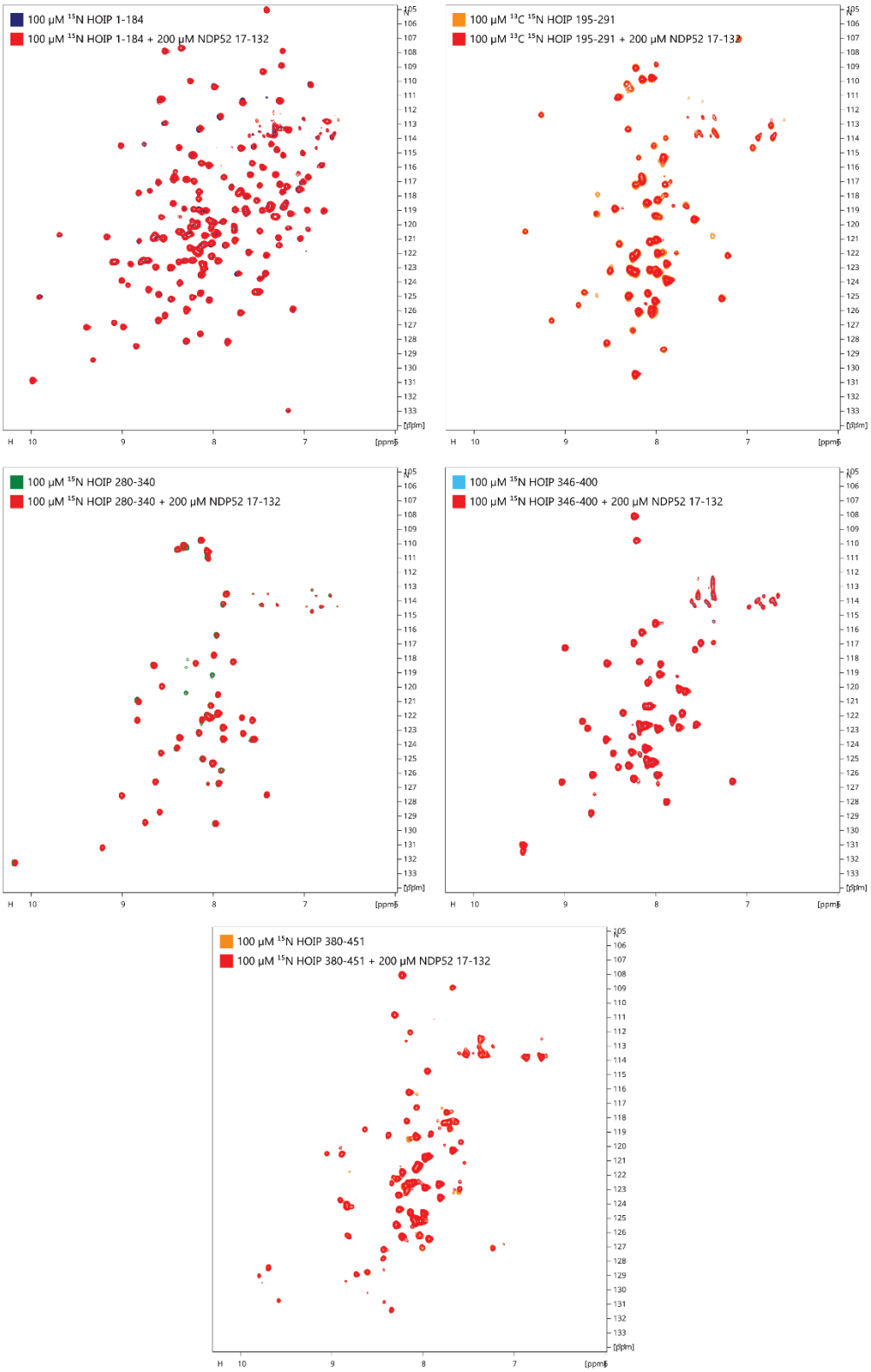
Supplementary Figure 15: (Left) BEST-TROSY spectra of ^{15}N-labelled HOIP NZF0 (aa 280-340, orange) and mixed with 1:4 molar excess NEMO CoZi domain (aa 257-364, green), showing minor peak shifting but no line broadening upon NEMO addition. (Right) BEST-TROSY spectra of ^{15}N-labelled HOIP NZF2 (aa 380-451, red) and mixed with 1:4 molar excess NEMO CoZi domain (aa 257-364, red), showing no peak shifting or broadening upon NEMO addition.



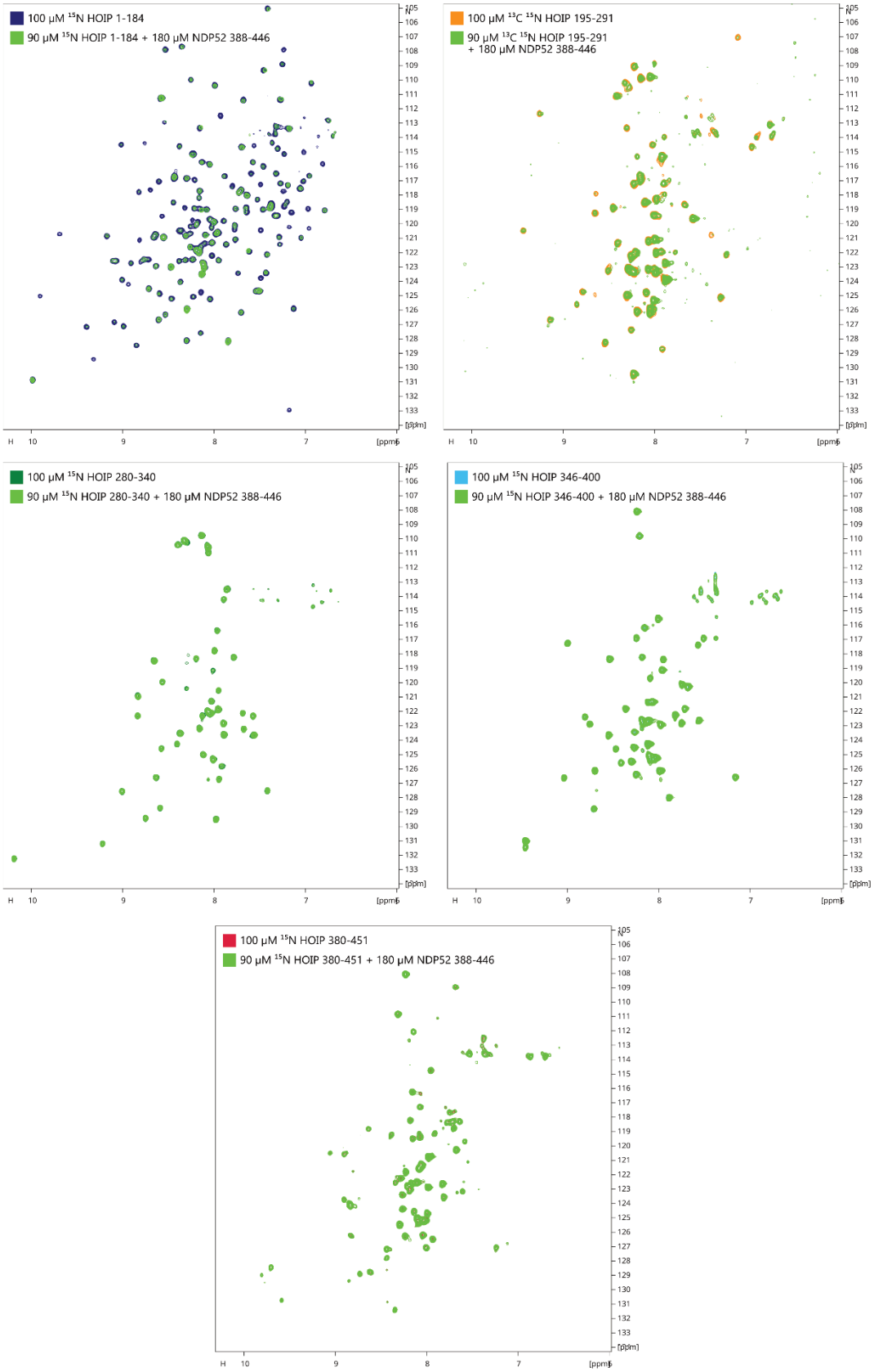
Supplementary Figure 16: BEST-TROSY spectra of ^{15}N-labelled HOIP B-box-NZF0-NZF1-NZF2 construct (aa 215-451, orange), mixed with 1:1 molar excess CARMA1 (aa 673-1028, purple), showing no peak shifting upon addition.



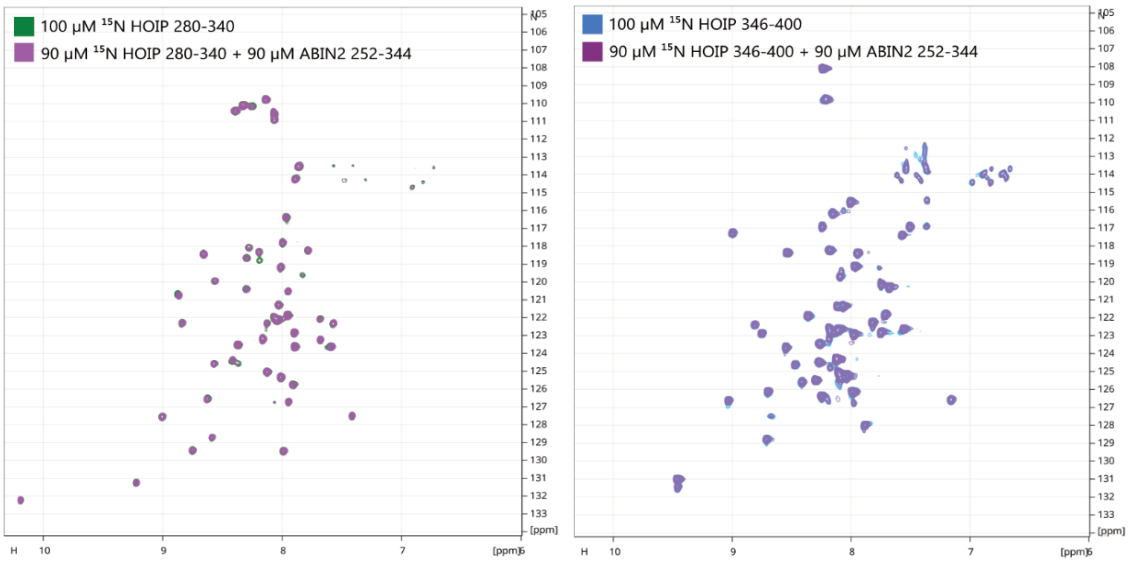
Supplementary Figure 17: BEST-TROSY spectra of ^{15}N-labelled HOIP PUB domain (aa 1-184, top left, dark blue), B-box (aa 195-291, top right, orange), NF0 (aa 280-340, green, center left), NZF1 (aa 346-451, center right, skyblue) and NZF2 (aa 380-451, bottom, red) on their own and mixed with 1:4 molar excess TRAF6 RING and Zf domains (aa 50-279, red), showing no peak shifting upon addition.



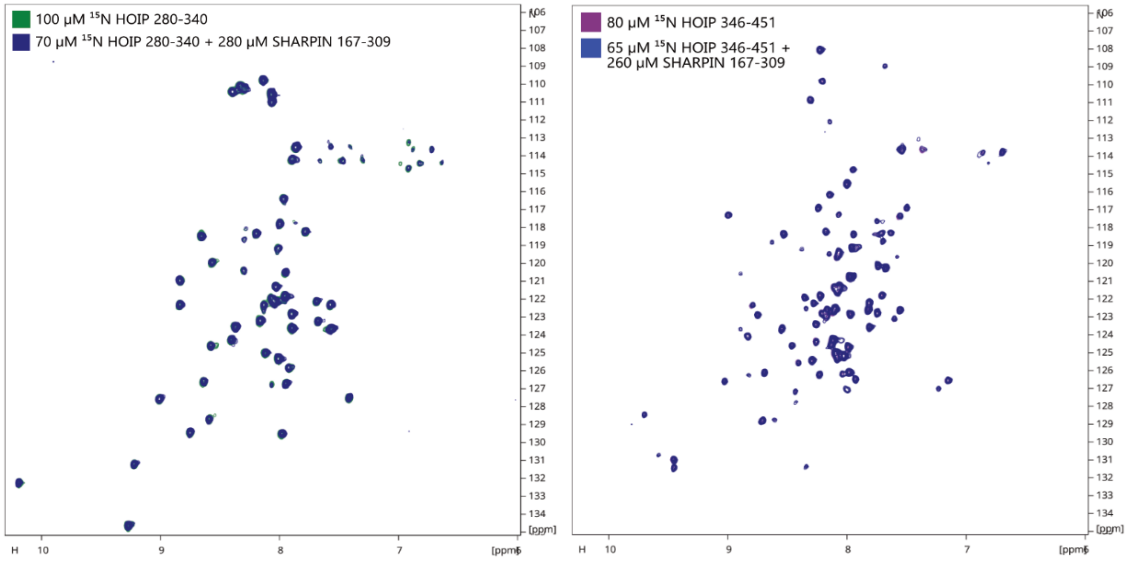
Supplementary Figure 18: BEST-TROSY spectra of ^{15}N-labelled HOIP PUB domain (aa 1-184, top left, dark blue), B-box (aa 195-291, top right, orange), NF0 (aa 280-340, green, center left), NZF1 (aa 346-451, center right, skyblue) and NZF2 (aa 380-451, bottom, orange) on their own and mixed with 1:2 molar excess NDP52 SKICH domain (aa 17-132, red), showing no peak shifting upon addition.



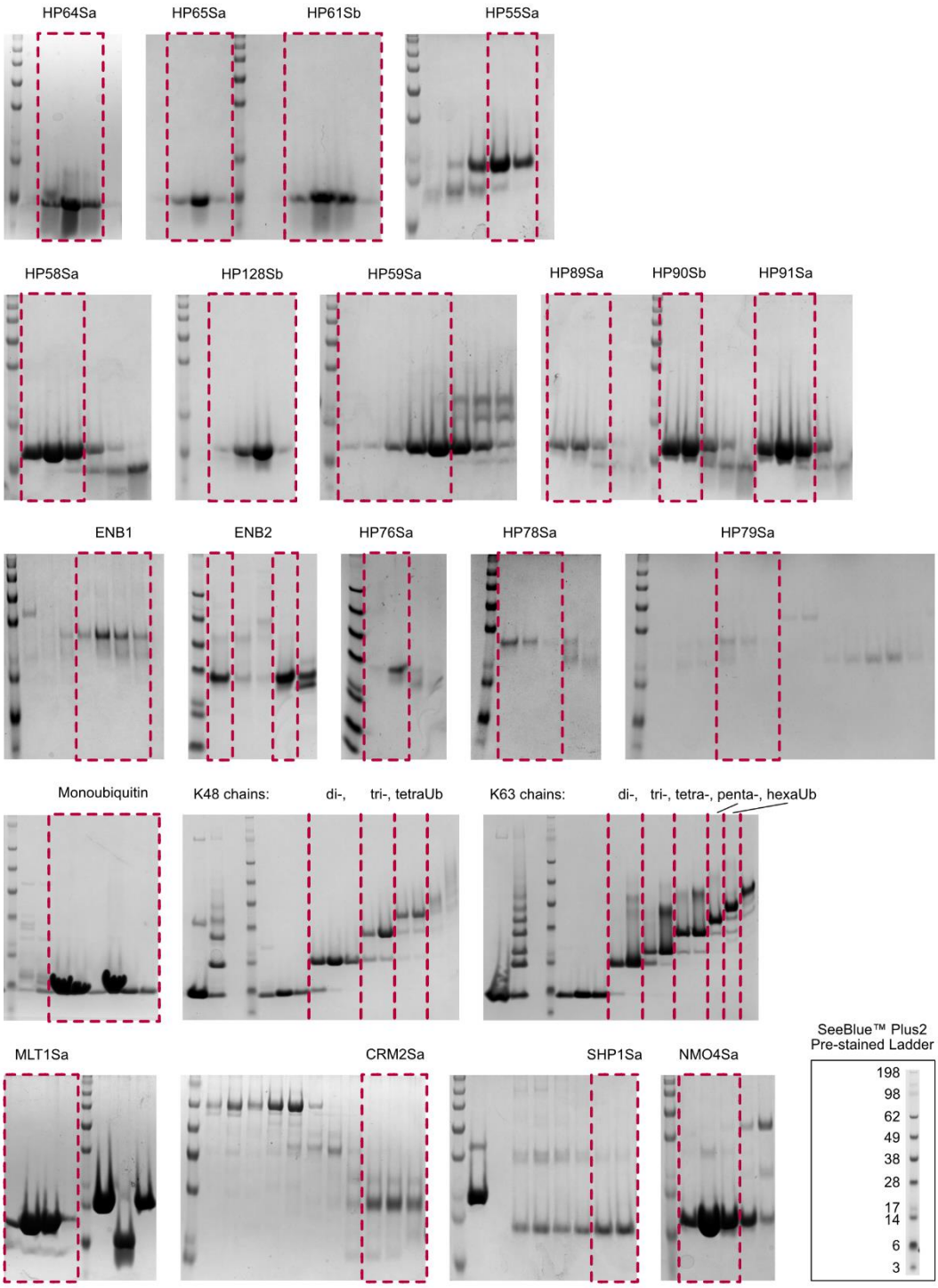
Supplementary Figure 19: BEST-TROSY spectra of ^{15}N-labelled HOIP PUB domain (aa 1-184, top left, dark blue), B-box (aa 195-291, top right, orange), NF0 (aa 280-340, green, center left), NZF1 (aa 346-451, center right, skyblue) and NZF2 (aa 380-451, bottom, red) on their own and mixed with 1:2 molar excess NDP52 UBZ domain (aa 388-446, lime), showing no peak shifting upon addition.



Supplementary Figure 20: (Left) BEST-TROSY spectra of ^{15}N-labelled HOIP NZF0 (aa 280-340, green, left) and NZF1 (aa 346-400, blue, right) mixed with 1:1 excess ABIN2 UBAN domain (aa 252-344, lilac), showing an overlap between the spectra.



Supplementary Figure 21: BEST-TROSY spectra of ^{15}N-labelled HOIP NZF0 (aa 280-340, left, green) and NZF1-NZF2 (aa 346-451, right, lilac) alone and mixed with 1:4 excess SHARPIN UBL domain (aa 167-309, dark blue), showing no shifts upon SHARPIN addition.



Supplementary Figure 22: SDS-PAGE analysis of all constructs purified for the purpose of this thesis. *Top row*: Constructs of individual NZF domains. HP64Sa (HOIP NZF1 aa 346-400, 6.01 kDa), HP65Sa (HOIP NZF2 aa 380-451, 7.75 kDa), HP61Sb (HOIP NZF0 aa 280-340, 6.25 kDa), HP55Sa (HOIP NZF0-NZF1-NZF2 aa 280-451, 18.11 kDa). *Second row*: NZF1-NZF2 wild-type and mutant constructs. HP58Sa (HOIP NZF1-NZF2 aa 346-451, 11.5 kDa), HP128Sb (HOIP NZF1-NZF2 aa 350-438, 9.7 kDa), HP59Sa (HOIP NZF1-NZF2 S383E aa 346-451, 11.5 kDa), HP89Sa (HOIP NZF1-NZF2 R375S aa 346-451, 11.5 kDa), HP90Sb (HOIP NZF1-NZF2 T360A aa 346-451, 11.5 kDa), HP91Sa (HOIP NZF1-NZF2 T419A aa 346-451, 11.5 kDa). *Third row:* Zinc finger region wild-type and mutant constructs. ENB1 (HOIP B-box-NZF0-NZF1-NZF2 aa 215-451, 24.89 kDa), ENB2 (HOIP B-box-NZF0-NZF1-NZF2 L219R aa 215-451, 24.89 kDa), HP76Sa (HOIP B-box-NZF0-NZF1-NZF2 L219D aa 215-451, 24.89 kDa), HP78Sa (HOIP B-box-NZF0-NZF1-NZF2 L219Y aa 215-451, 24.89 kDa), HP79Sa (HOIP B-box-NZF0-NZF1-NZF2

L219I aa 215-451, 24.89 kDa). *Fourth row*: Mono- and polyubiquitin purification. Monoubiquitin (aa 1-76, 8.6 kDa), K48 chain assembly products after cation exchange (products with more than four ubiquitin moieties per chain classified as “long chains” and pooled together), K63 chain assembly products after cation exchange (products with more than five ubiquitin moieties per chain classified as “long chains” and pooled together, aggregated of an apparent higher molecular weight can be seen in high concentrations). *Fifth row*: Signaling partner purifications. MLT1Sa (MALT1 aa 1-126, 13.54 kDa, lower molecular weight band stems from leak in well to the right of the gel containing monoubiquitin), CRM2Sa (CARMA1 aa 673-1028, 40.35 kDa), SHP1Sa (SHARPIN aa 167-309, 14.9 kDa), NMO4Sa (NEMO aa 257-364, 12.5 kDa). *Bottom right corner*: Note of protein ladder used for all gels, SeeBlue Plus2 Pre-stained Ladder.

References

1. Hershko, A. and A. Ciechanover, *The ubiquitin system.* Annu Rev Biochem, 1998. **67**: p. 425-79.
2. Hershko, A., A. Ciechanover, and I.A. Rose, *Resolution of the ATP-dependent proteolytic system from reticulocytes: a component that interacts with ATP.* Proc Natl Acad Sci U S A, 1979. **76**(7): p. 3107-10.
3. Goldstein, G., et al., *Isolation of a polypeptide that has lymphocyte-differentiating properties and is probably represented universally in living cells.* Proceedings of the National Academy of Sciences of the United States of America, 1975. **72**(1): p. 11-15.
4. Pickart, C.M. and M.J. Eddins, *Ubiquitin: structures, functions, mechanisms.* Biochim Biophys Acta, 2004. **1695**(1-3): p. 55-72.
5. Otten, E.G., et al., *Ubiquitylation of lipopolysaccharide by RNF213 during bacterial infection.* Nature, 2021. **594**(7861): p. 111-116.
6. Cohen, P. and S. Strickson, *The role of hybrid ubiquitin chains in the MyD88 and other innate immune signalling pathways.* Cell Death Differ, 2017. **24**(7): p. 1153-1159.
7. Pickart, C.M., *Mechanisms Underlying Ubiquitination.* Annual Review of Biochemistry, 2001. **70**(1): p. 503-533.
8. Fuseya, Y., et al., *The HOIL-1L ligase modulates immune signalling and cell death via monoubiquitination of LUBAC.* Nat Cell Biol, 2020. **22**(6): p. 663-673.
9. Komander, D. and M. Rape, *The ubiquitin code.* Annu Rev Biochem, 2012. **81**: p. 203-29.
10. Pruneda, J.N., et al., *Structure of an E3:E2~Ub complex reveals an allosteric mechanism shared among RING/U-box ligases.* Mol Cell, 2012. **47**(6): p. 933-42.
11. David, Y., et al., *E3 ligases determine ubiquitination site and conjugate type by enforcing specificity on E2 enzymes.* The Journal of biological chemistry, 2011. **286**(51): p. 44104-44115.
12. George, A.J., et al., *A Comprehensive Atlas of E3 Ubiquitin Ligase Mutations in Neurological Disorders.* Frontiers in Genetics, 2018. **9**(29).
13. Smit, J.J., et al., *The E3 ligase HOIP specifies linear ubiquitin chain assembly through its RING-IBR-RING domain and the unique LDD extension.* EMBO J, 2012. **31**(19): p. 3833-44.
14. Ye, Y., et al., *Ubiquitin chain conformation regulates recognition and activity of interacting proteins.* Nature, 2012. **492**(7428): p. 266-270.
15. Ikeda, F., N. Crosetto, and I. Dikic, *What determines the specificity and outcomes of ubiquitin signaling?* Cell, 2010. **143**(5): p. 677-81.
16. Emmerich, C.H., et al., *Lys63/Met1-hybrid ubiquitin chains are commonly formed during the activation of innate immune signalling.* Biochem Biophys Res Commun, 2016. **474**(3): p. 452-461.
17. Haglund, K. and I. Dikic, *Ubiquitylation and cell signaling.* EMBO J, 2005. **24**(19): p. 3353-9.
18. Dikic, I., S. Wakatsuki, and K.J. Walters, *Ubiquitin-binding domains — from structures to functions.* Nature Reviews Molecular Cell Biology, 2009. **10**(10): p. 659-671.
19. Fennell, L.M., S. Rahighi, and F. Ikeda, *Linear ubiquitin chain-binding domains.* FEBS J, 2018. **285**(15): p. 2746-2761.
20. Sato, Y., et al., *Structural basis for specific recognition of Lys 63-linked polyubiquitin chains by NZF domains of TAB2 and TAB3.* EMBO J, 2009. **28**(24): p. 3903-9.

21. Nielsen, C.P. and J.A. MacGurn, *Coupling Conjugation and Deconjugation Activities to Achieve Cellular Ubiquitin Dynamics.* Trends Biochem Sci, 2020. **45**(5): p. 427-439.
22. Heger, K., et al., *OTULIN limits cell death and inflammation by deubiquitinating LUBAC.* Nature, 2018. **559**(7712): p. 120-124.
23. Elliott, P.R., *Molecular basis for specificity of the Met1-linked polyubiquitin signal.* Biochem Soc Trans, 2016. **44**(6): p. 1581-1602.
24. van Wijk, S.J., et al., *Visualizing ubiquitination in mammalian cells.* EMBO reports, 2019. **20**(2): p. e46520.
25. Durcan, T.M., et al., *USP8 regulates mitophagy by removing K6-linked ubiquitin conjugates from parkin.* The EMBO Journal, 2014. **33**(21): p. 2473-2491.
26. Nucifora, F.C., Jr., et al., *Ubiqutination via K27 and K29 chains signals aggregation and neuronal protection of LRRK2 by WSB1.* Nat Commun, 2016. **7**: p. 11792.
27. Palicharla, V.R. and S. Maddika, *HACE1 mediated K27 ubiquitin linkage leads to YB-1 protein secretion.* Cell Signal, 2015. **27**(12): p. 2355-62.
28. Kulathu, Y. and D. Komander, *Atypical ubiquitylation — the unexplored world of polyubiquitin beyond Lys48 and Lys63 linkages.* Nature Reviews Molecular Cell Biology, 2012. **13**(8): p. 508-523.
29. Yuan, W.-C., et al., *K33-Linked Polyubiquitination of Coronin 7 by Cul3-KLHL20 Ubiquitin E3 Ligase Regulates Protein Trafficking.* Molecular Cell, 2014. **54**(4): p. 586-600.
30. Liwocha, J., et al., *Linkage-specific ubiquitin chain formation depends on a lysine hydrocarbon ruler.* Nat Chem Biol, 2021. **17**(3): p. 272-279.
31. Rohaim, A., et al., *Structure of a compact conformation of linear diubiquitin.* Acta Crystallogr D Biol Crystallogr, 2012. **68**(Pt 2): p. 102-8.
32. Komander, D., et al., *Molecular discrimination of structurally equivalent Lys 63-linked and linear polyubiquitin chains.* EMBO Rep, 2009. **10**(5): p. 466-73.
33. Rahighi, S., et al., *Specific recognition of linear ubiquitin chains by NEMO is important for NF-kappaB activation.* Cell, 2009. **136**(6): p. 1098-109.
34. Tokunaga, F., et al., *Involvement of linear polyubiquitylation of NEMO in NF-κB activation.* Nature Cell Biology, 2009. **11**(2): p. 123-132.
35. Haas, T.L., et al., *Recruitment of the linear ubiquitin chain assembly complex stabilizes the TNF-R1 signaling complex and is required for TNF-mediated gene induction.* Mol Cell, 2009. **36**(5): p. 831-44.
36. Shimizu, Y., L. Taraborrelli, and H. Walczak, *Linear ubiquitination in immunity.* Immunol Rev, 2015. **266**(1): p. 190-207.
37. Ikeda, F., *Linear ubiquitination signals in adaptive immune responses.* Immunological Reviews, 2015. **266**(1): p. 222-236.
38. Kirisako, T., et al., *A ubiquitin ligase complex assembles linear polyubiquitin chains.* EMBO J, 2006. **25**(20): p. 4877-87.
39. Tokunaga, F., et al., *SHARPIN is a component of the NF-kappaB-activating linear ubiquitin chain assembly complex.* Nature, 2011. **471**(7340): p. 633-6.
40. Rodriguez Carvajal, A., et al., *The linear ubiquitin chain assembly complex LUBAC generates heterotypic ubiquitin chains.* eLife, 2021. **10**: p. e60660.
41. Stieglitz, B., et al., *Structural basis for ligase-specific conjugation of linear ubiquitin chains by HOIP.* Nature, 2013. **503**(7476): p. 422-426.
42. Kelsall, I.R., et al., *The E3 ligase HOIL-1 catalyses ester bond formation between ubiquitin and components of the Myddosome in mammalian cells.* Proc Natl Acad Sci U S A, 2019. **116**(27): p. 13293-13298.
43. Shimizu, S., et al., *Differential Involvement of the Npl4 Zinc Finger Domains of SHARPIN and HOIL-1L in Linear Ubiquitin Chain Assembly Complex-Mediated Cell Death Protection.* Mol Cell Biol, 2016. **36**(10): p. 1569-83.
44. Ikeda, F., et al., *SHARPIN forms a linear ubiquitin ligase complex regulating NF-kappaB activity and apoptosis.* Nature, 2011. **471**(7340): p. 637-41.

45. Stieglitz, B., et al., *LUBAC synthesizes linear ubiquitin chains via a thioester intermediate.* EMBO Rep, 2012. **13**(9): p. 840-6.
46. Liu, J., et al., *Structural Insights into SHARPIN-Mediated Activation of HOIP for the Linear Ubiquitin Chain Assembly.* Cell Rep, 2017. **21**(1): p. 27-36.
47. Fujita, H., et al., *Cooperative Domain Formation by Homologous Motifs in HOIL-1L and SHARPIN Plays A Crucial Role in LUBAC Stabilization.* Cell Reports, 2018. **23**(4): p. 1192-1204.
48. Herhaus, L., et al., *Molecular Recognition of M1-Linked Ubiquitin Chains by Native and Phosphorylated UBAN Domains.* J Mol Biol, 2019. **431**(17): p. 3146-3156.
49. Alam, S.L., et al., *Ubiquitin interactions of NZF zinc fingers.* EMBO J, 2004. **23**(7): p. 1411-21.
50. Sato, Y., et al., *Specific recognition of linear ubiquitin chains by the Npl4 zinc finger (NZF) domain of the HOIL-1L subunit of the linear ubiquitin chain assembly complex.* Proc Natl Acad Sci U S A, 2011. **108**(51): p. 20520-5.
51. Fiil, B.K., et al., *OTULIN restricts Met1-linked ubiquitination to control innate immune signaling.* Mol Cell, 2013. **50**(6): p. 818-830.
52. Draber, P., et al., *LUBAC-Recruited CYLD and A20 Regulate Gene Activation and Cell Death by Exerting Opposing Effects on Linear Ubiquitin in Signaling Complexes.* Cell Rep, 2015. **13**(10): p. 2258-72.
53. Elliott, P.R., et al., *Molecular basis and regulation of OTULIN-LUBAC interaction.* Mol Cell, 2014. **54**(3): p. 335-48.
54. Elliott, P.R., et al., *SPATA2 Links CYLD to LUBAC, Activates CYLD, and Controls LUBAC Signaling.* Mol Cell, 2016. **63**(6): p. 990-1005.
55. Douglas, T. and M. Saleh, *Post-translational Modification of OTULIN Regulates Ubiquitin Dynamics and Cell Death.* Cell Rep, 2019. **29**(11): p. 3652-3663 e5.
56. Damgaard, R.B., et al., *The Deubiquitinase OTULIN Is an Essential Negative Regulator of Inflammation and Autoimmunity.* Cell, 2016. **166**(5): p. 1215-1230 e20.
57. Gerlach, B., et al., *Linear ubiquitination prevents inflammation and regulates immune signalling.* Nature, 2011. **471**(7340): p. 591-6.
58. Peltzer, N., et al., *LUBAC is essential for embryogenesis by preventing cell death and enabling haematopoiesis.* Nature, 2018. **557**(7703): p. 112-117.
59. Peltzer, N., et al., *HOIP Deficiency Causes Embryonic Lethality by Aberrant TNFR1-Mediated Endothelial Cell Death.* Cell Reports, 2014. **9**(1): p. 153-165.
60. Boisson, B., et al., *Human HOIP and LUBAC deficiency underlies autoinflammation, immunodeficiency, amylopectinosis, and lymphangiectasia.* Journal of Experimental Medicine, 2015. **212**(6): p. 939-951.
61. Oda, H., et al., *Second Case of HOIP Deficiency Expands Clinical Features and Defines Inflammatory Transcriptome Regulated by LUBAC.* Frontiers in Immunology, 2019. **10**(479).
62. Boisson, B., et al., *Immunodeficiency, autoinflammation and amylopectinosis in humans with inherited HOIL-1 and LUBAC deficiency.* Nature Immunology, 2012. **13**(12): p. 1178-1186.
63. Hrdinka, M. and M. Gyrd-Hansen, *The Met1-Linked Ubiquitin Machinery: Emerging Themes of (De)regulation.* Mol Cell, 2017. **68**(2): p. 265-280.
64. Oikawa, D., et al., *Linear Ubiquitin Code: Its Writer, Erasers, Decoders, Inhibitors, and Implications in Disorders.* Int J Mol Sci, 2020. **21**(9).
65. Seymour, R.E., et al., *Spontaneous mutations in the mouse Sharpin gene result in multiorgan inflammation, immune system dysregulation and dermatitis.* Genes Immun, 2007. **8**(5): p. 416-21.
66. Damgaard, R.B., et al., *OTULIN deficiency in ORAS causes cell type-specific LUBAC degradation, dysregulated TNF signalling and cell death.* EMBO Mol Med, 2019. **11**(3).

67. Hayden, M.S. and S. Ghosh, *NF-kappaB, the first quarter-century: remarkable progress and outstanding questions.* Genes Dev, 2012. **26**(3): p. 203-34.
68. Kumar, H., T. Kawai, and S. Akira, *Pathogen Recognition by the Innate Immune System.* International Reviews of Immunology, 2011. **30**(1): p. 16-34.
69. Liu, T., et al., *NF-κB signaling in inflammation.* Signal Transduction and Targeted Therapy, 2017. **2**(1): p. 17023.
70. Rieser, E., S.M. Cordier, and H. Walczak, *Linear ubiquitination: a newly discovered regulator of cell signalling.* Trends Biochem Sci, 2013. **38**(2): p. 94-102.
71. Rittinger, K. and F. Ikeda, *Linear ubiquitin chains: enzymes, mechanisms and biology.* Open Biol, 2017. **7**(4).
72. Wang, B., et al., *Structure and ubiquitin interactions of the conserved zinc finger domain of Npl4.* J Biol Chem, 2003. **278**(22): p. 20225-34.
73. De Franco, S., et al., *Exploring the suitability of RanBP2-type Zinc Fingers for RNA-binding protein design.* Sci Rep, 2019. **9**(1): p. 2484.
74. Michel, Martin A., et al., *Assembly and Specific Recognition of K29- and K33-Linked Polyubiquitin.* Molecular Cell, 2015. **58**(1): p. 95-109.
75. Kristariyanto, Yosua A., et al., *K29-Selective Ubiquitin Binding Domain Reveals Structural Basis of Specificity and Heterotypic Nature of K29 Polyubiquitin.* Molecular Cell, 2015. **58**(1): p. 83-94.
76. Fujita, H., et al., *Mechanism underlying IkappaB kinase activation mediated by the linear ubiquitin chain assembly complex.* Mol Cell Biol, 2014. **34**(7): p. 1322-35.
77. Noad, J., et al., *LUBAC-synthesized linear ubiquitin chains restrict cytosol-invading bacteria by activating autophagy and NF-kappaB.* Nat Microbiol, 2017. **2**: p. 17063.
78. Oikawa, D., et al., *Cellular and Mathematical Analyses of LUBAC Involvement in T Cell Receptor-Mediated NF-kappaB Activation Pathway.* Front Immunol, 2020. **11**: p. 601926.
79. Ozato, K., et al., *TRIM family proteins and their emerging roles in innate immunity.* Nat Rev Immunol, 2008. **8**(11): p. 849-60.
80. Thompson, H.G., et al., *Identification of the protein Zibra, its genomic organization, regulation, and expression in breast cancer cells.* Exp Cell Res, 2004. **295**(2): p. 448-59.
81. Feltham, R., A.I. Webb, and J. Silke, *SPATA2 - Keeping the TNF signal short and sweet.* The EMBO journal, 2016. **35**(17): p. 1848-1850.
82. Waterhouse, A.M., et al., *Jalview Version 2—a multiple sequence alignment editor and analysis workbench.* Bioinformatics, 2009. **25**(9): p. 1189-1191.
83. Michel, M.A., D. Komander, and P.R. Elliott, *Enzymatic Assembly of Ubiquitin Chains.* Methods Mol Biol, 2018. **1844**: p. 73-84.
84. Marion, D., *An introduction to biological NMR spectroscopy.* Mol Cell Proteomics, 2013. **12**(11): p. 3006-25.
85. Gao, G., J.G. Williams, and S.L. Campbell, *Protein-protein interaction analysis by nuclear magnetic resonance spectroscopy.* Methods Mol Biol, 2004. **261**: p. 79-92.
86. Barbato, G., et al., *Backbone dynamics of calmodulin studied by 15N relaxation using inverse detected two-dimensional NMR spectroscopy: the central helix is flexible.* Biochemistry, 1992. **31**(23): p. 5269-78.
87. Favier, A. and B. Brutscher, *NMRlib: user-friendly pulse sequence tools for Bruker NMR spectrometers.* J Biomol NMR, 2019. **73**(5): p. 199-211.
88. Folta-Stogniew, E. and K.R. Williams, *Determination of molecular masses of proteins in solution: Implementation of an HPLC size exclusion chromatography and laser light scattering service in a core laboratory.* J Biomol Tech, 1999. **10**(2): p. 51-63.

89. Kendrick, B.S., et al., *Online size-exclusion high-performance liquid chromatography light scattering and differential refractometry methods to determine degree of polymer conjugation to proteins and protein-protein or protein-ligand association states.* Anal Biochem, 2001. **299**(2): p. 136-46.
90. Wiseman, T., et al., *Rapid measurement of binding constants and heats of binding using a new titration calorimeter.* Anal Biochem, 1989. **179**(1): p. 131-7.
91. Duff, M.R., Jr., J. Grubbs, and E.E. Howell, *Isothermal titration calorimetry for measuring macromolecule-ligand affinity.* J Vis Exp, 2011(55).
92. Bromann, P.A., et al., *A putative ariadne-like E3 ubiquitin ligase (PAUL) that interacts with the muscle-specific kinase (MuSK).* Gene Expression Patterns, 2004. **4**(1): p. 77-84.
93. Robson, S., et al., *Nonuniform Sampling for NMR Spectroscopy.* Methods Enzymol, 2019. **614**: p. 263-291.
94. Karki, I., et al., *Entire-Dataset Analysis of NMR Fast-Exchange Titration Spectra: A Mg2+ Titration Analysis for HIV-1 Ribonuclease H Domain.* The Journal of Physical Chemistry B, 2016. **120**(49): p. 12420-12431.
95. Jumper, J., et al., *Highly accurate protein structure prediction with AlphaFold.* Nature, 2021.
96. Stetz, M.A., et al., *Chapter Seven - Characterization of Internal Protein Dynamics and Conformational Entropy by NMR Relaxation*, in *Methods in Enzymology*, A.J. Wand, Editor. 2019, Academic Press. p. 237-284.
97. Rinaldi, P.L., *Heteronuclear 2D-NOE spectroscopy.* Journal of the American Chemical Society, 1983. **105**(15): p. 5167-5168.
98. Fodor-Dunai, C., et al., *The phosphomimetic mutation of an evolutionarily conserved serine residue affects the signaling properties of Rho of plants (ROPs).* Plant J, 2011. **66**(4): p. 669-79.
99. Yamamoto, M., et al., *TNF receptor-associated factor 6 (TRAF6) plays crucial roles in multiple biological systems through polyubiquitination-mediated NF-κB activation.* Proceedings of the Japan Academy. Series B, Physical and biological sciences, 2021. **97**(4): p. 145-160.
100. Miyashita, H., et al., *Crosstalk Between NDP52 and LUBAC in Innate Immune Responses, Cell Death, and Xenophagy.* Frontiers in Immunology, 2021. **12**(831).
101. Herhaus, L., et al., *Molecular Recognition of M1-Linked Ubiquitin Chains by Native and Phosphorylated UBAN Domains.* Journal of Molecular Biology, 2019. **431**(17): p. 3146-3156.